REAL-TIME DETECTION OF *ESCHERICHIA COLI* USING BIOSENSORS FUNCTIONALIZED WITH LECTIN AND CARBON-HYDROGEL NANOSTRUCTURES

A Thesis

by

CASSIE ANN GIACOBASSI

Submitted to the Office of Graduate and Professional Studies of
Texas A&M University
in partial fulfillment of the requirements for the degree of

MASTER OF SCIENCE

Chair of Committee,	Carmen Gomes
Committee Members,	Matthew Taylor
	Elena Castell-Perez
Head of Department,	Stephen Searcy

May 2016

Major Subject: Biological and Agricultural Engineering

ABSTRACT

Foodborne pathogens are a major concern for the health and safety of the public. There is a need for a rapid, cost effective, and reliable detection method for foodborne pathogens to replace current highly technical and time consuming methods. *Escherichia coli* spp. are some of the most common foodborne bacteria. Concanavalin A was used in combination with platinum-graphene-platinum (PGP) and poly(N-isopropylacrylamide (PNIPAAm) to design an impedimetric biosensor for the real-time detection of non-pathogenic and pathogenic *E. coli* in PBS and in complex vegetable broth. Sensor performance was evaluated for sensitivity, lower detection limit (LOD), detection range, and detection time. Electroactive surface area (ESA) and actuation results testing for PNIPAAm were used to determine the most effective surface coating for *E. coli* detection. ESA values for bare, PGP, and PGP-PNIPAAm modified electrodes were calculated and generally increased ($p < 0.05$) with surface modification. Actuation of PNIPAAm, a thermo-responsive polymer, was tested, and results revealed 20 °C and 40 °C were the ideal temperatures for capturing and sensing bacteria, respectively. PGP results for ConA and antibody loaded at the same concentration were similar ($p > 0.05$). PGP-PNIPAAm yielded the best results with sensitivity of 38.005 ± 2.330 $(\log(CFU.mL^{-1}))^{-1}$ and 3.467 ± 0.297 $CFU.mL^{-1}$ LOD. ConA specificity to *E. coli* was tested in PBS with *Salmonella* Enteritidis and performance parameters were found to be similar ($p > 0.05$) to those with *E. coli* only. PGP-PNIPAAm-ConA was tested in vegetable broth inoculated with *E. coli* O157:H7 and performance was compared to

PGP-PNIPAAm-antibody. The antibody and ConA sensors performed similarly ($p > 0.05$) in broth regarding sensitivity, though the antibody was slightly superior with a larger detection range (10^2 –10^7 CFU.mL^{-1}) and lower ($p < 0.05$) LOD. The LOD for PGP-PNIPAAm-ConA was 39.06 ± 3.382 CFU.mL^{-1} and 21.850 ± 3.459 CFU.mL^{-1} for PGP-PNIPAAm-antibody. Response time for all sensors in this study was 17 minutes. Both ConA and antibody performance parameter results using PGP and PGP-PNIPAAm platforms were comparable to values reported in the literature. In PBS, ConA was superior to antibody in linear range of detection and the use of PNIPAAm for bacteria capture and sensing further improved sensitivity and LOD. The study showed there is great promise using ConA biosensors for pathogen detection in the food industry.

DEDICATION

To my family

Your love and support mean more than you know.

ACKNOWLEDGEMENTS

I would like to thank my committee chair and advisor, Dr. Gomes for her patient guidance throughout my graduate career; and my committee members, Dr. Taylor, and Dr. Castell, for their guidance, time, and support throughout the course of this research. Thank you, too, to Dr. McLamore and the research group at the University of Florida for their guidance and expertise regarding the subject.

Thank you also to my friends, colleagues, and the department faculty and staff for making my time at Texas A&M University a great experience. To my lab mates for all of their help through long days, late nights, and problem solving.

Finally, thank you to my family for their unconditional love and support, notes and words of encouragement, comic relief, and their patience with me through this process. Special thanks to my parents and sister for all of the late night, early morning, and middle of the day calls full of love and reassurance. My sincerest thanks and gratitude to all persons involved, directly or indirectly, in the completion of this work.

TABLE OF CONTENTS

Page

LIST OF FIGURES

Page

LIST OF TABLES

Page

1. INTRODUCTION

Foodborne pathogens are a constant concern in the food industry for the purpose of food safety (Kärkkäinen et al., 2011; Xu, 2012). According to the Centers for Disease Control and Prevention (CDC), known pathogens can be identified as the cause of an estimated 9.4 million foodborne illnesses annually in the United States (CDC, 2013c). Of the foodborne pathogens and illnesses the CDC keeps a record of, *Escherichia coli* spp. *(E. coli*), especially serogroups O157, O121, and O145 are some of the more common typically associated with beef and fresh produce (CDC, 2013c, 2014d). In 2009-2010, Shiga toxin-producing *Escherichia coli* (STEC) caused 58 confirmed outbreaks, with 53 being caused by serogroup O157 (CDC, 2013c).

Currently, the industry relies on conventional methods such as polymerase chain reaction (PCR), culture and colony counting, and enzyme-linked immunosorbent assay (ELISA) to detect foodborne pathogens (Lazcka, Campo, & Muñoz, 2007). While accurate, these methods can take from several hours to days to provide an answer (Lazcka et al., 2007).Therefore desirable to develop a more rapid, yet still accurate detection method for pathogens. An inexpensive, reliable detection method that could be used in a processing setting rather than require a laboratory and specially trained technicians to perform the test would be very advantageous in the food industry (Duncan, 2011). Biosensors, devices that use a biological material as part of the detection method, have been getting more attention in recent years as a possible alternative to traditional detection methods (Arora, Sindhu, Dilbaghi, & Chaudhury,

2011; Lazcka et al., 2007). In particular, electrochemical transduction has shown promise as well as optical, thermometric, and micromechanical transducing systems (Lazcka et al., 2007).

This project allows the food industry to begin to take advantage of the advances in nanotechnology by using the technology indirectly to improve pathogen detection techniques (Duncan, 2011). Along with the benefits of nanotechnology, the components to be used in the biosensor are washable, with removed pathogens being inactivated and properly disposed, and therefore the sensor will be able to be reused multiple times to not only reduce waste, but also cost (Campuzano et al., 2012). Implementation of such a sensor will have a significant, positive impact on food safety and public health.

2. RATIONALE AND SIGNIFICANCE

The number of foodborne pathogen disease outbreaks occurring in the United States and across the world negatively affecting the health, safety, and general well-being of consumers demonstrates the clear need to develop real-time detection biosensors. To get an idea of the breadth of the problem, 1 out 6 people in the United States become ill from contaminated food each year (CDC, 2013a). The use of biosensors could detect contamination sooner and prevent pathogens from reaching the public.

This project is a positive contribution to the overall knowledge of biosensors and their application within the food industry. It helps to further bridge the gap between the advances being made within nanotechnology in general and those technologies which are currently being applied in the food industry.

Studies have shown lectins, as biorecognition agents, to be a promising capture method for various types of pathogens, and for this reason were chosen for use in this study. The specificity, ease of attachment to biosensor surfaces, and availability of lectins make them excellent candidates for use in a biosensor for foodborne pathogen detection. This research is also an advancement in the area of immobilization efficiency of biorecognition molecules, lectins in this case, through the use of stimuli-responsive polymer nanobrushes. Actuation of the polymer enhances selective capture, benefitting the food industry through more efficient testing and accurate results. Previous studies investigating the characteristics of stimuli-responsive polymers and the use of lectins as

selective capture probes suggest that a biosensor combining these components will have superior capture and recognition of bacteria compared to current detection methods. Additionally, the use of platinum and graphene nanostructures in a platinum-graphene-platinum sandwich layer configuration on the electrode's surface has been shown to improve electrochemical performance of the sensor (Burrs et al., 2015; Vanegas et al., 2014). When lectin and stimuli-responsive polymers are combined with nanomaterial-modified electrodes, this approach is expected to have two distinct advantages over other published biosensors; enhanced capture of target bacteria due to less non-specific binding, and enhanced limit of detection and sensitivity.

This initial work exploring the combination of lectin and stimuli-responsive polymer nanobrushes over metallic nanostructures serves as a stepping-stone in the area of biosensing towards more efficient sensors. Furthermore, its contribution to food safety is significant in the work towards making the food supply safer and more reliable for consumers. Improved sensors using this technology can help to prevent future outbreaks of common foodborne pathogens, thus reducing the number of foodborne illnesses contracted each year.

The ConA biosensor will provide a significant advantage over current PCR and plate count methods in the long run. The new device is not only a quick detection method, but also as reliable and sensitive as conventional methods already in place within the industry. Along with saving time, the biosensor is easy to use and therefore reduces the need for extensive personnel training. Furthermore, this type of

nanotechnology has the potential to be produced in large batches adding to the economic feasibility of the sensor.

3. OBJECTIVES

3.1. Hypothesis

The combination of stimuli-responsive polymer brush interfaces and hybrid metallic nanostructures will enhance capture of target bacteria and increase the strength of transduction of electrochemical outputs as the acquisition signal. Furthermore, electrochemical detection of *Escherichia coli* (*E. coli*) through interactions between Concanavalin A (ConA) lectin with sections of the lipopolysaccharide (LPS) on the *E. coli* outer membrane will provide reduced time of detection, higher sensitivity, lower detection limit, broad linear range of detection, and overall efficient results when compared to plate count detection method and an antibody functionalized sensor for the purpose of food safety and quality applications.

3.2. Overall Objective

The overall goal of this research was to design and build a biosensor using ConA lectin and carbon-hydrogel nanostructures for real-time detection of *Escherichia coli* in a phosphate buffer solution (PBS) as well as a real-world scenario simulated by vegetable broth.

The specific objectives of this project were as follows:

3.2.1. Objective 1

Optimize immobilization and loading of ConA and *E. coli*-antibody on graphene-nanometal functionalized platinum electrodes through comparison of electroactive

surface area results from immobilization utilizing N-ethyl-N'-(3-dimethylaminopropyl) carbodiimide (EDC) and N-hydroxy-succinimide (NHS) chemistry.

3.2.2. Objective 2

Optimize immobilization and loading of ConA and *E. coli*-antibody on electrodes functionalized with poly(N-isopropylacrylamide) (PNIPAAm) nanobrushes and graphene-nanometal platform.

3.2.3. Objective 3

Determine the electrochemical response caused by interactions between ConA and *E. coli* K12 and *E. coli* O157:H7 using cyclic voltammetry (CV) and electrochemical impedance spectroscopy (EIS).

3.2.4. Objective 4

Determine the best test conditions for sensing bacteria using CV and EIS analysis.

3.2.5. Objective 5

Compare ConA biosensor detection limits, sensitivity, linear range, and total detection time with those of an antibody functionalized sensor and plate count methods in buffer suspension and food samples, i.e., vegetable broth.

3.2.6. Objective 6

Determine overall effectiveness of ConA biosensor compared to conventional plate count detection and an antibody functionalized sensor.

4. LITERATURE REVIEW

4.1. Biosensors

Biosensors, in general, are defined as analytical devices that use biological components as part of the detection method where the response of interaction between the component and the target analyte can be detected by a transducer and converted to a quantifiable signal (Arora et al., 2011; Lazcka et al., 2007). Figure 4.1. shows a schematic of a basic biosensor for the detection of an analyte. There are various types of transducers used for detection with the main types used for microbial detection being electrochemical, piezoelectric, and optical (Ivnitski, Abdel-Hamid, Atanasov, & Wilkins, 1999; Pejcic, De Marco, & Parkinson, 2006).

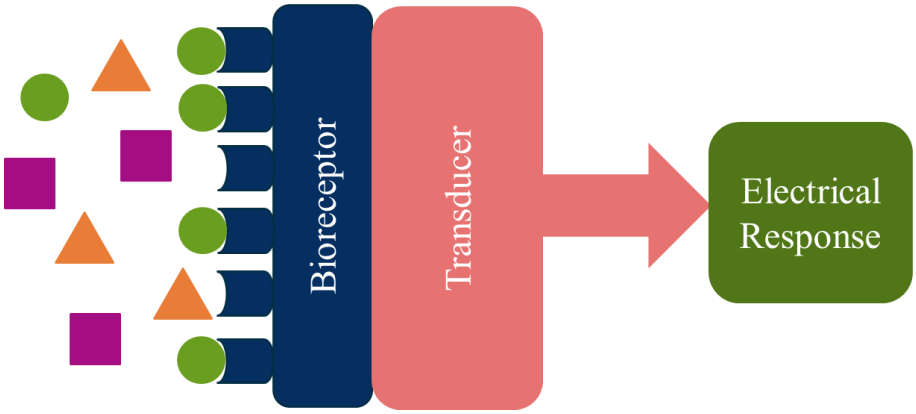

Figure 4.1. Schematic of a biosensor used to detect an analyte.

Electrochemical biosensors for pathogen detection are becoming a popular possible alternative to traditional methods (culture-based, immunological, and

molecular) as many of them can be made into very small, portable devices that are low in cost, yet high in selectivity (Vidal et al., 2013). The ability of electrochemical biosensors to detect bacteria in real time, in turn allowing for a higher throughput of samples than current detection methods adds to their appeal (Adams & Moss, 2008; Daniels & Pourmand, 2007; Varshney & Li, 2009). Despite the many improvements and advantages of biosensors, they have not replaced traditional methods as the standard in industry yet, mainly because the reproducibility is not to the level it needs to be for sustainable use within the industry (Daniels & Pourmand, 2007; Prodromidis, 2010). It is difficult to reuse the materials and still maintain the same limit of detection after the first use, particularly with sensors that involve the use of antibodies for detection (Daniels & Pourmand, 2007; Prodromidis, 2010).

However, biosensors are not a new concept. One of the first generation biosensors was the glucose sensor developed by Clark and Lyons in 1962, which used an oxygen sensor to measure the amount of oxygen consumed by an enzymatic reaction in order to determine the amount of glucose present in the sample as cited by Wang (2001). Through the years, the use for biosensors has expanded beyond glucose to include other medical, environmental, and food safety applications (Abu-Rabeah, Ashkenazi, Marks, Atias, & Amir, 2009; Daniels & Pourmand, 2007; Pöhlmann et al., 2009).

4.1.1. Electrochemical

In particular, electrochemical biosensors are valuable due to low cost, high sensitivity, real-time detection, and compact, mobile size (Pejcic et al., 2006; Skládal et al., 2013; Varshney & Li, 2009). Additionally, electrochemical biosensors are relatively

easy to miniaturize, require small sample volumes, and can be used in turbid solutions (Grieshaber, MacKenzie, Voros, & Reimhult, 2008; Ivnitski et al., 1999). Electrochemical biosensors detect an analyte by measuring the changes in electrical properties, which are caused by biochemical reactions (Grieshaber et al., 2008).

A common way to differentiate between types of electrochemical sensors is by the parameter they measure. Some of the most widespread electrochemical sensors are amperometric, potentiometric, conductometric, and impedimetric (Arora et al., 2011; Grieshaber et al., 2008).

Amperometric sensors work by measuring the current, which results from oxidation and reduction reactions between the biological component and analyte, when the sensor is set to a constant potential (Grieshaber et al., 2008; Lazcka et al., 2007). Typically, enzyme systems such as horse radish peroxidase (HRP) and alkaline phosphatase (AP) are used in amperometric biosensors due to their ability to convert non-electrochemically active analytes to electrochemically active in order to elicit a response in the sensor (Arora et al., 2011; Pöhlmann et al., 2009). Results are interpreted based on the notion that the relationship between the analyte concentration present and the peak current value is linear and directly proportional (Grieshaber et al., 2008; Lazcka et al., 2007). The surface of amperometric sensors is often prepared using thin-films of gold, platinum, or carbon in order to transmit the signal from the reaction through the sensor (Arora et al., 2011).

One of the least common among biosensors, potentiometric sensors detect changes in ion activity in the sample solution (Arora et al., 2011; Lazcka et al., 2007).

The change that is detected occurs due to the charge potential that builds up on the working electrode in comparison to a reference electrode when no current is passed between them (Grieshaber et al., 2008). A disadvantage contributing to the unpopularity of potentiometric biosensors is the lower signal to noise ratio in contrast to amperometric and impedimetric sensors (Vidal et al., 2013). The signal produced shows the concentration of the analyte present as a logarithmic relationship, which allows for detection of small changes in concentration over a large range (10^{-6} to 10^{-1} mol L^{-1}) (Arora et al., 2011; Ivnitski et al., 1999; Lazcka et al., 2007). A commonly used potentiometric sensor is the pH meter electrode. Potentiometric sensors have had limited use in the area of new drug studies and environmental toxicity studies (Lazcka et al., 2007). The most successful use of the sensors has been when they are combined with optical detection and used for food pathogen detection (Arora et al., 2011; Lazcka et al., 2007).

Conductometric biosensors, sometimes categorized as a subset of impedimetric sensors, are not the most widely used type in the area of biosensors for pathogen detection (Grieshaber et al., 2008). Some studies have shown conductometric sensors detecting various foodborne pathogens in less than 10 min over a wide range of concentrations; however, these studies failed to prove the method was reliable when compared to a standard immunoassay method (Pejcic et al., 2006) Conductometric sensors have also been explored for use in drug detection in urine samples and for environmental pollution detection (Grieshaber et al., 2008). They work by measuring the conductance change in the medium containing the analyte or rather the ability of the

solution to conduct electrical current is measured between two electrodes or reference nodes (Grieshaber et al., 2008; Pejcic et al., 2006). Similarly to amperometric sensors, conductometric biosensors commonly rely on enzymes and the subsequent enzymatic reactions that cause changes in the ionic strength (Grieshaber et al., 2008). The widespread use of conductometric sensors is limited by the inevitable variability of the ionic strength of samples coupled with the need to detect minute changes in the conductivity (Grieshaber et al., 2008).

Impedimetric biosensors use the change in impedance response of a material, which occurs due to a small amplitude sinusoidal excitation signal formed from a combination of capacitive, inductive, or resistive properties of the material for analyte detection (Arora et al., 2011; Varshney & Li, 2009). Responses seen in the capacitance, resistance, inductance, and the effect they have on the overall impedance show that all of these are merely different ways to measure the same reaction and they are all interconnected (Ivnitski et al., 1999). To achieve the impedance measurement, the instrument uses an alternating current (AC) steady state with constant direct current (DC) bias conditions to collect data over a range of frequencies or at one particular frequency (Daniels & Pourmand, 2007; Pejcic et al., 2006).

An assortment of analytes can be detected using impedance biosensors because the probe used can be varied to accommodate differing targets that do not need to be electroactive, making impedance sensors attractive versus other types of sensors and methods (Daniels & Pourmand, 2007). Impedance biosensors have been used to detect DNA, proteins, bacteria, specific food pathogens, and viruses without the need for labels

(Daniels & Pourmand, 2007; Ivnitski et al., 1999; Pejcic et al., 2006). Another big advantage impedimetric sensors have over other methods of detection is that they differentiate between viable and non-viable bacterial cells because only live cells can elicit a change in the conductivity of the sample (Varshney & Li, 2009).

The most common measurement used in impedimetric biosensors, impedance, encompasses all opposition a circuit gives against the flow of electrons and ions when a single-frequency is applied (Barsoukov & Macdonald, 2005; Prodromidis, 2010). This impedance (Z) is represented as the ratio of V(t)/I(t) where V is the voltage and I is the current (Barsoukov & Macdonald, 2005; Prodromidis, 2010). Difficulties on fully understanding impedance arise due to impedance being expressed as a complex number made up of real and imaginary components, which can make the mathematics difficult (Barsoukov & Macdonald, 2005; Lazcka et al., 2007; Prodromidis, 2010). With regard to impedance being a complex number, the real component consists of the ohmic resistance and is not dependent on frequency, while the imaginary component refers to the capacitive reactance and is dependent on frequency (Barsoukov & Macdonald, 2005; Prodromidis, 2010). Results can be interpreted either by solving the complex system of partial differential equations or, more favorably, by using equivalent circuits to understand the data collected (Lazcka et al., 2007).

The solution of differential equations includes capacitive and inductive components given by the equations (Barsoukov & Macdonald, 2005):

$$i(t) = \left[\frac{dv(t)}{dt} \right] C \tag{4.1}$$

$$v(t) = \left[\frac{di(t)}{dt}\right]L \tag{4.2}$$

where i represents current in Amperes, v is voltage (Volts) in both equations and both capacitive (C) and inductive (L) elements in Farads and Henrys are represented by Eqs. 4.1 and 4.2, respectively (Barsoukov & Macdonald, 2005). Impedance (Z), when reported as a single, complex vector quantity is represented by Eq. 4.3 where Z is impedance in Ohms , Z' is the real portion in Ohms, Z" is the imaginary portion in Ohms, *j* is the imaginary number representing $\sqrt{-1}$, and ω is the frequency in Hertz (Barsoukov & Macdonald, 2005). The phase angle (θ) is given by $\theta = tan^{-1}(Z''/Z')$ (Barsoukov & Macdonald, 2005).

$$Z(\omega) = Z' + jZ'' \tag{4.3}$$

Empirical equivalent circuits are often used to analyze the experimental impedance data collected (Barsoukov & Macdonald, 2005; Lazcka et al., 2007). Equivalent circuits are made up of a combination of ideal resistors and capacitors arranged in a plausible order to represent the physical system (Barsoukov & Macdonald, 2005; Lazcka et al., 2007). A simple and often used equivalent circuit in Electrochemical Impedance Spectroscopy (EIS) experiment analysis is the Randles circuit (Prodromidis, 2010). The Randles circuit, demonstrated in Figure 4.2., is made up of the resistance of the electrolyte (R_s), the capacitance of the dielectric layer (C_{dl}), and the charge-transfer resistance (R_{ct}) (Prodromidis, 2010). The resistance and capacitance are connected in series, while the capacitance and the charge-transfer resistance are connected in parallel (Prodromidis, 2010). There is also the Warburg

impedance (Z_w) connected in series with the charge transfer resistance, which takes into account the diffusion of ions from the bulk electrolyte to the electrode surface (Prodromidis, 2010).

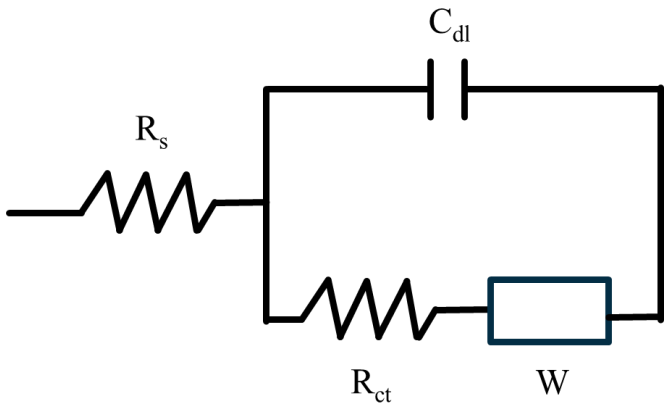

Figure 4.2. Depiction of Randles equivalent circuit.

While this method is accepted widely, it is important to use caution to ensure the equivalent circuit used makes physical sense as the same data may be fitted by more than one circuit (Lazcka et al., 2007). Measuring the impedance at different frequencies can be useful if several parameters need to be determined to complete the circuit (Lazcka et al., 2007). Residual properties, given by the real resistance, are of negligible importance over large frequency ranges and therefore the system can be approximated by ideal resistance in the equivalent circuit (Barsoukov & Macdonald, 2005). A disadvantage to using equivalent circuits is that ideal circuits represent lumped constant properties and

therefore the ideal elements used may not be adequate in describing the electrical response detected (Barsoukov & Macdonald, 2005).

Common ways to report impedance data for further analysis are the Nyquist and Bode plots (Prodromidis, 2010). The Nyquist plot displays the imaginary impedance portion, Z", against the real component, Z', at each frequency, while the Bode plot shows the log of the absolute impedance, $|Z|$, and the phase shift, θ, against the log of the frequency, ω (Prodromidis, 2010). Examples of Nyquist and Bode plots can be seen in Figures 4.3. and 4.4., respectively.

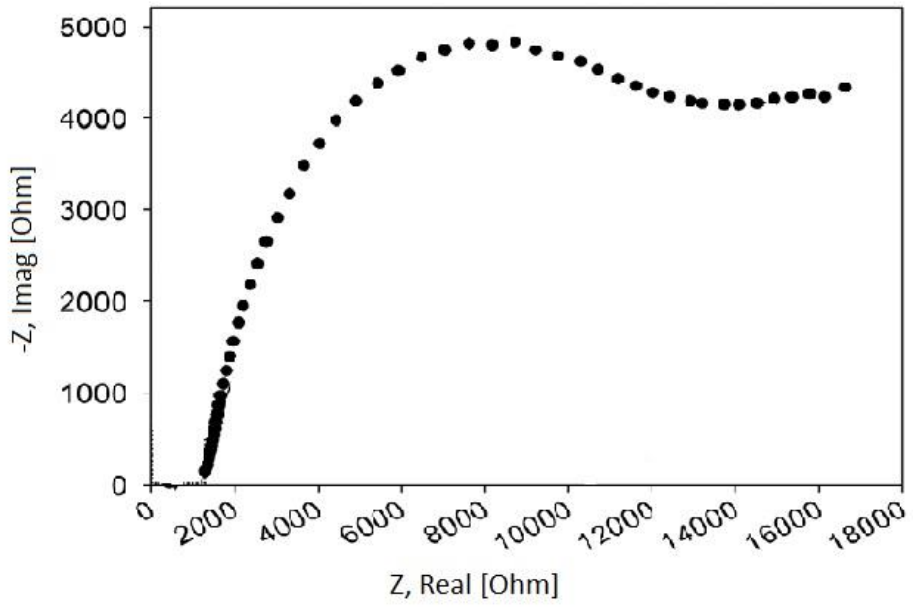

Figure 4.3. Representative Nyquist plot of bare electrode adapted from Burrs et al. (2015).

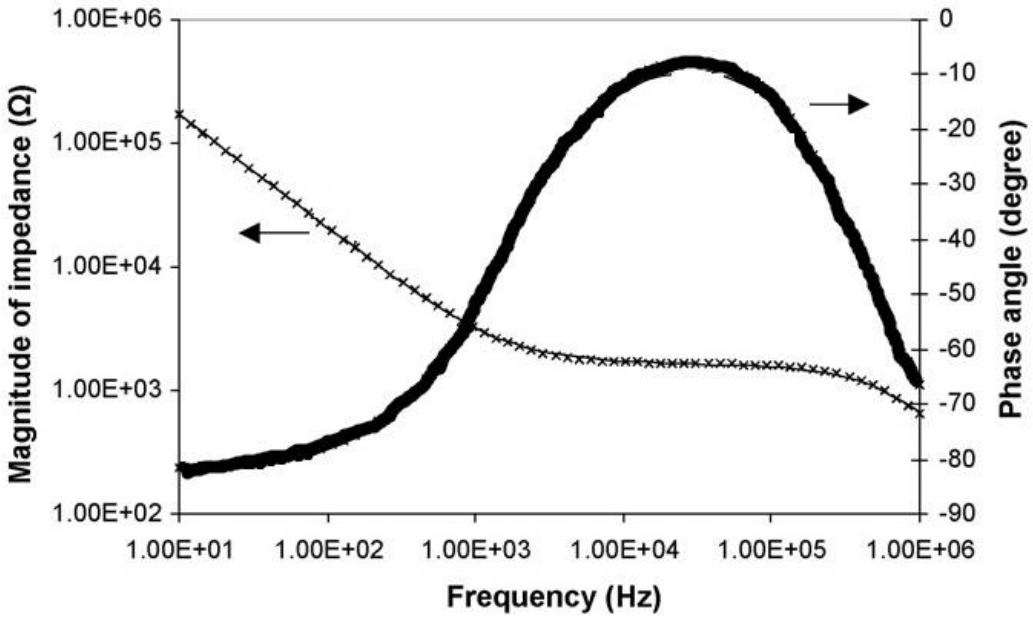

Figure 4.4. Example Bode plot of simulated data adapted from Varshney and Li (2007).

Conventional EIS (Electrochemical Impedance Spectroscopy) reports Z, described above, as a function of *v* or ω over a range of frequencies (Barsoukov & Macdonald, 2005). The electrical properties of the entire system are derived from the Z(ω) vs. ω responses (Barsoukov & Macdonald, 2005).

4.1.2. Impedance Biosensors for Detection of *E. coli* O157:H7

E. coli O157:H7 has been the target of many impedance sensors due to its large impact on human health causing serious illness and, in some cases, death (A. D. Chowdhury, De, Chaudhuri, Bandyopadhyay, & Sen, 2012; Radke & Alocilja, 2005; Varshney & Li, 2007). Several studies have shown great promise in sensitivity of detection and success in developing sensors micro in size (A. D. Chowdhury et al., 2012; Radke & Alocilja, 2005; Varshney & Li, 2007, 2008). Reproducibility of consistent,

reliable, and rapid sensors is one of the hurdles to overcome in the quest for creating a widely available sensor for industry use (Daniels & Pourmand, 2007; Prodromidis, 2010). The limit of detection is not at the level needed to prevent infection, i.e., equivalent or lower than the infectious dose, which for *E. coli* O157:H7 is estimated to be 10-100 viable cells (Feng, Weagant, & Jinneman, 2011). Therefore, using these sensors in the industry would risk missing a potentially hazardous product contamination at a dose below the limit of detection.

Chowdhurry et al. (2012) published a study on using a label free impedimetric sensor based on polyaniline specifically for the detection of *E. coli* O157:H7. The sensor was made up of a polyaniline surface immobilized with an antibody through covalent linking (A. D. Chowdhury et al., 2012). Unfortunately, for best results, their method required purification of the samples by centrifugation, which, as with conventional methods, was the most time consuming part of detection (A. D. Chowdhury et al., 2012). The group was successful in producing a sensor that utilized a simple method capable of detecting *E. coli* O157:H7 at a range of 10^2-10^7 CFU mL^{-1}, though they found their sensor to be most accurate over in the range of 10^2-10^5 CFU mL^{-1} (A. D. Chowdhury et al., 2012).

Using a high density microelectrode array for the structure of their biosensor, the group of Radke and Alocilja (2005) were successful in detecting *E. coli* O157:H7 at a detection level of 10^4 CFU mL^{-1}. While the infectious dose is much lower than the detection limit (10^4 CFU mL^{-1}), the work was novel and important in the design of the sensor as far as size and dimensions (Radke & Alocilja, 2005). The width and spacing

of each finger were such that the contribution each bacterium had on the impedance was increased (Radke & Alocilja, 2005). Spacing close to the size of the individual bacterium increased the contribution of the immobilized bacteria to the measured impedance (Radke & Alocilja, 2005). Finally, their work also contributed to the overall improvement of biosensors through the exploration of testing real samples in the form of lettuce water without any purification steps (Radke & Alocilja, 2005).

The group of Varshney and Li (2007) also explored the use of microelectrode arrays and their application in detecting *E. coli* O157:H7 in food samples. The microelectrode array was coupled with magnetic nanoparticle-antibody conjugates (MNAC) to isolate a bacterial sample (Varshney & Li, 2007). The use of a magnetic field aided in concentrating the bacteria onto the surface of the electrode allowing the sensor to detect bacteria at 7.4×10^4 CFU mL^{-1} in pure samples and 8.0×10^5 CFU mL^{-1} in ground beef samples with a detection time of 35 min (Varshney & Li, 2007).

4.1.3. Piezoelectric

Piezoelectric biosensors have been shown to have applications as a direct (label-free) bacteria detection system within environmental, food industry, clinical diagnostics, and biotechnology settings (Ivnitski et al., 1999). Direct detection methods do not require any type of additional label attached to the target such as fluorescent antibodies for detection, but rather they use direct measurement of physical phenomena that take place during biochemical reactions (Arora et al., 2011; Ivnitski et al., 1999). At their core, piezoelectric sensors detect pathogens by monitoring the change in frequency observed due to the change in mass on the transducer surface (Arora et al., 2011; Ivnitski

et al., 1999; Lazcka et al., 2007; X.-L. Su & Li, 2004). The relationship between the change in resonant frequency and the change in mass observed is given by the Sauerbrey equation (Eq. 4.4), where ΔF is the change in frequency in Hertz, F_0 is the resonant frequency of the crystal in MHz, Δm is the mass in grams deposited on the surface, and A is the coated area in cm^2 (Lazcka et al., 2007).

$$\Delta F = \frac{-2.3x10^6 F_0^2 \Delta m}{A} \tag{4.4}$$

The change in mass occurs because of bacteria adsorption onto the antibody coated sensor surface, which occurs due to biochemical reactions that take place between the bacteria and the antibody (Pejcic et al., 2006; X.-L. Su & Li, 2004). Antibodies used in piezoelectric sensors are chosen with high specificity to the desired pathogen of concern and they are therefore a highly desired and useful tool in the food industry (Arora et al., 2011).

An ultra-sensitive surface is required to detect the minute changes in mass that take place during the binding of the bacteria (X.-L. Su & Li, 2004). The most common surface used as transducers today is the quartz crystal microbalance (QCM) (Arora et al., 2011; Lazcka et al., 2007; X.-L. Su & Li, 2004). In addition to quartz, lithium niobate and potassium sodium tartrate have recently become more accepted and used as a raw material used for the surface of piezoelectric biosensors (Arora et al., 2011; Nayak, Kotian, Marathe, & Chakravortty, 2009).

Recently, there have been a few studies using piezoelectric sensors to detect foodborne pathogens. Protein-A antibody has been used in stop flow analysis (SFA) piezoelectric sensors to detect *Salmonella* Typhimurium at relatively high concentrations

in the range of 10^6-10^9 CFU mL^{-1} (Babacan, Pivarnik, Letcher, & Rand, 2002). The group of Su and Li used affinity-purified antibodies for the detection of *E. coli* O157:H7 within the range of 10^3-10^8 CFU mL^{-1} (X.-L. Su & Li, 2004). Some disadvantages associated with piezoelectric biosensors are the multiple steps required for washing and drying as well as regeneration of the surface crystals in order to reuse the sensors (Ivnitski et al., 1999). Alternative production methods such as dip-and-dry, while more sensitive, are not feasible for automation at this time, and therefore, sensitivity remains a concern for piezoelectric sensors that may be used in industrial applications (Lazcka et al., 2007). Advantages affiliated with piezoelectric sensors include rapid detection of various bacteria as the sensors can be made with specific antibodies to match the target bacteria as well as the simplicity of the technique (Arora et al., 2011; X.-L. Su & Li, 2004).

4.1.4. Optical

Optical biosensors utilize the energy gathered from the electromagnetic spectrum to provide a visual representation of the minute changes detected in the environment immediately surrounding the target (Pejcic et al., 2006). Cells bind to receptors immobilized on the transducer surface causing the changes in refractive index or thickness which can be observed by the sensor (Ivnitski et al., 1999).

Using optical transducers allows for real-time, label-free, in situ bacteria detection, which are desirable attributes for use in industry applications (Grieshaber et al., 2008; Ivnitski et al., 1999; Nayak et al., 2009). High selectivity and sensitivity also contribute to optical sensors being some of the most popular sensors for detection of

bacteria (Arora et al., 2011; Lazcka et al., 2007). A number of sensors use optical detecting techniques including direct fluorescence, bioluminescence, optical waveguide lightmode spectroscopy (OWLS), and, most commonly, surface plasmon resonance (SPR) (Grieshaber et al., 2008; Ivnitski et al., 1999; Lazcka et al., 2007).

Surface plasmon resonance (SPR) is a direct optical-sensing method that utilizes optical illumination of metal surfaces for pathogen detection (Amano & Quan, 2005; Arora et al., 2011). More specifically, changes in the refractive index occur due to biospecific interactions between immobilized antibodies and antigens thus causing a shift in the resonance angle, which is proportional to the amount of antigens present on the surface (Amano & Quan, 2005; Arora et al., 2011; Subramanian, Irudayaraj, & Ryan, 2006). SPR typically uses gold film as the attachment surface where, at particular wavelengths, resonance is generated with the electron cloud in the metal (Arora et al., 2011). Pathogen detection is measured by the change in the angle of incidence from the original angle, which is based solely on the properties of the gold-solution surface before any antibody-antigen binding (Lazcka et al., 2007).

Not only is SPR a label-free sensing technique, it is also non-invasive and provides results in real-time through analysis in less processed samples than typically required for bacteria detection and is generally more sensitive than electrochemical techniques (Lazcka et al., 2007; Pejcic et al., 2006). SPR has been shown to detect *E. coli* O157:H7 as low as 10^3 CFU mL^{-1} by Subramanian et al. (2006) as well as in other studies with detection limits in the range of 10^2-10^7 CFU mL^{-1} (Deisingh & Thompson, 2004; Lazcka et al., 2007). Unfortunately, SPR is at a disadvantage in that it is very

complex, expensive to perform, and the equipment currently available is large in size (Lazcka et al., 2007).

4.2. Platinum and Graphene in Biosensing

Metal and carbon nanomaterials have been increasingly used in electroanalytical applications (Vanegas et al., 2014). In particular, graphene and platinum are being explored due to their potential to enhance biosensing, especially when used together (Shi et al., 2012; X. Su, Ren, Meng, Ren, & Tang, 2013; Vanegas et al., 2014).

In biosensing, graphene has the potential to increase electron transfer during the oxidation or reduction of electroactive intermediate species (Shi et al., 2012). Graphene along with reduced graphene sheets have also been shown to increase the surface area of the sensing platform, exhibit superior electric conductivity, strong mechanical strength, excellent biocompatibility, and ease of functionalization (X. Su et al., 2013; Yixian, Zunzhong, & Yibin, 2012). The electrical conductivity of graphene modified electrodes has been shown to be higher than that of carbon nanotubes due to the increased sp^2 bonding content (Shi et al., 2012). While the addition of graphene has been shown to aid the electrical conductivity of the sensor, the carbon concentration present in the graphene to be attached has an effect on the overall conductivity (Vanegas et al., 2014). Too little carbon present and there is poor conjugation to the electrode surface; too much carbon and the graphene stacks on itself and lowers the overall electrical conductivity (Vanegas et al., 2014).

An advantage of graphene and its derivatives (reduced graphene, graphene oxide) is their ability to be dispersed in aqueous solution, which aids in preparation of sheets,

composites, and films (Choi et al., 2010). Graphene oxide is particularly easy to disperse in aqueous solution due to its high concentration of hydroxyl and carboxyl groups (X. Su et al., 2013). One major challenge encountered when using graphene is the deposition onto the electrode surfaces by van der Waals forces (Shi et al., 2012). Sometimes graphene is suspended in polymers then deposited on electrode surfaces, though this can cause its own problems as the polymers are non-conductive and can form a diffusion barrier decreasing the active surface area of sensors and decreasing the sensitivity (Shi et al., 2012).

Platinum deposited as nanoparticles has been shown to improve biosensor performance as a result of its biocompatibility and electrocatalytic activities (Shi et al., 2012). Often, nanoplatinum (platinum black) is applied to electrode surfaces in layers of amorphous clusters as electrocatalytic platforms to aid in sensitivity, limit of detection, and response time in biosensors (McLamore et al., 2011; Shi et al., 2012; Vanegas et al., 2014). Platinum is a desired choice due to its high resistance to chemicals, stability at high temperatures, resistance to wear and tarnish, and excellent electrocatalytic activity (Carraro, Maboudian, & Magagnin, 2007; Claussen, Franklin, ul Haque, Porterfield, & Fisher, 2009). Addition of immobilized conductive nanoplatinum improves electrochemical sensing due to higher current densities and faster mass transport compared to larger macro particles as well as providing more favorable Faradic-to-capacitive current ratios and increased electrocatalytic behavior attributed to quantum confinement (Claussen et al., 2012).

There are several common ways for nanoplatinum to be deposited onto the surface of an electrode including galvanic displacement, pulsed electrodeposition, and electrodeposition, which result in differing surface structures and, consequently, electrochemical performance (Carraro et al., 2007; Chandrasekar & Pushpavanam, 2008; Chen et al., 2007; Coleman & Co, 2014; Penner, 2002; Vanegas et al., 2014). Galvanic displacement is achieved when the metallic ion in solution has a lower oxidation potential than the displaced base material and while the base dissolves into the solution the metallic ions are reduced on the surface (Carraro et al., 2007). The particle size can be controlled during galvanic displacement through the adjustment of deposition time and temperature as well as the starting concentration of platinum used in solution (Coleman & Co, 2014). Pulsed electrodeposition (PED) is accomplished by alternating the potential or current between two different values in a series of pulses, separated by zero current, with equal amplitude, polarity, and duration (Chandrasekar & Pushpavanam, 2008). The deposited film composition and thickness can be regulated by controlling the pulse amplitude and width (Chandrasekar & Pushpavanam, 2008). Electrodeposition is carried out similarly to pulsed electrodeposition, though all at one time rather than in pulses. Nanoplatinum deposited via electrodeposition occurs at a constant voltage for a specific amount of time (Burrs et al., 2015; Vanegas et al., 2014). Electrochemical properties, such as electrocatalytic activity, resulting from deposition of nanoplatinum can also be affected by the properties of the supporting materials (i.e. various carbon materials) used during deposition (Chen et al., 2007).

While platinum and graphene offer many benefits to biosensor performance when incorporated onto the electrode surface, they are most effective at efficiently enhancing electron transport when used in combination (Shi et al., 2012; Vanegas et al., 2014). Testing of several combinations revealed that the best combination of graphene and platinum is a sandwich formation starting with a layer of nanoplatinum, then graphene, and ending with another layer of nanoplatinum (Burrs et al., 2015; Vanegas et al., 2014). This sandwich structure yielded the highest electrochemical performance (ESA and sensitivity toward hydrogen peroxide) with enhanced electrocatalytic activity of platinum and graphene used in combination or on their own due to combined effects of nanocomposite soldering to the electrode surface and electrical junctions formed between nanocarbons (Vanegas et al., 2014). To assemble the nanomaterials onto the surface, both Vanegas et al. (2014) and Burrs et al. *(2015)* utilized sonoelectrodeposition to form nanoplatinum layers and spin coating in two cycles to deposit reduced graphene oxide.

4.3. Poly(N-isopropylacrylamide)

Much attention has been paid to stimuli-responsive polymers and the role they can play in the improvement of biosensors by utilizing the transition between collapsed and expanded states (Zhao, Liu, Lu, Zhou, & Li, 2012). Stimuli-sensitive materials are capable of undergoing chemical and conformational changes in response to small external variations in the environment (Gil & Hudson, 2004; Zhao et al., 2012). Numerous stimuli including pH, ionic strength, temperature, and electromagnetic

radiation have been shown to produce changes in stimuli-responsive polymers (Ju, Kim, & Lee, 2001).

Some of the most widely researched of these are temperature responsive polymers (Ju et al., 2001). An important parameter to be aware of when working with thermal responsive polymers is the lower critical solution temperature (LCST) (Ju et al., 2001; Yin, Zhang, Jiang, & Zhu, 2009). The LCST is the temperature at which the polymer changes from shrunken to swollen and vice versa. In the case of poly(N-isopropylacrylamide) (PNIPAAm), the polymer is expanded when exposed to temperatures below the LCST and collapsed when above the LCST, which is typically around 32-35° C (Ju et al., 2001; Yin et al., 2009). The physical properties exhibited above and below the LCST by PNIPAAm are fully reversible in aqueous solution due to the changes in the hydrogen-bonding interfaces of the amide group (Yin et al., 2009).

When the polymer is exposed to temperatures below the LCST hydrogen-bonds form between the hydrophilic (acylamino) groups in the PNIPAAm and the water causing the hydrogel to swell (Burrs et al., 2015; Hill & Gomes, 2014). Exposed to temperatures above the LCST, the polymer collapses due to a breakdown of the hydrogen bonds between the water and the PNIPAAm, which allows for the interactions between hydrophobic (isopropyl) groups to dominate (Burrs et al., 2015; Hill & Gomes, 2014). Figure 4.5. A depicts the structure of PNIPAAm while the physical change observed above and below the LCST is shown schematically in Figure 4.5. B. Through the use of co-polymerization with other molecules, the LCST of PNIPAAm can be adjusted allowing for a wider range of uses (Zhang, 2005).

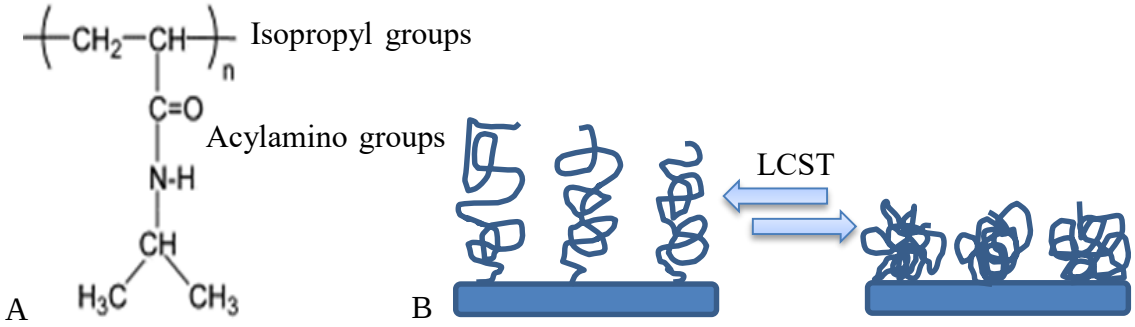

Figure 4.5. A) PNIPAAm structure adapted from Gil & Hudson (2004) and Burrs et al. (2015). B) PNIPAAm below and above LCST, respectively.

PNIPAAm is also a beneficial polymer to explore in the use of biosensors because it can easily be manipulated to have different endings, such as carboxyl or amine, depending on the group needed for any further attachment (Ju et al., 2001; Leal, De Borggraeve, Encinas, Matsuhiro, & Müller, 2013; Lee, Ha, Cho, Lee, & Kim, 2004). To synthesize PNIPAAm with a carboxyl group ending, radical polymerization can be used along with 3-Mercaptopropionic acid (MPA) as the chain-transfer agent and N,N'-Azobisisobutyronitrile (AIBN) as the initiator (Lee et al., 2004; Liu et al., 2008). In order to have an amine termination, free radical polymerization can be carried out using AIBN as the initiator and 2-Aminoethanethiol (AESH) as the chain transfer agent (Leal et al., 2013).

Polymers can be attached to electrode surfaces to form nanobrushes through 'grafting-to' and 'grafting-from' techniques (Nasir, Ali, & Ensinger, 2012). The grafting-to technique involves reactive surface functional groups interacting with end-functionalized polymer molecules (Nasir et al., 2012). When grafting-from, covalently

immobilized initiator groups jump start the polymerization reaction from the substrate surface (Nasir et al., 2012). One grafting-from technique commonly used is the atom transfer radical polymerization (ATRP) process, which has been known to provide better control of the polymerization process, i.e., brush length (Mendes, 2008; Minko, 2006). This technique has been used as the method of grafting polymer brushes onto a gold electrode surface, for example (Lokuge, Wang, & Bohn, 2007).

Electrochemical techniques are commonly used to prepare as well as investigate polymer-modified surfaces and other sensitive interfaces (Zhou et al., 2007). Electropolymerization technique is also known to improve control over polymer length and also to limit aggregation by pulsing electrical potential. This technique has been used extensively in preparation of dispersed nanomaterials (X. Yang, Shi, Liu, Bentley, & Payne, 2009; Zhao et al., 2012). The group of Zhao et al. (2012) used electrochemistry to induce the polymerization of PNIPAAm nanobrushes onto a gold substrate in order to investigate the interaction with and sensitivity to 1,4-dihydro-β-nicotinamide adenine dinucleotide (NADH). The same method of electrochemical-induced polymerization of N-isopropylacrylamide onto a gold substrate to form polymer chains of PNIPAAm was also used by Zhou et al. (2007) to aid in understanding the capabilities of PNIPAAm chains and the switching behavior exhibited under temperature changes.

In addition to the many studies conducted to characterize and better understand the properties, especially swelling and shrinking capabilities, PNIPAAm nanobrushes have been studied as a method for immobilization of materials such as cells, enzymes,

proteins among others for biosensing applications (Burrs et al., 2015). Liu and coworkers (2008) used PNIPAAm combined with an antibody to create a renewable immunosensor. The sensor was tested using bovine serum albumin (BSA) to demonstrate the concept (Liu et al., 2008). Immobilized antibodies were able to maintain their specificity and activity for more than 30 reproducible assays due to the control of PNIPAAm-antibody conjugates achieved through the use of temperature changes (Liu et al., 2008). Another study compared PNIPAAm and several other hydrogels as encapsulants in a biosensor to detect hydrogen peroxide (Burrs et al., 2015). The sensor fabricated using PNIPAAm proved to be the most sensitive and have the highest response time when compared to the same sensor fabricated using silk fibroin or cellulose nanocrystals (CNC). Similar results were observed for chitosan hydrogel (Burrs et al., 2015).

4.4. Lectins

Lectins are non-immune plant or animal proteins, or glycoproteins, involved in various life processes (Nilsson, 2007). While there are many different lectins, the group best characterized come from the plant kingdom as these are typically produced in large amounts (Nilsson, 2007). Lectins are known to bind to carbohydrates of polysaccharide structures that are major structural components of bacteria cell surfaces (Cambi et al. 2005). Specific lectins can bind explicitly to carbohydrates associated with the membrane of different bacteria, especially Gram-negative bacteria such as *E. coli* (Campuzano et al., 2012; Haseley, 2002; Lu et al., 2009; Nilsson, 2007). This interaction between lectins and carbohydrates is both selective and reversible, which is a

beneficial trait when looking at lectins for the use in biosensing (Gamella, Campuzano, Parrado, Reviejo, & Pingarrón, 2009). Lectins used for target bacteria identification through the recognition of surface carbohydrates contain one or more carbohydrate recognition domain (CRD) and the physical structure of these domains determine the specificity of the lectin (Cambi, Koopman, & Figdor, 2005).

In sensing applications, soluble proteins are more desirable than transmembrane proteins due to their superior stability over the lipophilic transmembrane lectins (Cambi et al., 2005). Lectins can then be further divided into groups depending on mode of action and structure including C-type (Ca^{2+}-dependent), MBL (mannose-binding lectins), N-linked (N-acetylglucosamine), and FBL (fucose-binding lectins) (Audfray et al., 2012; Cambi et al., 2005; Eddie Ip, Takahashi, Alan Ezekowitz, & Stuart, 2009; Ghazarian, Idoni, & Oppenheimer, 2011).

Concanavalin A (Con A), a mannose-binding lectin, was first isolated in nearly pure form by Sumner and his team in 1935 (T. K. Chowdhury & Weiss, 1975). They crystallized the lectin from *Canabalia ensiformis*, more commonly referred to as the jack bean (T. K. Chowdhury & Weiss, 1975). Con A is conventionally isolated and purified from jack bean through a multistep process that includes protein precipitation, dialysis, size exclusion, and affinity (Ahirwar & Nahar, 2015).

The use of ConA is relatively new and would be beneficial due to its specificity to *E. coli*, yet broad enough to detect any strain of *E. coli* bacteria that may be present in the sample. The lectin Con A binds multivalently to carbohydrate components

specifically found in the membrane of *E. coli* (Lu et al., 2009). The particular carbohydrate binding site known for *E. coli* is G_{M1} ganglioside (Haseley, 2002).

Several sensors have been explored using Con A. One in particular uses wireless, remote-query to detect *E. coli* in distilled and deionized water showing that Con A can indeed be used as a detection method with a limit of detection of 60 cells mL^{-1} and a response range of 6.0×10^1 to 6.1×10^9 cells mL^{-1} (Lu et al., 2009). Also detecting *E. coli*, the group of Gamella et al. (2009) utilized absorption of Con A onto screen-printed gold electrodes as the platform for detection. The screen-printed gold electrodes utilizing Con A showed a linear response to *E. coli*, diluted in deionized water, between 5×10^3 and 5×10^7 CFU mL^{-1} and a limit of detection of 5×10^3 CFU mL^{-1} (Gamella et al., 2009). Another group explored the use of Con A recognition of sulfate-reducing bacteria for the detection and monitoring of microbial populations (Wan, Zhang, & Hou, 2009). The study revealed that the sensor was capable of detecting sulfate-reducing bacteria over a range of 1.8 to 1.8×10^7 CFU mL^{-1} when tested in PBS (Wan et al., 2009). Another study showed a detection limit of 7.5×10^2 cells mL^{-1} and a linear range between 7.5×10^2 and 7.5×10^7 cells mL^{-1} for *E. coli* when using Con A with a quartz crystal microbalance (QCM) in a PBS test solution (Shen et al., 2007). Cyclic voltammetry (CV) and electrochemical impedance spectroscopy (EIS) were both used to show the attachment of the Con A to the carbohydrate showing that Con A can be used with CV and EIS to detect *E. coli* in foods (Gamella et al., 2009; Lu et al., 2009; Wan et al., 2009).

4.5. Antibodies

Antibodies are normally occurring protein molecules produced by B lymphocyte cells (B cells) in the body (*Funk & Wagnalls new world encyclopedia*, 2015; Lipman, Jackson, Trudel, & Weis-Garcia, 2005). The primary function of antibodies is to act as a defense against foreign substances invading the body and can be found in the blood of all vertebrates and play an important role in the immune system (Cunningham, 1998; *Funk & Wagnalls new world encyclopedia*, 2015). Typically, antibodies have a well-defined Y-shape structure and float freely in the blood (*Funk & Wagnalls new world encyclopedia*, 2015; Trilling, Beekwilder, & Zuilhof, 2013). Antibodies are a small subset of glycoproteins and possess only one binding site (Trilling et al., 2013). Substances recognized by antibodies, such as proteins in bacteria, are called antigens (Cunningham, 1998; *Funk & Wagnalls new world encyclopedia*, 2015).

One type of antibody commonly used in biosensing applications is immunoglobulin G (IgG), seen in Figure 4.6. (Trilling et al., 2013). IgG type antibodies are made up of four chains, two heavy and two light, which are linked by disulfide bonds and form the Y-shape (Cunningham, 1998; Trilling et al., 2013). Each chain consists of constant and variable regions and it is the variable region that is responsible for antibody-antigen specific interactions (Trilling et al., 2013). Through engineering, conventional antibodies have been miniaturized into more stable and smaller portions called fragments (Lipman et al., 2005; Trilling et al., 2013).

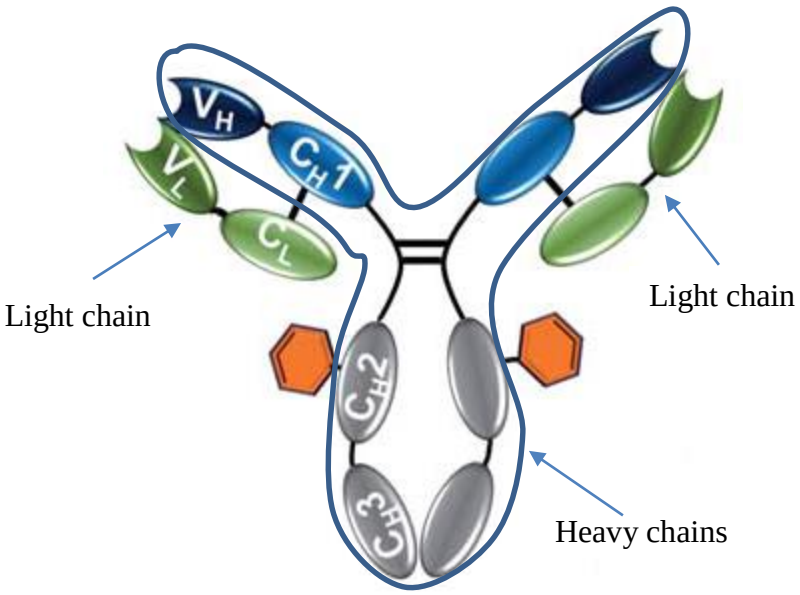

Figure 4.6. Schematic of IgG antibody structure with antigen binding areas are denoted by V_L and V_H. Image adapted from Trilling et al. (2013).

For biosensing purposes, IgG antibodies are normally immobilized on electrode surfaces through covalent linking (Skládal et al., 2013). Covalent immobilization is thought to be one of the best methods for longevity of the surface combined with high sensitivity because this type of immobilization results in a more specific orientation than others (Varshney & Li, 2007).

Some advantages of using antibodies for biosensing include their high specificity and high affinity constants (Cunningham, 1998; Skládal et al., 2013). Specificity can be adjusted through the type of antibody used (polyclonal vs. monoclonal) (Lipman et al., 2005). Monoclonal antibodies are produced by a single B lymphocyte clone, while polyclonal antibodies come from many and this affects the specificity with monoclonal

being more specific responding to only one type of antigen (Lipman et al., 2005). This difference in antibody type can be advantageous when designing sensors.

There are also several disadvantages to using antibodies such as the need for live animals for production and different affinities depending on whether the antibodies are monoclonal or polyclonal (Cunningham, 1998). Antibody performance can be variable from batch to batch meaning reoptimization must be performed somewhat regularly and the kinetic parameters of antibodies interacting with antigens cannot be changed (Jayasena, 1999). Sensitivity to temperature and irreversible denaturation along with their very limited shelf life are major challenges faced working with antibodies, especially for biosensing applications (Jayasena, 1999). Another problem encountered performing antibody immobilization is low capture efficiency (Varshney & Li, 2007). This results in less than optimal use of the functional surface area of the sensor for detection (Varshney & Li, 2007). To achieve the desired robustness for the sensors, many are fabricated by attaching the antibodies onto electrode surfaces that have been activated using self-assembled monolayers (SAM) as attaching to bare electrode surfaces directly can lead to slow release of the proteins (Skládal et al., 2013).

Some of the work incorporating antibodies into biosensors includes studies with electrochemical impedance, amperometric, and piezoelectric immunosensors. Immunosensors are a subset of the larger biosensor category. Biosensors are made up of a biological receptor element to bind specific analytes and a transducing element, which detects the receptor/analyte binding (North, 1985). Essentially, immunosensors are

biosensors with the receptor and analyte being specifically defined as antibodies and their selective antigens (North, 1985).

The group of Geng et al. (2008) studied the use of antibodies in an electrochemical impedance immunosensor through immobilization of the *E. coli* antibodies onto Au electrodes by self-assembled monolayers (SAM). It was determined that the *E. coli* cells binding to the antibodies increased electro-transfer resistance and this could be detected by EIS and a relationship was determined from the responses detected (Geng et al., 2008). Using antibodies in conjunction with EIS, *E. coli* could be detected as low as 50 CFU mL^{-1} in river water samples, but this was with pre-concentration and pre-enrichment steps (Geng et al., 2008). The study by Li et al. (2012) showed the use of *E. coli* antibodies combined with chitosan-multiwalled carbon nanotubes on Au electrodes to create an amperometric sensor capable of detecting *E. coli* at 4.12 x 10^2 CFU mL^{-1} under optimal conditions. Along with these works on electrochemical impedance and amperometric sensors, the group of Su and Li (2004) developed a piezoelectric immunosensor to detect *E. coli* O157:H7 in the range of 10^3-10^8 CFU mL^{-1} using antibodies immobilized onto a SAM on an Au electrode surface using NHS covalent binding reaction for antibody immobilization.

4.6. *Escherichia coli*

Enterohaemorrhagic *Escherichia coli* spp. (EHEC *E. coli*) are some of the most common pathogens to contribute to foodborne illness and, according to the World Health Organization (WHO), was first recognized as a public health problem in 1982 after an outbreak in the United States (CDC, 2013c, 2014d; WHO, 2011). The Centers for

Disease Control and Prevention (CDC) estimates 9.4 million foodborne illnesses occurring annually in the United States are caused by known pathogens (CDC, 2013c).

First isolated in 1885, *E. coli* is likely one of the best understood free-living organisms today (Adams & Moss, 2008). The majority of *E. coli* are harmless and contribute positively as a part of the total microflora in the intestinal tract and gut of healthy humans and other warm-blooded animals (Adams & Moss, 2008; CDC, 2014b; WHO, 2011). Pathogenic *E. coli* are divided into six groups or pathotypes: enterotoxigenic *E. coli* (ETEC), enteropathogenic *E. coli* (EPEC), enteroinvasive *E. coli* (EIEC), enteroaggregative *E. coli* (EAEC), diffusely adherent *E. coli* (DAEC), and enterohemorrhagic *E. coli* (EHEC) (CDC, 2014b; FDA, 2012). The most prevalent of these being EHEC, which accounts for about 63,000 cases of foodborne illness in the United States, is sometimes referred to as Shiga toxin-producing *E. coli* (STEC) or Verotoxin-producing *E. coli* (VTEC) (Adams & Moss, 2008; CDC, 2014b; FDA, 2012). Included in the EHEC group is *E. coli* O157:H7, which is the most common type reported and associated with foodborne illness (Adams & Moss, 2008).

EHEC is closely monitored due to its transmission through food and water, but also because of the wide range of conditions associated with EHEC (Adams & Moss, 2008; FDA, 2012; WHO, 2011). The infectious dose of *E. coli* O157:H7, in particular, is thought to be very low, in the range of 10-100 cells (FDA, 2012; Feng et al., 2011). Other EHEC serotypes are estimated to have a slightly higher infectious dose (FDA, 2012). Onset of EHEC infections is typically 3-4 days, but can occur anywhere from 1-9 days after ingestion of the organism (CDC, 2014b; FDA, 2012). Symptoms often

include diarrhea and abdominal cramps, which in uncomplicated cases in otherwise healthy adults, resolve within 2-9 days (CDC, 2014b; FDA, 2012; WHO, 2011).

The illnesses can range from relatively mild diarrhea and cramps to hemorrhagic colitis and even life threatening conditions thrombotic thrombocytopaenic purpura (TTP) and haemolytic uremic syndrome (HUS) (Adams & Moss, 2008; WHO, 2011). TTP is not a common complication and is usually only found in adults. Symptoms of TTP include fever, some kidney damage, and neurological symptoms from blood clots in the brain (Adams & Moss, 2008). HUS is characterized by acute renal failure, reduction of red blood cells (haemolytic anemia), and reduction of blood platelets (thrombocytopaenia) (Adams & Moss, 2008). HUS is most common in children under 10 and has a mortality rate of 3-5% (Adams & Moss, 2008; FDA, 2012).

The *E. coli* organism is a Gram-negative, short, fermentative, oxidase-negative, catalase-positive, non-sporing rod (Adams & Moss, 2008). It is a mesophile with an optimum growth temperature of 37°C within the range of 7-50°C (Adams & Moss, 2008; WHO, 2011). EHEC grows best at a near-neutral pH, but can also grow in acidic foods down to a pH of 4.4 with a minimum water activity (Aw) of 0.95 (Adams & Moss, 2008; WHO, 2011).

Food and water supplies can become infected with *E. coli* due to contamination from fecal matter introduced by food handlers, cross contamination, improper washing of raw vegetables, and undercooked ground beef (Adams & Moss, 2008; WHO, 2011). Contamination can be prevented through basic good manufacturing practices in the industry and food hygiene at home (WHO, 2011). Regular hand washing, washing of

foods (especially those to be consumed raw), and reaching the proper internal cooking temperature of 70°C can protect against infection (CDC, 2014b; WHO, 2011).

The government's recent action signing the FDA Food Safety Modernization Act (FSMA) into law in January of 2015 is another major indication of the need for more preventative actions within food safety such as real-time pathogen detection (FDA, 2015). The goal of the FSMA is to shift the focus of food safety from reactive to proactive measures to improve the safety and quality of our food supply (FDA, 2015). By concentrating on implementing better manufacturing practices, detection, and other science-based preventive controls, future outbreaks can be prevented rather than contained. These new regulations are in addition to and to compliment the practices already in place through Hazard Analysis Critical Control Point (HACCP) plans.

According to the CDC, *E. coli* (STEC) O157 ranked fifth amongst the pathogens monitored in 2011 that contribute to domestically acquired foodborne illnesses resulting in hospitalization (CDC, 2014a). The Foodborne Diseases Active Surveillance Network (FoodNet) closely monitors 10 geographical areas in the U.S. and in 2014, *E. coli* (STEC O157 and STEC non-O157) ranked fifth in total number of cases of bacterial and parasitic infections reported (CDC, 2015).

Some of the most notable outbreaks of *E. coli* in recent years affected raw, leafy produce and ground beef (CDC, 2014d). In 2014, outbreaks of *E. coli* O157:H7 and O121 were reported in ground beef and raw clover sprouts, respectively. The O157:H7 outbreak resulted in 12 reported cases across 4 states and a product recall was issued for 1.8 million pounds of ground beef products that were possibly contaminated (CDC,

2014c). Ready-to-eat salad contaminated with *E. coli* O157:H7 was recalled in 2013 after 33 cases were reported across 4 states with 7 individuals being hospitalized and two infected persons developing HUS (CDC, 2013b). One of the worst outbreaks in the last several years affected a total of 58 people by contaminated Romaine lettuce and reports of cases spread across 9 different states (CDC, 2012). People infected during this outbreak ranged in age from 1 to 94, 33 were hospitalized, and 3 went on to develop HUS though no deaths were reported (CDC, 2012).

4.7. Current Detection Methods

The most popular conventional methods used for bacteria detection include culture and colony counting, polymerase chain reaction (PCR), and enzyme-linked immunosorbent assay (ELISA) (Lazcka et al., 2007; Yixian et al., 2012; Zelada-Guillén, Bhosale, Riu, & Rius, 2010). While these methods are still trusted in the industry today due to their proven reliability, detection time, training required, cost, and complicity are all disadvantages (Lazcka et al., 2007; Yixian et al., 2012).

4.7.1. Plate Count

Culture and colony counting, often referred to as plate counts, is still the standard method for detecting bacteria (Lazcka et al., 2007). Plate counting is reliable, provides high selectivity, and, with enrichment, can detect just a single bacteria colony in a 1 mL sample, yet can take days to reach a negative result and, in some cases, upwards of 15 days to confirm a positive result (Adams & Moss, 2008; Lazcka et al., 2007; Xu, 2012). Given a controlled, normal laboratory setting, plate counting is one of the most accurate ways to identify the presence of viable cells (Adams & Moss, 2008). Cost also becomes

a factor as replications required for proper detection require many Petri dishes, a lot of growth media, and many man hours of trained personnel to complete the detection process (Adams & Moss, 2008). Plate counting is achieved by preparing Petri dishes with media, pipetting a thoroughly mixed sample onto the plate, and spreading the sample evenly onto the plate (Adams & Moss, 2008). In order to ensure the plate counts are within the desired range, between 30 and 300 colonies, the sample must be diluted (Adams & Moss, 2008). Typically a ten-fold dilution series is used, however; unknown samples require plating of more dilutions to make sure the plates are within the range to be counted properly (Adams & Moss, 2008).

4.7.2. Polymerase Chain Reaction

Polymerase chain reaction (PCR) is considered to be a rapid detection method when compared to culture and colony counting (Lazcka et al., 2007; Shen et al., 2014; Yixian et al., 2012). The detection time itself is in the range of a few hours, though this does not include any enrichment steps necessary prior to the detection (Lazcka et al., 2007; Yixian et al., 2012). PCR has another advantage in that it is sensitive enough to theoretically detect a single copy of the target DNA/RNA sequence and selective enough to recognize the serotype group based on the sequence present in the sample (Adams & Moss, 2008; Lazcka et al., 2007). In addition to requiring pretreatment steps, PCR is a technical process and therefore requires highly trained and qualified technicians and complex equipment and set-up to carry out the preparation as well as the testing (Shen et al., 2014). Due to the small DNA fragment needed for detection, PCR results may be

based on DNA from non-viable cells (Adams & Moss, 2008). Therefore, PCR cannot distinguish between viable and non-viable cells.

Developed in the 1980's, PCR works through amplification of specific portions of DNA (Adams & Moss, 2008; Lazcka et al., 2007). Theoretically, only a short chain is required in order to detect just a single copy of the intended sequence, which includes the bacteria's genetic material (Adams & Moss, 2008; Lazcka et al., 2007). A schematic of the PCR method can be seen in Figure 4.7. The basic process is that DNA is denatured through the use of heat from 94-98 °C, which allows oligonucleotide primer sequences to hybridize onto each strand in the cooled mixture between 37 °C and 65 °C (Adams & Moss, 2008). Following catalysis by DNA polymerase, the primers extend and produce double-stranded copies of the two target regions (Adams & Moss, 2008). Once the first copies have been made, the process is repeated any number of times, though it is important for the DNA polymerase to be heat stable in order to endure the heat steps (Adams & Moss, 2008).

There are several different PCR methods extended from the basic technique that are used for the purpose of detecting bacteria including real-time, multiplex, nested, and reverse transcriptase (Adams & Moss, 2008; Lazcka et al., 2007; Miller & Andre, 2014).

Real-time PCR reduces the detection time by eliminating the need for amplification steps following the initial process (Lazcka et al., 2007). This reduction of time is achieved through the use of fluorescent signal (Adams & Moss, 2008; Lazcka et al., 2007; Miller & Andre, 2014). As the DNA is synthesized, the fluorescent signal intensifies (Adams & Moss, 2008; Miller & Andre, 2014). The signal not only

intensifies with increasing PCR cycles, but the fluorescence is also directly proportional to the amount of bacteria initially present, which means real-time PCR is both a quantitative and qualitative test (Adams & Moss, 2008; Miller & Andre, 2014). Multiplex PCR incorporates multiple sets of primers in one PCR mixture and simultaneously produces amplification of several targets of varying sizes (Adams & Moss, 2008; Tarabees, Hassanin, El Rahman, & El Bagoury, 2015).

Nested PCR uses two separate sets of primers, outer and inner, to improve the sensitivity (Adams & Moss, 2008). The outer primers amplify a larger portion of DNA beyond the target section, and then inner primers amplify the shorter portion of the sequence included in the already amplified portion (Adams & Moss, 2008). Reverse transcriptase PCR uses DNA that has been transcribed from RNA (Adams & Moss, 2008). This method is useful for detecting RNA viruses and has a higher sensitivity than conventional PCR due to multiple RNA copies present within a cell (Adams & Moss, 2008).

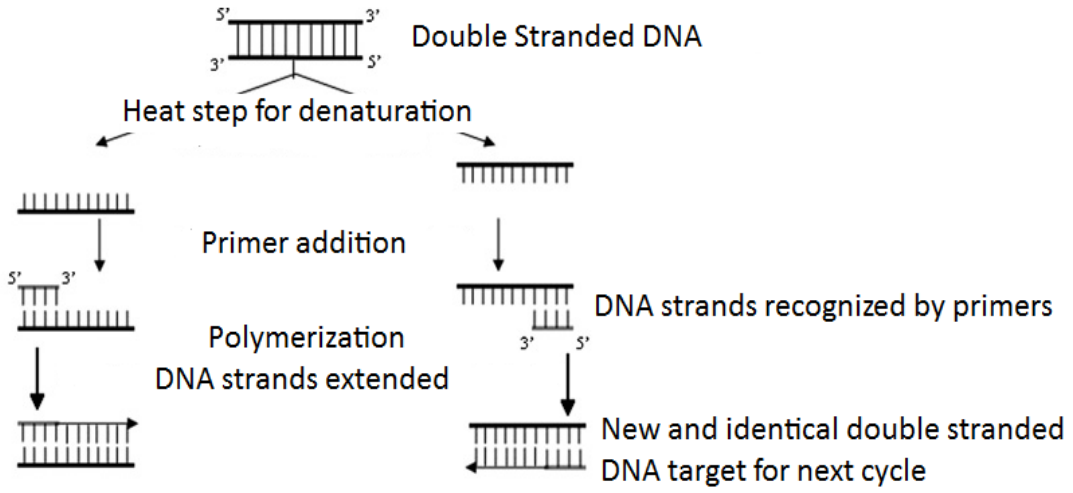

Figure 4.7. Schematic of one PCR cycle modified from Lazcka et al. (2007).

4.7.3. Enzyme-Linked Immunosorbent Assay

Polyclonal and monoclonal antibodies have shown promising specificity when used in immunoassays (Adams & Moss, 2008). Enzyme-linked immunosorbent assay (ELISA) is one of the most established immunological methods used to detect microorganisms including *E. coli*, *Salmonella*, and *Listeria monocytogenes* (Adams & Moss, 2008; Lazcka et al., 2007; Shen et al., 2014; N. Wang, He, & Shi, 2007). ELISA is recognized as a reputable technique due to its relatively high reproducibility and specificity in its detection of various antigens from bacteria to viruses and proteins (Bomans et al., 2013; Lazcka et al., 2007; Shen et al., 2014). However, ELISA is not reliable in distinguishing between viable and non-viable bacteria cells (N. Wang et al., 2007).

At their simplest, ELISAs detect antigens through binding by antibodies (Adams & Moss, 2008; N. Wang et al., 2007). There are several different configurations of ELISA, the most common being the sandwich ELISA (Adams & Moss, 2008; Lazcka et al., 2007). Figure 4.8. shows the direct sandwich structure in which a capture antibody is attached to a plate and a sample containing the antigen to be analyzed is introduced followed by the introduction of an enzyme labeled antibody. After washing to remove any unattached enzymes and antibodies, the substrate changes color in the presence of the enzyme. The intensity of the color change is directly proportional to the concentration of antigen present in the sample (Adams & Moss, 2008). Alternative methods to color change are also used for detection such as agglutination in the presence of the antigen when antibodies are attached to latex and fluorescence-labeled antibodies that can be seen using a fluorescence microscope (Adams & Moss, 2008).

While ELISAs are available and used commercially, they are not a perfect solution for microorganism detection (Adams & Moss, 2008; Shen et al., 2014). One of the main concerns surrounding the use of ELISA is the number of organisms required to be present in the sample in order for reliable detection (Adams & Moss, 2008). The number of target organisms essential for detection, depending on the target organism, typically ranges from 10^5-10^7 organisms (Adams & Moss, 2008; Shen et al., 2014). This is an inadequate detection limit as, in the case of *E. coli* O157:H7, the infectious dose is a mere 100 cells (Shen et al., 2014). To combat this challenge, the sample in question must be amplified or concentrated before analysis (Adams & Moss, 2008). The additional step to concentrate the organism adds significant time onto the total time

necessary for detection essentially resulting in ELISA taking as long or longer than other conventional methods used (Adams & Moss, 2008). Along with the undesirable detection limit, ELISA also has some variability among target organisms due to the inconsistency of the strength of the antibody to antigen interaction (Daniels & Pourmand, 2007).

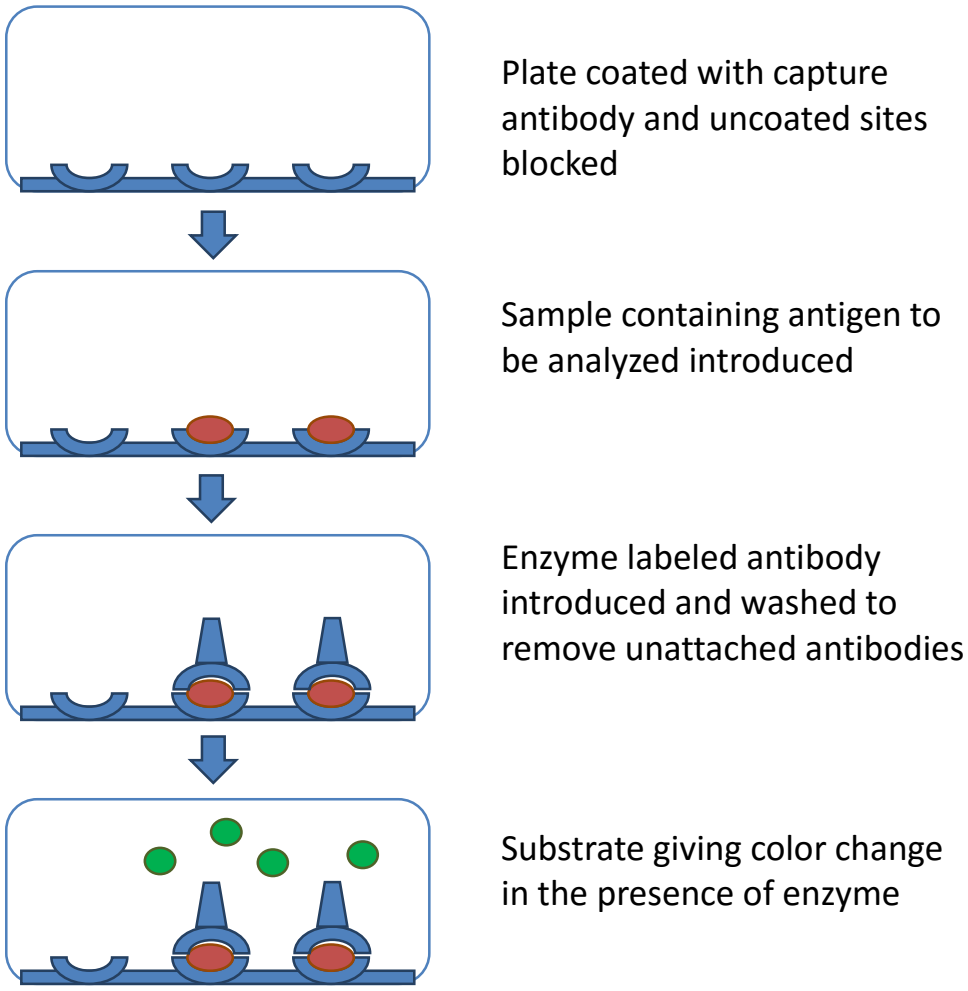

Figure 4.8. Schematic of direct sandwich ELISA modified from Adams and Moss (2008).

5. MATERIALS AND METHODS

5.1. Materials

5.1.1. Reagents

Lead acetate (30% w/v), chloroplatinic acid (8% w/w), 2-aminoethanethiol hydrochloride (AESH), ascorbic acid, potassium phosphate monobasic, Concanavalin A (ConA) from *Canavalia ensiformis* (Jack bean), sodium chloride, sodium phosphate dibasic, 11-mercaptoundecanoic acid (11-MUA), Anti-GroEL antibody produced in rabbit, and potassium chloride were purchased from Sigma-Aldrich (St. Louis, MO). Calcium chloride, 1-ethyl-3-(3-dimethylaminopropyl)carbodiimide HCl (EDC), sodium persulfate ($Na_2S_2O_8$), sodium nitrate ($NaNO_3$), and manganese chloride were obtained from Thermo Fisher Scientific (Waltham, MA). Potassium ferrocyanide trihydrate was purchased from Ward's Science (Rochester, NY). N-Hydroxysuccinimide (NHS), potassium nitrate, 2-(morpholino)ethanesulfonic acid) (MES) buffer, glutaraldehyde, and platinum wire (99.95% Pt, 1.2 mm dia.) were obtained from Alfa Aesar (Ward Hill, MA). Single-layered graphene oxide (GO) was purchased from ACS Material (Medford, MA). N-Isopropylacrylamide (NIPAAm) was obtained from Tokyo Chemical Industry Co. (Portland, OR).

5.1.2. Bacteria

Escherichia coli (ATCC 35218) was used for sensitivity and selectivity testing in phosphate buffer saline (PBS, pH 7.4). *Salmonella* Enteritidis (ATCC 1045) was used for selectivity testing in PBS. *Escherichia coli* O157:H7 (ATCC 43895) was used for

real-world testing in vegetable broth. All bacteria were grown using BD Bacto™ Tryptic Soy Broth (TSB) (Franklin Lakes, NJ) and verified through plate count on 3M™ Petrifilm™ Aerobic Count Plates (Saint Paul, MN).

5.1.3. Equipment

Cyclic voltammetry and electrochemical impedance spectroscopy were performed on a CH Instruments Electrochemical analyzer/Workstation (Model 600 E Series) and supporting software (CH Instruments Software version 12.04) (Austin, TX). Pt wire auxiliary electrode, Ag/AgCl reference electrode, and PTFE platinum/iridium (Pt/Ir) working electrodes (2 mm internal diameter) for voltammetry from BASi (West Lafayette, IN). A Revlon 1875 Watt Ionic Styler dryer (New York, NY) was used to apply heat for drying electrodes. BK Precision single output programmable DC power supply (Yorba Linda, CA) was used for deposition of platinum and a variable speed spin coater was used for deposition of reduced graphene oxide. A benchtop router table with 1-3/4 HP router was used in conjunction with a router speed control dial, both from Harbor Freight (Calabasas, CA) for the spin coating of reduced graphene oxide. Hielscher UP400S Ultrasonic Processor (Ringwood, NJ) was used for the ultrasonication of graphene oxide.

5.2. Electrode Coating/Functionalization

5.2.1. Platinum-Graphene-Platinum Coating

Before applying any type of coating to the Pt/Ir electrodes, they were polished according to manufacturer instructions and rinsed with distilled water. Platinum/Iridium

(Pt/Ir) electrodes were prepared through the application of a platinum-graphene-platinum (PGP) layer following a procedure adapted from Vanegas et al. (2014).

The first layer of platinum was applied as follows: bare platinum wire and the working electrode were connected to the power supply and submerged in a solution of chloroplatinic acid, lead acetate, and RO water. The power supply was set to 10 V and 90 s for the deposition of platinum to occur.

Reduced graphene oxide (rGO) was prepared according to Vanegas et al. (2014) through ultrasonification of graphene oxide for 30 min at 40% amplitude and the cycle set to 0.9. Subsequently, the ultrasonicated graphene oxide was vortex mixed for 5 min with L-ascorbic acid at a concentration of 2 mg/ 250 μL.

Platinum coated electrodes were allowed to dry before drop coating rGO onto the surface. Following the reduction reaction, 2 μL rGO was drop coated onto the surface of the platinum treated electrode and dried at room temperature for 1 min followed by 30 sec of heat on medium setting at a distance of approximately 25 cm. The semi-dry electrode was then spun in the spin coater for 30 s at 1700 rpm and then increased to 3500 rpm for 1 min.

Working electrodes were then coated with a second layer of platinum in the manner aforementioned for 30 s. Completed PGP coated electrodes were stored at room temperature prior to further coating attachment or testing.

5.2.2. PNIPAAm Nanobrush Attachment

The following procedure used to modify PGP Pt/Ir electrodes with PNIPAAm-NH_2 was adapted from Zhau et al. (2012). It was dissolved in 20 mL RO water; 1 M

NIPAAm, 0.2 M $NaNO_3$, 0.01 M $Na_2S_2O_8$, and 4.85 mM AESH. The AESH was added to serve as a chain transfer agent in order to have the amine end group needed for attachment of ConA (Ju et al., 2001; Leal et al., 2013).

The PGP coated electrode was then connected to the CHI workstation and submerged in the NIPAAm solution. Polymerization of PNIPAAm-NH_2 onto the electrode was achieved using CV with the following settings: potential range from -0.35 V to -1.35 V and a scan rate of 100 mV/s for 60 cycles (Zhao et al., 2012). Completed electrodes were stored in 10 mM PBS, pH 7.4 in the refrigerator until biosensor testing or characterization of biorecognition agent was carried out. Figure 5.1. shows a schematic of the electrode set up used for PNIPAAm nanobrush attachment as well as all CV and EIS testing.

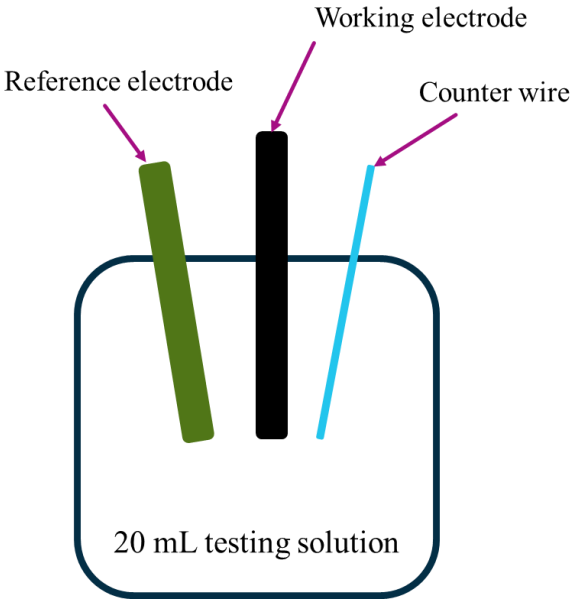

Figure 5.1. Schematic of electrode set up for use with the potentiostat.

5.2.3. ConA Deposition on PGP Functionalized Electrode Using Self-Assembly Monolayer

Deposition of ConA onto the PGP functionalized electrode was conducted using a procedure adjusted from Thermo Scientific instructions for EDC/NHS crosslinking of carboxylates with primary amines and the procedure by Jantra et al. (2011; Scientific).

In ethanol, 150 mM of 11-MUA was dissolved. PGP coated electrodes were immersed in the 11-MUA solution for 30 min in order for a self-assembled monolayer (SAM) to form on the surface (Jantra et al., 2011; Safina, van Lier, & Danielsson, 2008). EDC and NHS were added directly to an activation buffer consisting of 0.1 M MES (pH 6.5) and 0.5 M NaCl. Electrodes treated with SAM were rinsed with RO water, immersed in the EDC/NHS solution, and agitated for 50 min at room temperature to allow for the activation of SAM (Jantra et al., 2011). The solution activated free carboxyl groups on the electrodes preparing them for the ConA immobilization process (Devi, Yadav, & Pundir, 2011; Jantra et al., 2011).

After the reaction between EDC/NHS and the 11-MUA SAM treated electrodes occurred, electrodes were immersed in solutions of various concentrations (50 nM, 100 nM, and 200 nM) of ConA in 10 mM PBS, pH 7.4 with 1 mM Ca^{2+} and 1mM Mn^{2+} and allowed to react for 2 hrs with agitation (Hu, Zuo, & Ye, 2013; Scientific). Ca^{2+} and Mn^{2+} ions were added to the PBS solution to promote carbohydrate binding and achieve optimum ConA activity (Gamella et al., 2009; Lu et al., 2009; Safina et al., 2008). The ConA was immobilized on the surface of the electrode by means of EDC/NHS coupling chemistry (Campuzano et al., 2012; Scientific).

5.2.4. PNIPAAm-ConA Attachment

Following PNIPAAm-NH_2 attachment, electrodes were exposed to an aqueous solution containing glutaraldehyde in a 2:1 molar ratio to AESH and allowed to react with agitation for 2 hrs at room temperature (Hill & Gomes, 2014). Electrodes were then exposed to several concentrations of ConA (50 nM, 100 nM, 200 nM) with agitation for 2 hrs at room temperature.

5.2.5. PNIPAAm-Antibody Attachment

Electrodes were treated with PNIPAAm-NH_2 nanobrushes to prepare for antibody attachment. Anti-GroEL antibodies were immobilized on the PNIPAAm-NH_2 treated electrodes following the same procedure used for ConA attachment using glutaraldehyde as crosslinker to form amine-amine bonds (Hill & Gomes, 2014; Kim, 2000; Prodromidis, 2010; Shi et al., 2011; X. Su et al., 2013). Electrodes were reacted with antibodies at 50 nM, 100 nM, and 200 nM concentrations.

5.3. Electrochemical Characterization

5.3.1. Electroactive Surface Area

The electroactive surface area (ESA) was used to characterize the different surface configurations of the electrodes and ultimately determine the optimal concentration of ConA and antibody to use for bacteria detection. An increase in ESA indicates enhanced signal transduction (Shi et al., 2011). As a strong signal is desirable for any sort of detection, ConA and antibody concentrations shown to have the highest ESA's were chosen as the optimum concentration. ESA's from bare, PGP-modified, ConA-modified, and ConA-PNIPAAm nanobrush modified electrodes were all

compared in order to determine the optimal ConA concentration on the biosensor. Likewise, bare, PGP-modified, antibody-modified, and antibody-PNIPAAm nanobrush modified ESA's were compared to determine the optimal antibody concentration on the biosensor. The cyclic voltammetry (CV) tests required to calculate the ESA were performed using a CHI Electrochemical Analyzer/Workstation.

Electrodes were immersed in a solution of 4 mM $Fe(CN)_6$/1 M KNO_3 in order to help eliminate noise and gather a clear reading of the response (Devi et al., 2011; McLamore et al., 2011; Shi et al., 2011; X. Su et al., 2013; Vanegas et al., 2014). Using comparable, previous studies as a reference point, CV was carried out using scan rates 50, 100, 150, and 200 mVs^{-1} with a varied potential between -0.65 V and 0.65 V (Hu et al., 2013; Shi et al., 2011; Vanegas et al., 2014). The corresponding current peak (i_p) at each scan rate was used to find the ESA. For each electrode, the ESA was calculated using the Randles-Sevcik equation (Shi et al., 2011; Vanegas et al., 2014). The Randles-Sevcik equation can be rearranged to solve for A:

$$A = \frac{k}{\left(2.69x10^5\right)n^{3/2}D^{1/2}C} \tag{5.1}$$

where A is the electroactive surface area (cm^2), k is the slope of the Cottrell plot of i_p (A) vs. $v^{1/2}$ ($(Vs^{-1})^{0.5}$), *n* is the number of transferred electrons in the redox reaction, D is the diffusion coefficient (cm^2s^{-1}), and C is the molar concentration of the working solution (Vanegas et al., 2014). The values for *n*, D, and C are one, 6.70 x 10^{-6} cm^2s^{-1}, and 4 mM, respectively (Shi et al., 2011). As these values were known based on the properties

of the working solution; A was calculated directly based on k, the slope of the Cottrell plot of i_p vs. $v^{1/2}$ (Vanegas et al., 2014).

5.3.2. PNIPAAm Nanobrush Actuation

Stimuli conditions for PNIPAAm were tested to determine the best capture and test scenarios for the sensor. The PNIPAAm-modified electrode was tested using cyclic voltammetry (CV) above and below the LCST (40 °C and 25 °C, respectively). The temperature resulting in the lowest ESA was the temperature used for capture of the bacteria and the temperature demonstrating the highest ESA was used for EIS and CV analysis. These results were indicative of the shrinking and swelling behavior of the PNIPAAm in response to the change in stimuli (Ju et al., 2001; Yin et al., 2009; Zhao et al., 2012).

5.4. Bacteria Growth and Traditional Testing

Bacteria used for electrochemical detection testing was kept viable by completing weekly 0.1 mL transfers into 9.9 mL of Bacto™ Tryptic Soy Broth (TSB). Transfers were incubated at 35 °C for 24 hours and then stored at 4 °C.

Total aerobic plate counts were performed using 3M™ Petrifilm™ Aerobic Count Plates. Dilutions of eight and nine fold were made in nine milliliters of buffered peptone water (BPW). Plates were inoculated with 1 mL of eight and nine fold dilutions and then incubated at 35 °C for 24 hours. After incubation, colonies were counted and reported as CFU mL^{-1} to be used for comparison to biosensor results.

5.5. Electrochemical Detection

Electrochemical impedance spectroscopy (EIS) was used to measure any electrochemical response produced by the biosensor when exposed to bacteria at concentrations varying from 0-10^9 CFU mL^{-1}. EIS tests were run at a frequency range of 1-100,000 Hz with amplitude of 0.1 V and initial potential 0.25 V (Burrs et al., 2015; Joung et al., 2013).

Sensitivity to the target bacterium was determined by the slope of the linear portion of the calibration curve consisting of the change in impedance (Ohm) vs. the concentration of cells (CFU mL^{-1}) (Shi et al., 2011; Vanegas et al., 2014). Sensitivity testing was initially performed in PBS (pH 7.4) and then again with the optimized ConA and antibody sensors in commercially sterile vegetable broth.

Selectivity of the sensor to *E. coli* in the presence of *Salmonella* Enteritidis was calculated with the same approach as sensitivity, but using the resulting calibration curve with both bacteria present (Shi et al., 2011). Tests for selectivity were performed on the optimized ConA biosensor configuration in PBS.

The range of detection was determined as the linear portion of the calibration curve to have a favorable R^2 value (>0.98) (McLamore et al., 2011). The lower limit of detection (LOD) was calculated for each type of sensor under both testing conditions. The 3σ method was used to calculate the LOD (Hu et al., 2013; McNaught & Wilkinson, 1997; Vanegas et al., 2014).

5.6. Microscopic Imaging Analysis

The morphology of the electrode coatings was observed through field emission scanning electron microscopy (SEM) images using an FEI Quanta 600F (Hillsboro, OR) at the Texas A&M University Microscopy Imaging Center (College Station, TX). Prior to imaging, a Cressington sputter coater 208 HR (Waterford, United Kingdom) was used to coat electrodes with a 10 nm layer of platinum to improve the conductivity of the electrodes' surface. Samples were placed on the base plate inside the sputter coater chamber and then the top plate was closed. The coater, equipped with a thickness controller, was turned on and argon gas supply opened to zero out the thickness monitor. Once ready, the instrument was turned on and the coating process was carried out until the desired thickness was reached and the coater stopped automatically. Prior to imaging, electrodes were retrieved from the sputter coater and allowed to ventilate. Images were taken at 5,000 and 10,000 times magnification with an operating voltage of 5 kV.

5.7. Statistical Analysis

All electrochemical tests were performed at least in triplicate with a randomized experimental design. Statistical analysis was performed using SPSS PASW Statistics, version 23. In order to determine if there was statistical significance among results from the different sensors, analysis of variance (ANOVA) was used with Tukey's test to separate means. Statistical significance was expressed at the 95% confidence interval ($P < 0.05$).

6. RESULTS AND DISCUSSION

6.1. Electroactive Surface Area

6.1.1. Electrode Coatings

Cyclic voltammetry (CV) performed on bare, PGP-modified, and PGP-PNIPAAm-modified electrodes demonstrated reversible redox couples with well-defined redox peaks. Figures 6.1. A and B show representative CV curves for PGP and PGP-PNIPAAm- modified electrodes at the various scan rates tested. The defined oxidation peaks on the curves indicate that the reaction is diffusion controlled at the interface of the electrode-solution (Vanegas et al., 2014).

Using the value of the oxidation peak at each scan rate and the square root of the corresponding scan rates, a Cottrell plot, seen in Figure 6.2., was configured in order to obtain the slope value needed in the Randles-Sevcik equation (Eq. 5.1) to calculate the ESA. Calculated ESA (cm^2) values observed for bare, PGP, and PGP-PNIPAAm coated electrodes were found to be 0.018 ± 0.0001, 0.028 ±0.002, and 0.03 ±0.004, respectively. These values were compared to those found in the literature to determine the effectiveness of different coatings and the resulting ESA.

The studies by Burrs et al. (2015) and Vanegas et al. (2014) reported ESA (cm^2) values for bare electrodes to be 0.015 ± 0.0004 and 0.019 ± 0.003, respectively. For bare electrodes, ESA values were found to be similar to those reported by both Vanegas et al. (2014) and Burrs et al. (2015). For PGP-modified electrodes ESA values were calculated and reported as 0.21 ±0.02 cm^2 and 0.148 ± 0.064 cm^2 by Burrs et al. (2015)

and Vanegas et al. (2014), respectively. The ESA for PGP-PNIPAAm coatings observed by Burrs et al. (2015) to be 0.19 ± 0.02 cm^2. These results from the literature for both PGP and PGP-PNIPAAm were higher than the ESA values observed in this study. These differences in ESA could be attributed to differences in fabrication procedures for both PGP and PGP-modified electrodes, particularly the use of spin coating of graphene. Graphene for this study was ultrasonicated 15 min longer than reported by Vanegas et al. (2014) and Burrs et al. (2015) and it is unknown if the ultrasonicator power used in those studies was the same as the one used in this study or if the settings were exactly the same. For the spin coating process, speeds of 1700 rpm and 3500 rpm were used in this study while Burrs et al. (2015) reported speeds of 2621 rpm and 5738 rpm. Procedures for depositing platinum onto the electrode surface similarly involved using a sonoelectrodeposition process, which has been shown to improve nanoplatinum deposition in terms of quantity and uniformity onto sensor surfaces (Burrs et al., 2015). A platinum wire was immersed in a solution of chloroplatinic acid and lead acetate and the wire and electrode were connected to a power supply and ultrasonicator; nanoplatinum deposition was carried out via sonoelectrodeposition at 10 V for 90 seconds (Burrs et al., 2015; Vanegas et al., 2014). The different procedures most likely resulted in different amounts of platinum and graphene deposited on the electrode surfaces.

While lower than literature values, PGP and PGP-PNIPAAm values were both significantly higher ($p < 0.05$) than the ESA found for bare electrodes, consistent with the findings of Burrs et al. (2015). Higher ESA values indicate that coating the

electrodes with PGP and PGP-PNIPAAm improves electron transport at the electrode surface.

Analysis of variance (ANOVA) and Tukey HSD were used to verify the significant difference between bare electrodes and those coated with PGP ($p = 0.011$) and PGP-PNIPAAm ($p = 0.004$). The ESA for PGP-PNIPAAm-modified electrodes did not differ from that of the PGP-modified electrodes at the 95% confidence interval ($p = 0.550$). Figure 6.3. gives a visual representation of the ESA's for each of the electrode coatings. All further testing for the development of the biosensor in this study were carried out using PGP and PGP-PNIPAAm-modified electrodes based on the results from the ESA values calculated, i.e., these coatings showed the best results.

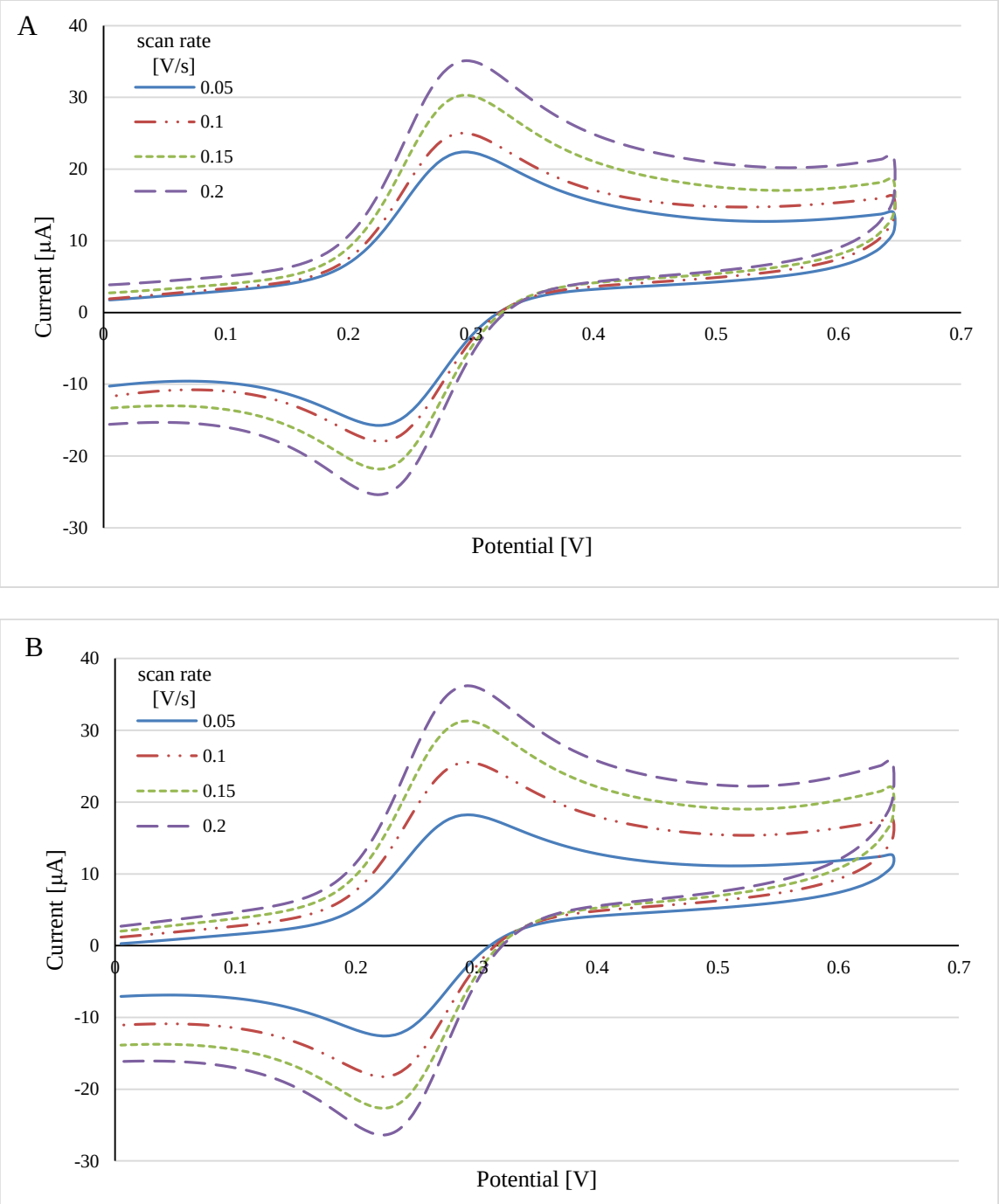

Figure 6.1. Representative CV curves for A) PGP coated and B) PGP-PNIPAAm coated electrodes at various scan rates. Curves represent the average of 3 repetitions.

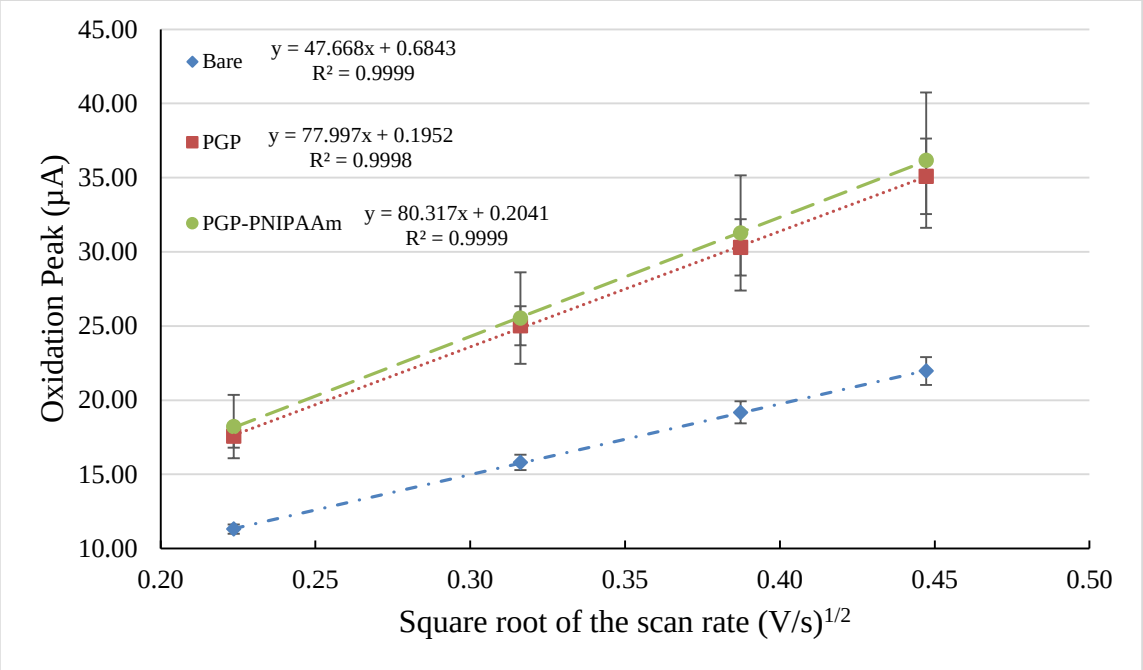

Figure 6.2. Cottrell plot comparing the oxidation peak of Bare, PGP, and PGP-PNIPAAm electrode coatings at various scan rates. Each line represents the average from 3 repetitions. Equations are listed to the right of their respective coating.

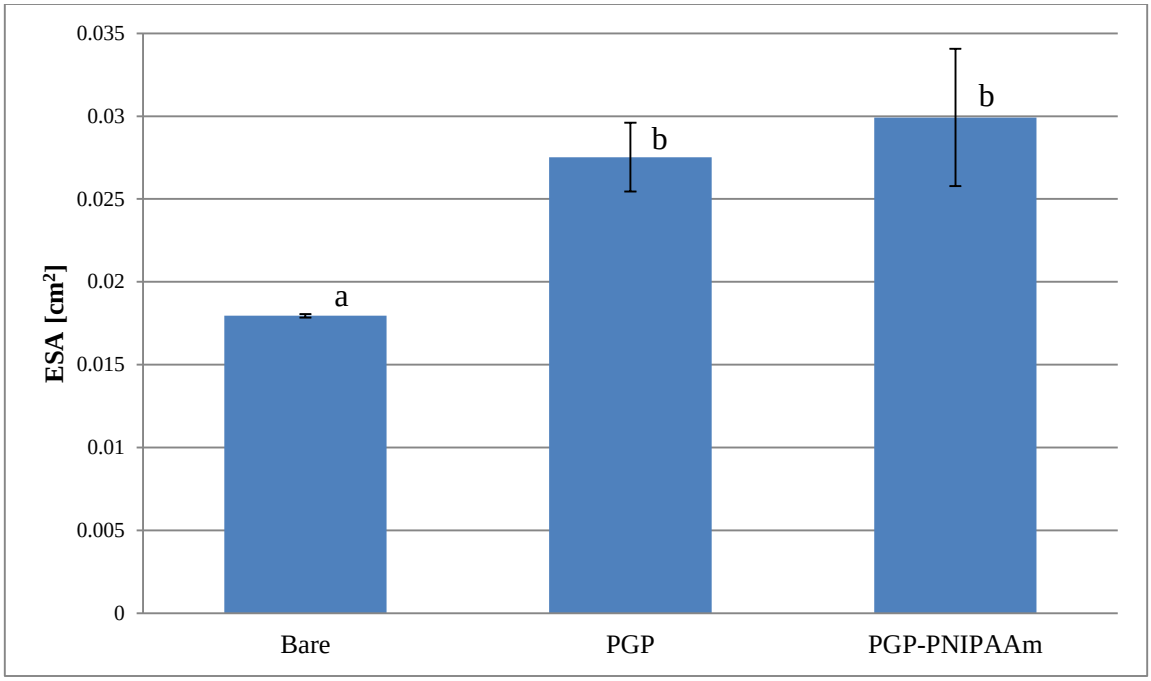

Figure 6.3. Comparison of ESA in cm^2 for Bare (0.018 ± 0), PGP (0.028 ±0.002), and PGP-PNIPAAm (0.03 ±0.004) electrodes. Each ESA value was calculated from 3 repetitions. Bars denoted by different letters are significantly different from each other ($p<0.05$)

6.1.2. Concanavalin A Loading

The optimum ConA loading concentration was determined from the ESA values found at several different ConA concentrations (50 nM, 100 nM, 200 nM) for both PGP and PGP-PNIPAAm coated electrodes. As with the electrode coatings, cyclic voltammetry (CV) was performed and similarly, they have demonstrated reversible redox couples with well-defined redox peaks. Figures 6.4. A and B show representative CV curves for PGP-modified electrodes at the various ConA concentrations and PGP-PNIPAAm- modified electrodes at different ConA concentrations, respectively. All tests were run at neutral pH at room temperature. The reaction showed to be diffusion

controlled as the oxidation peaks are defined similarly to the peaks observed in the CV curves for the PGP and PGP-PNIPAAm-modified electrodes (Vanegas et al., 2014).

A Cottrell plot, seen in Figure 6.5., was constructed using the value of the oxidation peak at each scan rate and the square root of the corresponding scan rates. From the Cottrell plot, the slope values were obtained and used in the Randles-Sevcik equation (Eq. 5.1) to calculate each ESA. Electrodes modified with PGP demonstrated higher ($p < 0.05$) ESA values than those modified with PGP-PNIPAAm when compared at the same concentration of ConA. At 100 nM and 200 nM ConA, the ESA for PGP was significantly larger than the ESA found for PGP-PNIPAAm ($p < 0.05$) at the same concentrations, but for 50 nM, the difference between PGP and PGP-PNIPAAm was not significant ($p > 0.05$). The ESA values at each ConA concentration for both PGP and PGP-PNIPAAm-modified electrodes can be seen in Table 6.1.

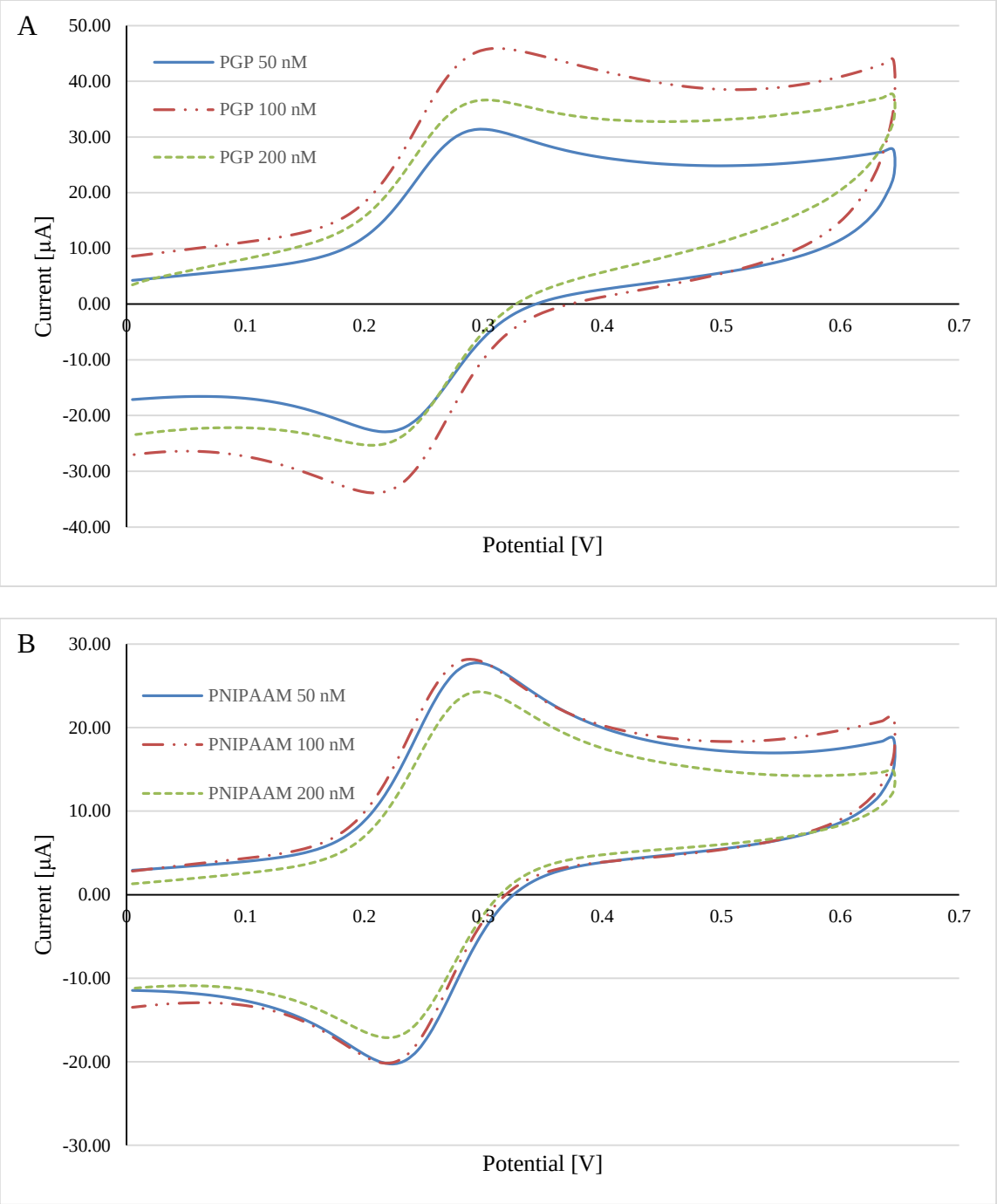

Figure 6.4. Representative CV curves at 100 mVs^{-1} for A) PGP coated and B) PGP-PNIPAAm coated electrodes at various ConA concentrations. Curves represent the average of 3 repetitions.

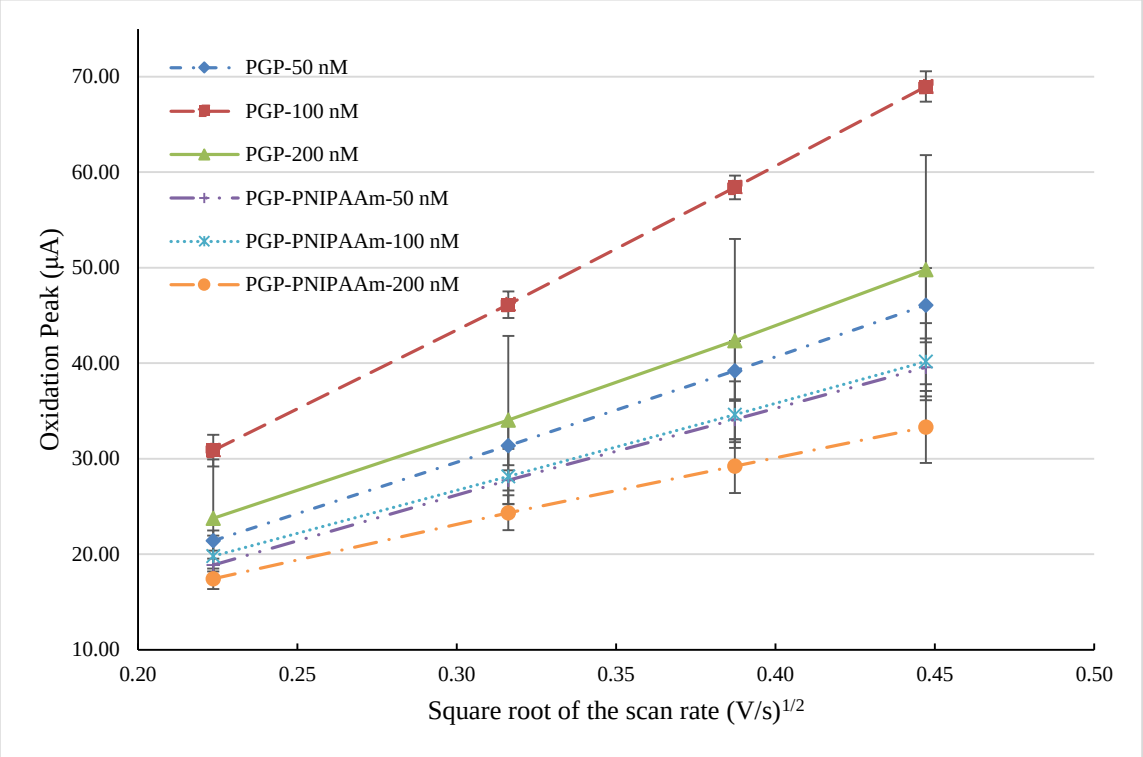

Figure 6.5. Cottrell plot comparing the oxidation peak (µA) for PGP and PGP-PNIPAAm-modified electrodes with various ConA loading concentrations. Each line represents the average from 3 repetitions. Error bars represent the standard deviation.

Table 6.1. Comparison of ESA values from PGP and PGP-PNIPAAm coated electrodes at various ConA concentrations.

Electrode Coating	ConA Concentration [nM]	ESA [cm^2]
PGP	50	$0.0359^{b} \pm 0.0000$
	100	$0.0718^{c} \pm 0.0000$
	200	$0.0347^{b} \pm 0.0021$
PGP-PNIPAAm	50	$0.0323^{a,b} \pm 0.0036$
	100	$0.0323^{a,b} \pm 0.0036$
	200	$0.0263^{a} \pm 0.0041$

Values given are averages of three replicates ± standard deviations. Means that are not followed by a common superscript letter are significantly different ($p < 0.05$).

ConA deposition onto PGP-modified electrodes was achieved through the use of 11-MUA SAM's, while glutaraldehyde and AESH were used to initiate ConA attachment to PGP-PNIPAAm-modified electrodes. This difference in methods for ConA attachment likely contributes to the differences in ESA observed for ConA loading. A study examining the effect of different types of SAM's concluded that MUA SAM's are preferable for electrochemistry analysis compared to longer SAM's chains, this finding supports the higher ESA values observed with ConA attached using 11-MUA SAM's in this study (Claussen, Wickner, Fisher, & Porterfield, 2011). Furthermore, covalent crosslinking between the biosensor platform of the non-conductive material of ConA and PNIPAAm was expected to negatively affect the resulting ESA (Burrs et al., 2015). The overall conductivity of the electrode surface with PGP-PNIPAAm-ConA would be lower than for just PGP-PNIPAAm and in turn lower than the conductivity of the electrode surface coated only with PGP or PGP-ConA, which is observed by the reported ESA values.

Results of ANOVA and Tukey HSD testing show that PGP-modified electrodes loaded with 100 nM of ConA were significantly different from PGP electrodes with 50 nM and 200 nM ConA as well as from all concentration of ConA loaded on PNIPAAm-modified electrodes. For this reason, 100 nM of ConA was determined to be the optimum loading concentration for electrodes modified with PGP. According to the ANOVA and Tukey HSD results, there was no significant difference between PNIPAAm-modified electrodes loaded with 100 nM of ConA and PNIPAAm-modified electrodes loaded with 50 nM and 200 nM of ConA. Though there was no significant

difference, 100 nM was determined to be the concentration to use for the remainder of PNIPAAm-modified tests including actuation and bacteria testing due to the consistency observed when loading at this concentration. Using 50 nM with the PNIPAAm-modified electrode yielded the highest ESA ($p > 0.05$) of the PNIPAAm-ConA load testing, though the standard deviation was much higher and results were difficult to replicate. In the study by Hu et al. (2013), several concentrations of ConA were tested and a concentration of 100 nM of ConA was determined to be the optimum concentration, which is consistent with the findings of this study. For ConA attachment, Hu et al. (2013) used a similar method to this study, which included the use of 11-mercaptoundecanoic acid (MUA) and self-assembled monolayers (SAM).

While ESA was not determined in the study by Hu et al. (2013), CV curves were observed for each ConA concentration and the peak of the curve became lower and less defined as the concentration was increased indicating the charge between the surface of the electrode and the solution was being interrupted by the lectin immobilized on the surface. Low concentrations of ConA (1 nM and 10 nM) elicited CV responses similar to that of a bare electrode and concentrations above 100 nM (500 nM and 1 μM) resulted in curves with nearly non-distinguishable peaks, therefore 100 nM of ConA was chosen as the optimum concentration for the study (Hu et al., 2013). Figures 6.6. A and B give a visual representation of the ESA's for each of the electrode coatings at the different ConA concentrations tested.

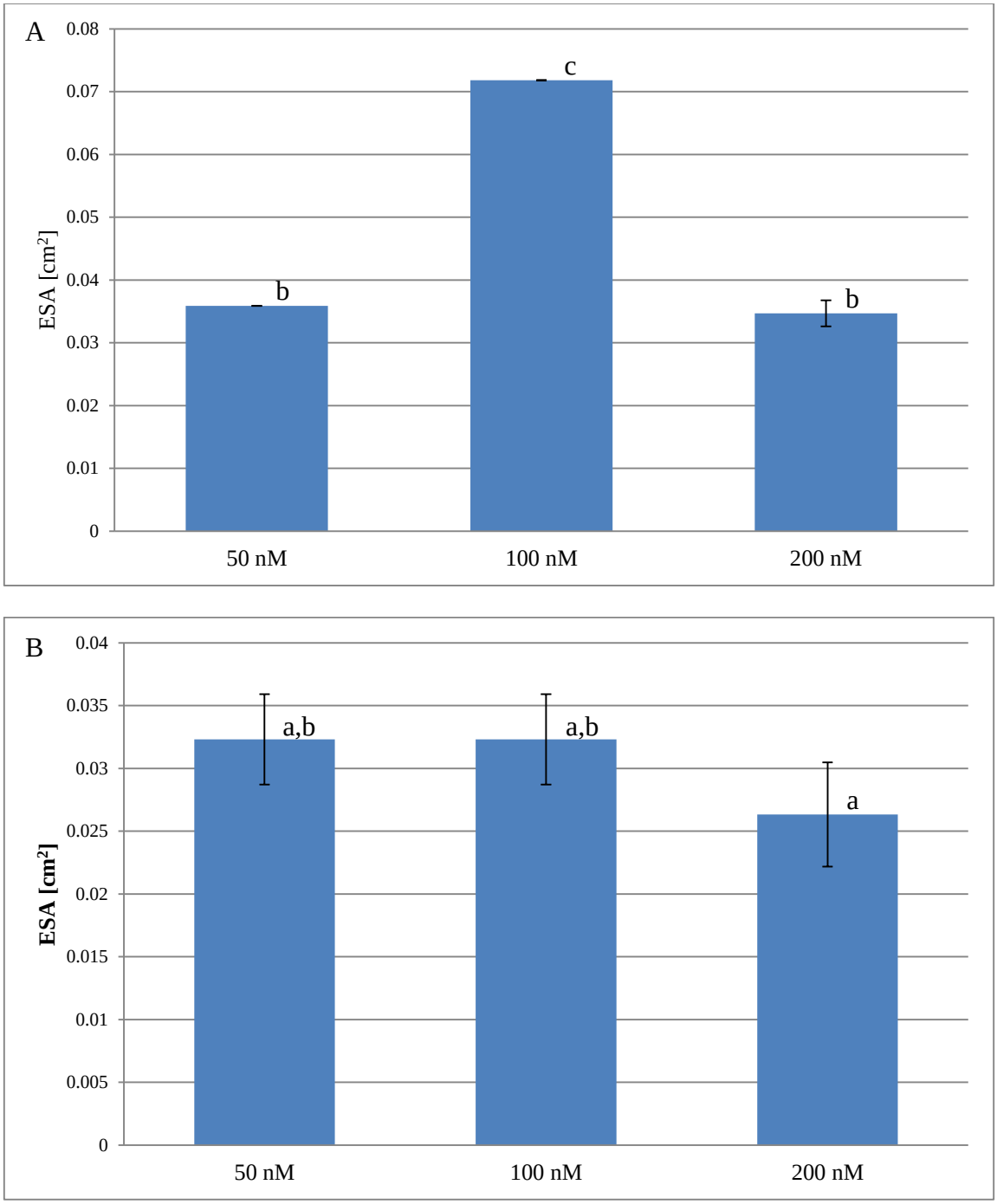

Figure 6.6. A) Comparison of ESA in cm^2 for PGP-modified electrodes at various ConA concentrations. B) Comparison of ESA in cm^2 for PGP-PNIPAAm electrodes at various ConA concentrations. All values represent the average of 3 replicates. Bars denoted by different letters are significantly different from each other ($p<0.05$). Error bars represent the standard deviation.

6.1.3. Antibody Loading

The optimum *E. coli* antibody loading concentration was determined from the ESA values found at several different antibody concentrations (50 nM, 100 nM, 200 nM) for both PGP and PGP-PNIPAAm coated electrodes. Antibody concentrations chosen for comparison were based on the concentrations used for ConA loading optimization.

As with the electrode coatings, cyclic voltammetry (CV) was performed and again demonstrated reversible redox couples with well-defined redox peaks. Figures 6.7. A and B show representative CV curves for PGP and PGP-PNIPAAm electrodes at the various antibody concentrations tested, respectively. Similar to all other coatings in this study, the reaction was diffusion controlled. This is due to the oxidation peaks being well defined (Vanegas et al., 2014).

A Cottrell plot, seen in Figure 6.8., was constructed using the value of the oxidation peak at each scan rate and the square root of the corresponding scan rates. From the Cottrell plot, the slope values were obtained and used in the Randles-Sevcik equation (Eq. 5.1) to calculate ESA. The ESA values at each antibody concentration for both PGP and PGP-PNIPAAm-modified electrodes can be seen in Table 6.2.

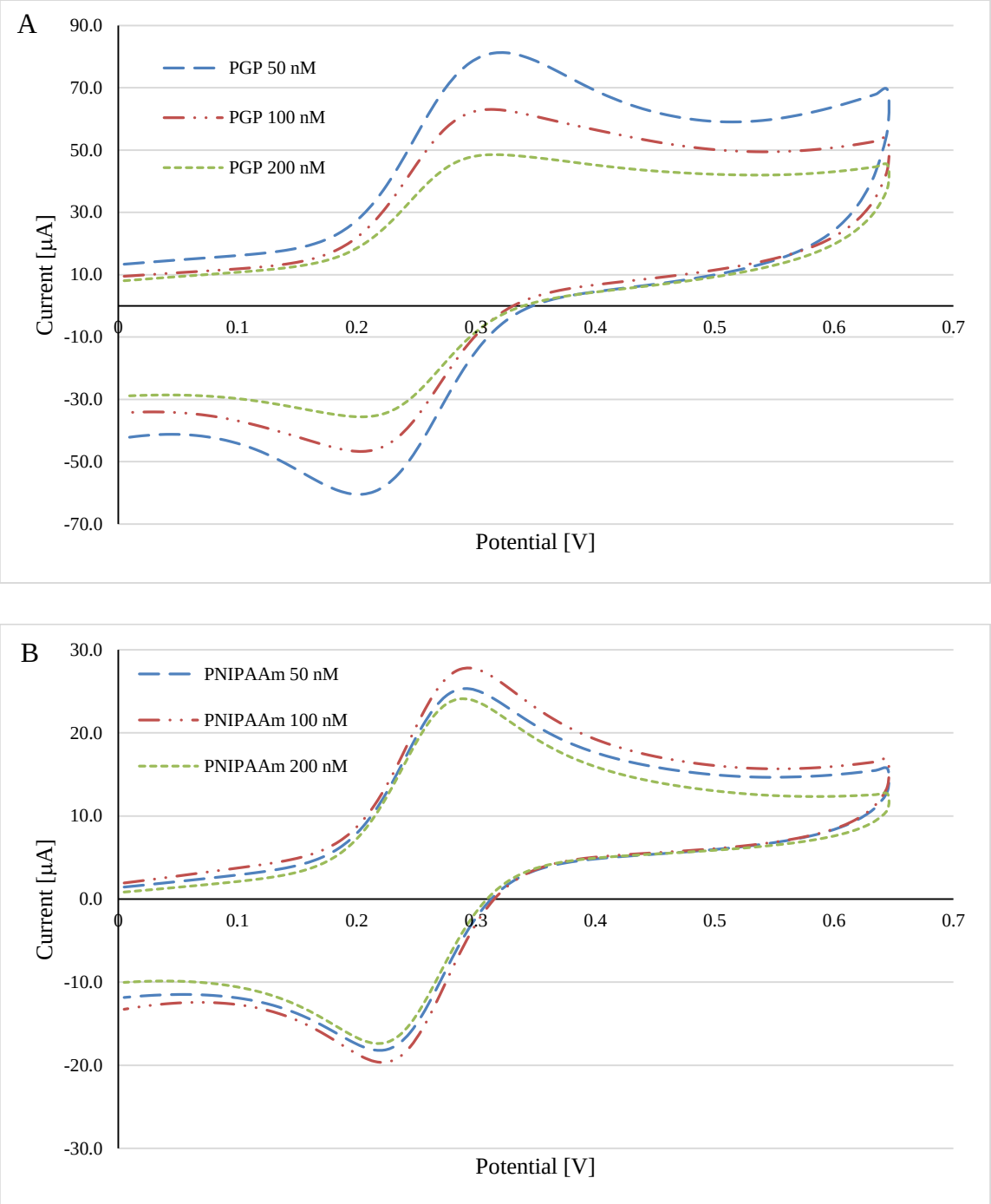

Figure 6.7. Representative CV curves at 100 mVs^{-1} for A) PGP coated and B) PGP-PNIPAAm coated electrodes at various antibody concentrations. Each curve represents the average of 3 repetitions.

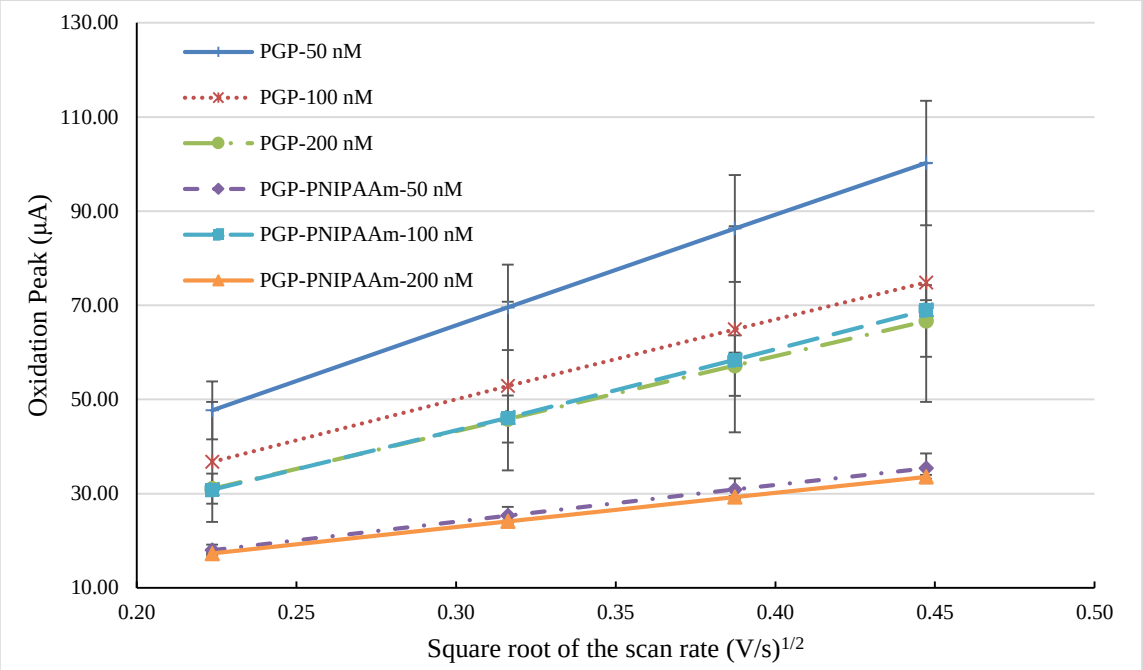

Figure 6.8. Cottrell plot comparing the oxidation peak for PGP and PGP-PNIPAAm-modified electrodes with various antibody loading concentrations. Each line represents the average of 3 replicates. Error bars represent the standard deviation.

Table 6.2. Comparison of ESA values from various electrode coatings.

Electrode Coating	Antibody Concentration [nM]	ESA [cm^2]
PGP	50	$0.0993^{b} \pm 0.0145$
	100	$0.0598^{a} \pm 0.0207$
	200	$0.0598^{a} \pm 0.0207$
PGP-PNIPAAm	50	$0.0275^{a} \pm 0.0021$
	100	$0.0311^{a} \pm 0.0021$
	200	$0.0251^{a} \pm 0.0000$

Values given are averages of three replicates ± standard deviations. Means that are not followed by a common superscript letter are significantly different ($p < 0.05$).

Results of ANOVA and Tukey HSD testing showed only PGP electrodes modified with 50 nM of *E. coli* antibodies were significantly different from other

loading concentrations for PGP or PGP-PNIPAAm. There was no significant difference between any of the other antibody loading concentrations tested for either PGP-modified or PGP-PNIPAAm-modified electrodes. Figures 6.9. A and B give a visual representation of the ESA's for each of the electrode coatings at the antibody concentrations tested.

For PGP-modified electrodes, an antibody loading concentration of 50 nM resulted in the highest ($p < 0.05$) ESA and was therefore chosen as the loading concentration to be used for bacteria testing with PGP-antibody as the capture set up. In addition to 50 nM producing the highest ESA, the oxidation peak appeared to be much higher than those observed for the other concentrations tested. Furthermore, it seems that above 50 nM loading the electrodes have reached saturation.

In the case of PGP-PNIPAAm-modified electrodes, 100 nM loading concentration of antibody yielded the highest ESA, similar to ConA loading results. For this reason 100 nM was the chosen concentration for further PGP-PNIPAAm testing with antibodies. As antibody loading data is not readily available within the literature, it was decided to test the antibody loading at the same concentration as it was tested for ConA loading. This also allowed for a direct comparison between the two capture probes.

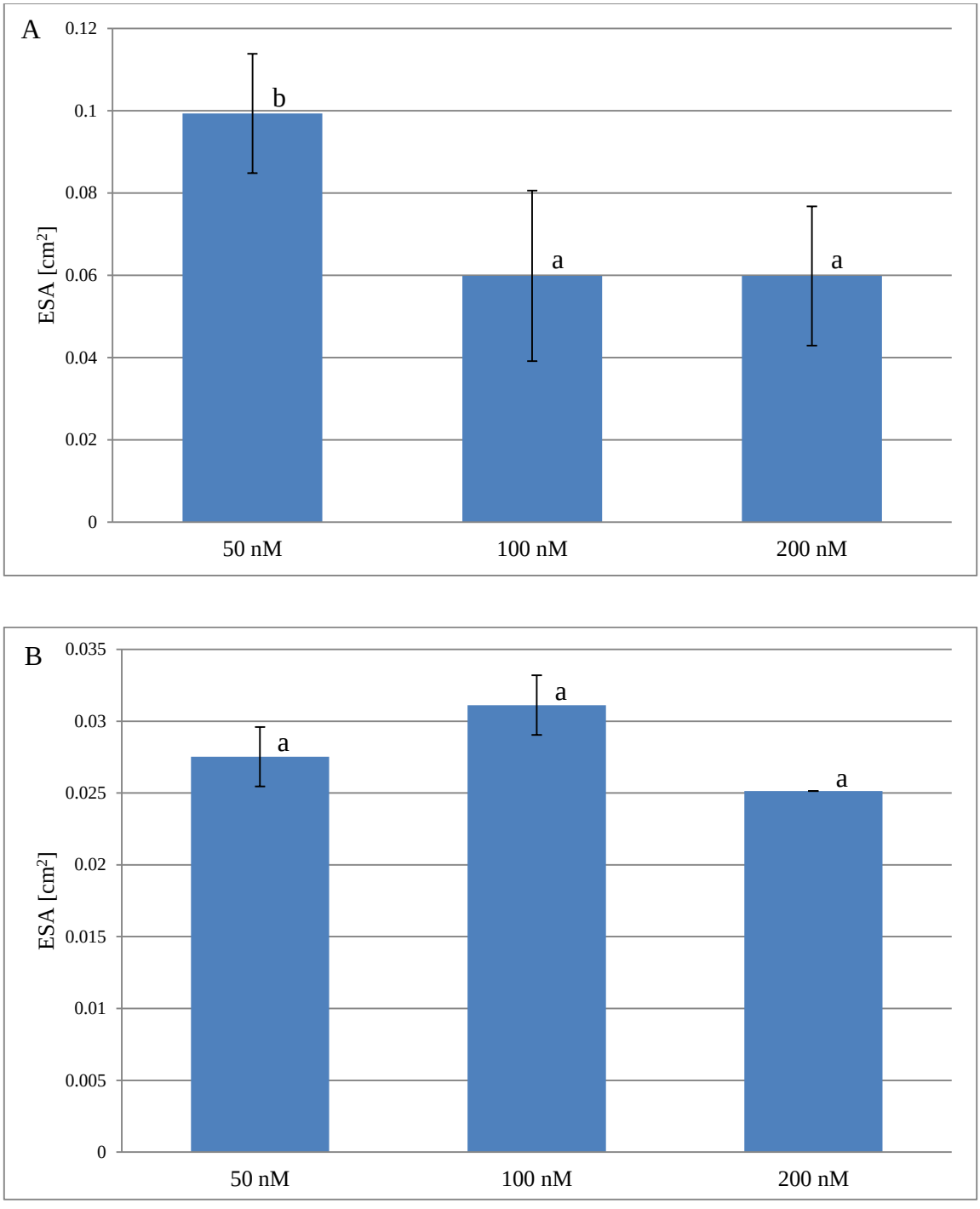

Figure 6.9. Comparison of ESA in cm^2 for A) PGP-modified and B) PGP-PNIPAAm-modified electrodes at various antibody concentrations. Values represent the average of 3 replicates. Bars denoted with different letters were found to be significantly different from each other ($p < 0.05$). Error bars represent the standard deviation.

6.2. Testing Conditions

6.2.1. PNIPAAm Nanobrush Actuation

Cyclic voltammetry (CV) performed on electrodes modified with PGP-PNIPAAm-ConA loading at 100 nM above and below the PNIPAAm lower critical solution temperature or LCST (40 °C and 20 °C, respectively) demonstrated the same reversible redox couples with well-defined redox peaks as the other ESA tests in this study. Figure 6.10. shows representative CV curves for PGP-PNIPAAm-ConA modified electrodes at 20 °C and 40 °C. Similarly to the other coatings tested (bare, PGP, PGP-PNIPAAm, PGP-PNIPAAm-ConA), the defined oxidation peaks on the curves indicate that the reaction is diffusion controlled at the interface of the electrode-solution (Vanegas et al., 2014).

As shown in Figure 6.10., the highest peak values were observed when electrodes were tested above the LCST at 40 °C when the PNIPAAm nanobrushes are in a collapsed state. The collapsed nanobrushes likely improve conductivity through the PGP-PNIPAAm-ConA layer compared to when the nanobrushes are expanded. Each coated electrode was tested at 20 °C then 40 °C, brought back down to 20 °C, tested at 20 °C and again tested at 40 °C; i.e., two cycles. Varying the temperature multiple times was to test the hypothesis that the state of the PNIPAAm nanobrushes is switchable and that causing the PNIPAAm to swell does not destroy the nanobrushes or affect the loading of the ConA. The actuation of PNIPAAm was also hypothesized to be beneficial to the capture of bacteria with PNIPAAm nanobrushes expanded, ConA would be available to capture bacteria and when PNIPAAm collapsed at 40 °C closer

contact to the surface of the biosensor would facilitate electron transport for testing. This was verified by the peak current values and ESA values being similar at each corresponding temperature tested for both cycles as shown in Figure 6.10.

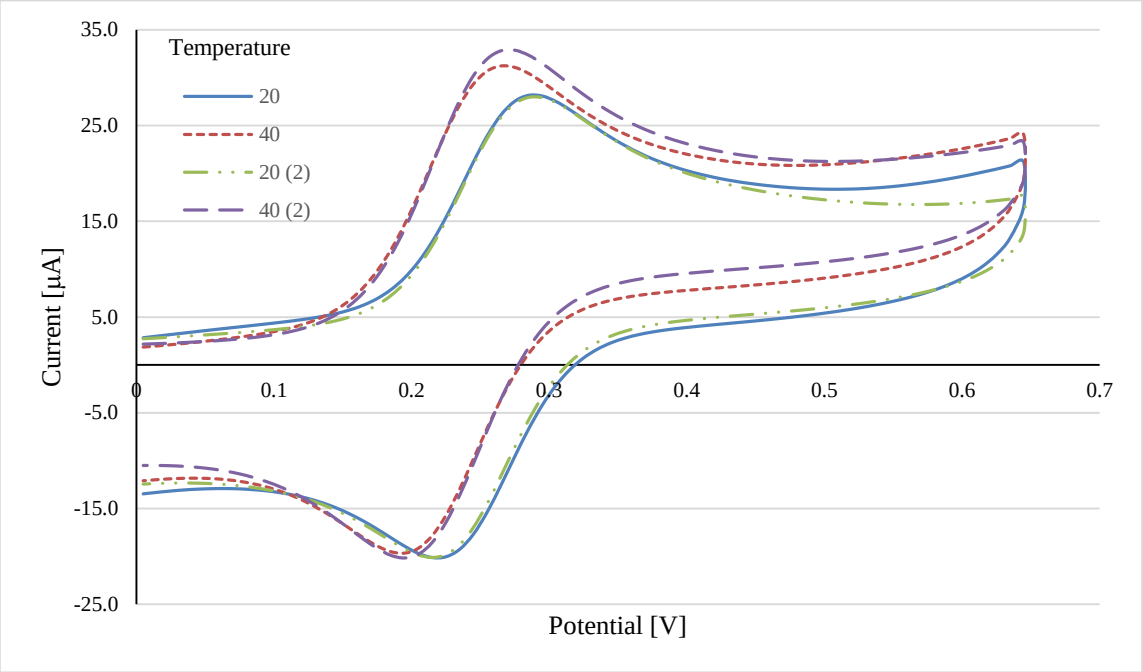

Figure 6.10. Representative CV curves at 100 mVs^{-1} for PGP-PNIPAAm-ConA coated electrodes above (40 ºC) and below (20 °C) the lower critical solution temperature. Curves denoted 20 and 40 represent the first set of tests and curves denoted 20 (2) and 40 (2) denote the second tests run at the respective temperatures on the same electrodes.

Studies by Yin et al. (2009) and Zhao et al. (2012) have also investigated the effect of temperature changes above and below the LCST of PNIPAAm had on electrodes modified with PNIPAAm. Results from both studies were opposite of those found in this study in that CV curves from PNIPAAm-modified electrodes tested below the LCST showed current peaks higher than electrodes tested above the LCST (Yin et

al., 2009; Zhao et al., 2012). This difference could be attributed to the type of electrodes used and additional components on the sensors differing from those used in this study.

In the study by Yin et al. (2009), PNIPAAm brushes were fabricated similarly to PNIPAAm nanobrush fabrication in this study, but polymerization was carried out by cycling the potential between 100 and -800 mV at a scanning rate of 100 mV s^{-1}. Also, the PNIPAAm was attached to an indium tin oxide (ITO) film, the model protein hemoglobin (Hb) was used and electrodes were tested in a PBS solution. Zhao et al. (2012) tested Au (gold) electrodes grafted with multiwalled carbon nanotubes (MWNT) onto a PNIPAAm-modified surface and PNIPAAm-modified electrodes with no platinum-graphene-platinum layer. PNIPAAm brushes were synthesized using similar electropolymerization process as was the case with this study, though no chain transfer agent was used when attaching MWNT to PNIPAAm brushes (Zhao et al., 2012). The testing solution used by Zhao et al. (2012) was similar to that used in this study. The CV results reported by Zhao et al. (2012) not only differ from this study's results in peak current values, but also in the general shape of the curve further confirming differences in the electrodes and coating contribute to differences in results from actuation testing even though PNIPAAm was used in both studies. ESA values were not reported by either Yin et al. (2009) or Zhao et al. (2012) and therefore cannot be used for comparison.

Using the value of the oxidation peak at each scan rate and the square root of the corresponding scan rates, a Cottrell plot (Figure 6.11.) was configured in order to obtain the slope value needed in the Randles-Sevcik equation (Eq. 5.1) to calculate the ESA.

ESA values calculated below the LCST were compared to those from above the LCST (Table 6.3.) to observe the effect of temperature on the PNIPAAm nanobrushes. Higher ESA values were observed at the higher temperature and indicate that PGP-PNIPAAm-ConA modified electrodes tested above PNIPAAm's LCST with the PNIPAAm in a collapsed state improves electron transport at the electrode surface. Furthermore, results from two cycles of testing support the hypothesis that PNIPAAm actuation is reversible and switching the state of the polymer from expanded to collapsed and vice versa does not damage the coating of the electrode. Results also indicate 20 °C should probably be used for most efficient capture of bacteria while the PNIPAAm nanobrushes are expanded and ConA is easily accessible for the bacteria and 40 °C should probably be used as the test temperature when the PNIPAAm nanobrushes are in a shrunken state. A visual representation of the ESA values can be seen in Figure 6.12.

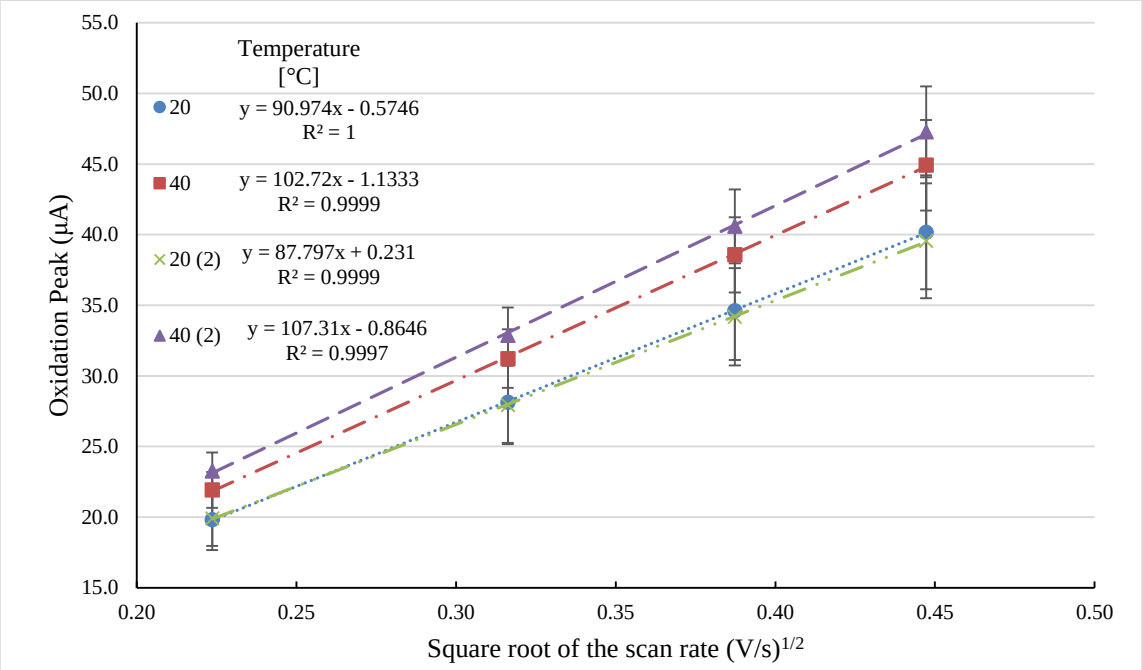

Figure 6.11. Cottrell plots for PGP-PNIPAAm-ConA coated electrodes below (20 °C) and above (40 °C) the lower critical solution temperature. Each electrode tested twice for comparison. The number (2) following the temperatures denotes the second set of tests and equations displayed are to the right of the respective test. Each line represents the average from 3 repetitions. Error bars represent the standard deviation.

Table 6.3. Comparison of ESA values for PGP-PNIPAAm-ConA coated electrodes above and below the LCST.

Temperature [°C]	ESA [cm^2]
20	$0.0323^a \pm 0.0036$
40	$0.0347^a \pm 0.0021$
20 (2)	$0.0311^a \pm 0.0021$
40 (2)	$0.0359^a \pm 0.0000$

Values given are averages of three replicates ± standard deviations. Means that are not followed by a common superscript letter are significantly different ($p < 0.05$). The number (2) following the temperatures denotes the second set of tests.

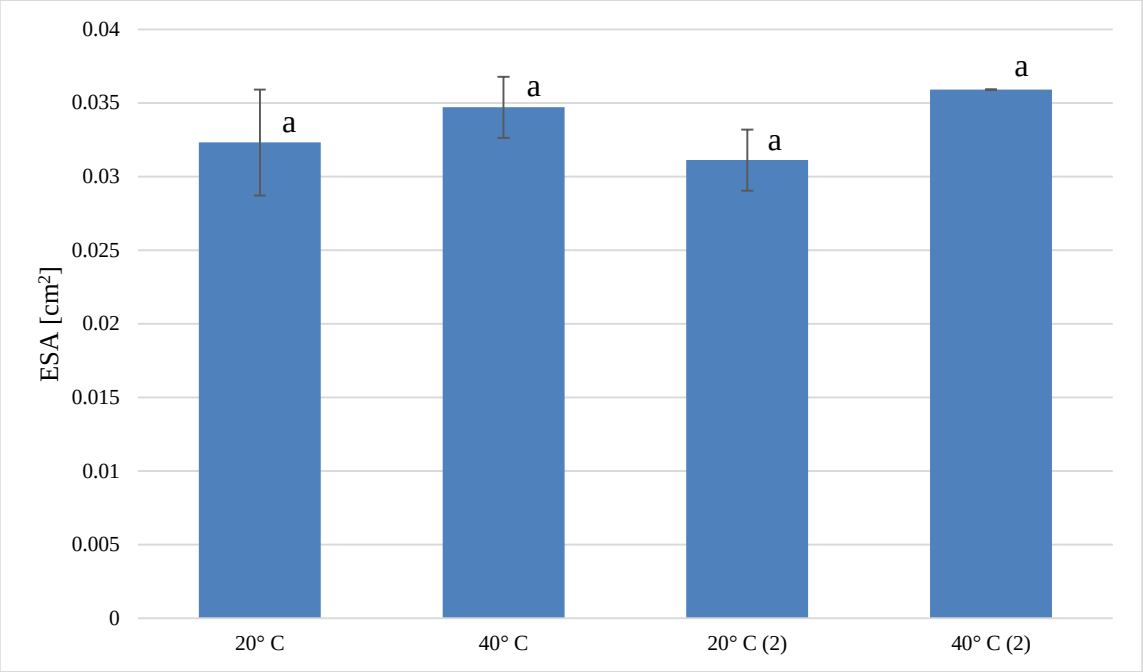

Figure 6.12. Comparison of ESA in cm^2 for PGP-PNIPAAm-ConA coated electrodes below and above the lower critical solution temperature. Tests run in triplicate and each electrode tested twice at each temperature for comparison. The number (2) following the temperatures denotes the second set of tests. Bars denoted by different letters were found to be significantly different ($p<0.05$). Error bars represent the standard deviation.

6.2.2. Bacteria Capture and Detection Conditions

Cyclic voltammetry (CV) performed on electrodes modified with PGP-PNIPAAm-ConA loading at 100 nM after being exposed to *E. coli* K12 at a concentration of 1.32×10^4 CFU mL^{-1}. Two different scenarios of capture and detection conditions were explored using PBS at a neutral pH as the capture and test solution. The different capture/sensing combinations were analyzed and compared to results from the actuation results (section 6.2.1.) to optimize the testing conditions for detecting bacteria using the PGP-PNIPAAm-ConA modified sensor. For three electrodes, capture of bacteria was carried out at 20 °C and CV testing was performed at 40 °C. Three more

replicates were performed this time capturing bacteria in solution at 40 °C and testing at 20 °C.

The lower critical solution temperature (LCST) is the temperature at which the polymer changes from shrunken to swollen and vice versa. In the case of PNIPAAm, the polymer is expanded when exposed to temperatures below the LCST and collapsed when above the LCST, which is typically around 32-35° C (Ju et al., 2001; Yin et al., 2009). As shown in Figure 6.13., the test performed with capture occurring at 20 °C (below the LCST of PNIPAAm) and sensing at 40 °C (above the LCST of PNIPAAm) resulted in CV curves with higher current values for both reduction and oxidation cycles than the testing scenario with capture at 40 °C and sensing at 20 °C. This trend held true over several scan rates (50 mV s^{-1}, 100 mV s^{-1}, 150 mV s^{-1}, 200 mV s^{-1}) tested. ESA values could not be calculated for capture and sensing scenarios due to the inability to definitively define oxidation peak values for the CV curves for the Randles Sevcik equation (Eq. 5.1).

These results indicate 20 °C should be used for most efficient capture of bacteria while the PNIPAAm nanobrushes are expanded and ConA is easily accessible for the bacteria and 40 °C should be used as the sensing temperature when the PNIPAAm nanobrushes are in a shrunken state. This is consistent with the findings from the actuation testing (section 6.2.1) with ESA values being higher for PGP-PNIPAAm-ConA coated electrodes tested at 40 °C than at 20 °C. Based on these results, all further testing for the development of the biosensor in this study were carried out by capturing bacteria at 20 °C and sensing at 40 °C.

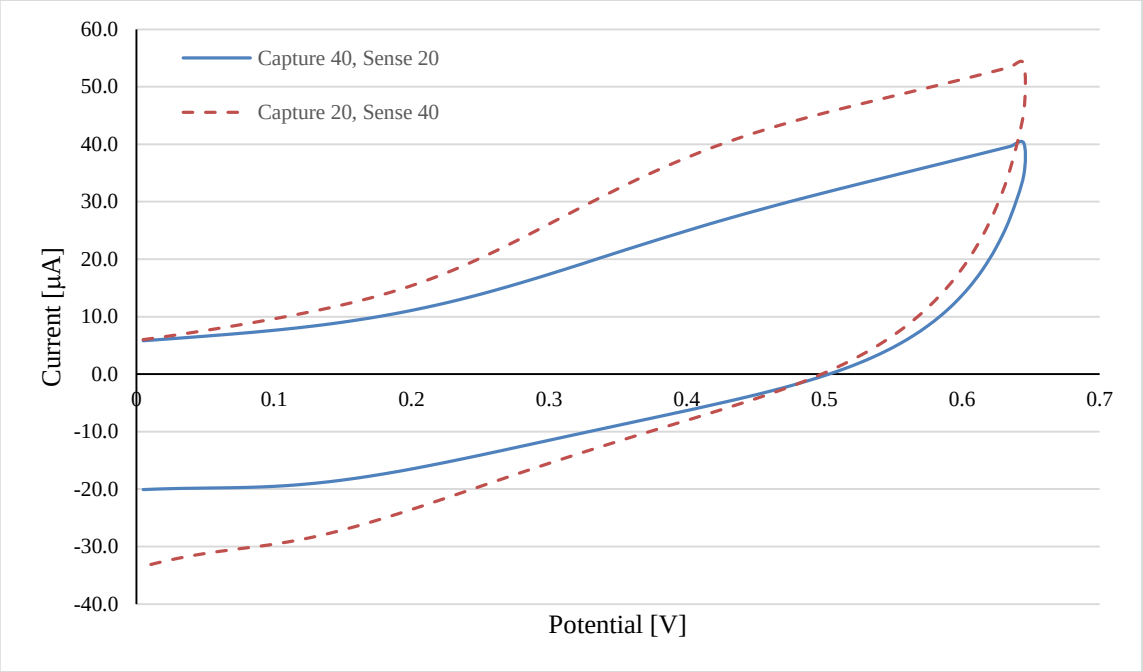

Figure 6.13. Representative CV curves at 100 mVs^{-1} for PGP-PNIPAAm-ConA (100 nM) coated electrodes tested in PBS at a neutral pH in the presence of 1.32 x 10^4 CFU mL^{-1} *E. coli* K12. The numbers 20 and 40 refer to the solution temperature [°C] for the respective portion of the test, i.e.: Capture 40 means the bacteria was captured in a PBS solution at 40 °C. Each curve represents the average of 3 replicates.

6.3. Circuit Fitting

Equivalent circuits, particularly the Randles equivalent circuit, have been used to explain the physical system made up of the solution, electrode surface, and analyte in various biosensor systems (Barsoukov & Macdonald, 2005; Lazcka et al., 2007; Prodromidis, 2010). The Randles circuit, demonstrated in Figure 4.2., is composed of the resistance of the solution (R_s), the capacitance of the dielectric layer (C_{dl}), the charge-transfer resistance (R_{ct}), and the Warburg impedance (Z_w) (Prodromidis, 2010).

The group of Burrs et al. (2015) observed a semicircular region when examining Nyquist plots for bare electrodes indicating a slow electron transfer; this was verified by

the high charge transfer resistance for bare electrodes compared to other electrode treatments in their study. Figures 6.14. A and B show representative Nyquist plots showing the real (Z') and imaginary (-Z") impedance values over the frequency range 1 Hz to 100 kHz and 400 Hz to 100 kHz, respectively, for Bare, PGP-ConA, and PNIPAAm-ConA modified electrodes. As the figure indicated, no semicircular region was observed for any of the electrode modifications tested. The absence of the semicircular region suggests fast electron transfer with negligible charge transfer resistance (Burrs et al., 2015). Figure 6.15. shows an alternative representation of the EIS data in the form of a Bode plot relating the imaginary portion of impedance (-Z") to the testing frequency from 1-100,000 Hz.

Equivalent circuit values were found using CH Instruments Software version 12.04 (Austin, TX) based on the best fit between EIS data collected using the CH Instruments Electrochemical analyzer/Workstation (Model 600 E Series) and the simulated circuit. Randles equivalent circuit was fitted for data from bare, PGP-ConA, and PGP-PNIPAAm-ConA modified electrodes. Results from the circuit fitting are shown on Table 6.4.

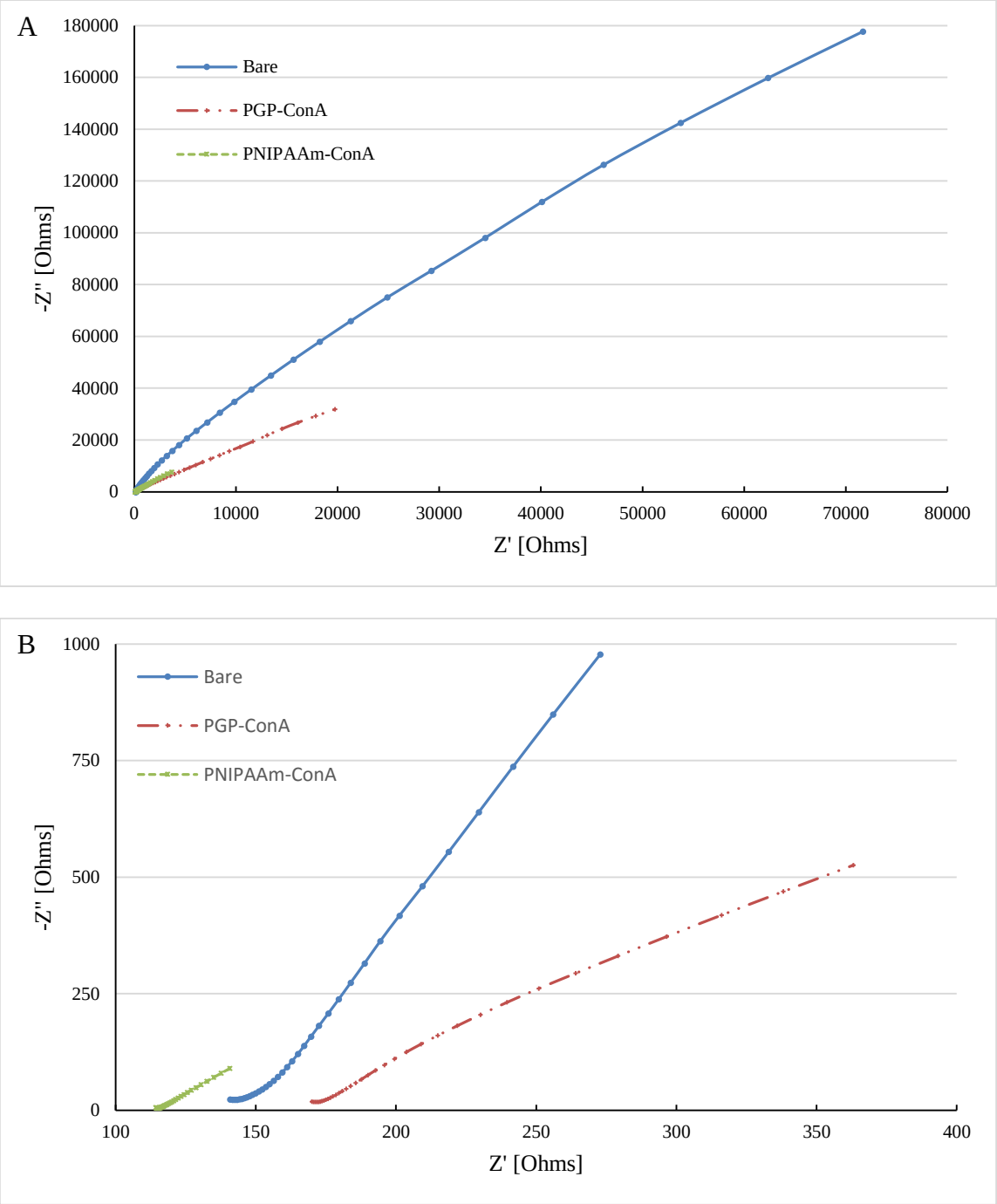

Figure 6.14. A) Representative Nyquist plot over the frequency range of 1-100,000 Hz for Bare, PGP-ConA, and PNIPAAm-ConA modified electrodes. B) Exploded view of Nyquist plot for Bare, PGP-ConA, and PNIPAAm-ConA modified electrodes over the frequency range of 400-100,000 Hz.

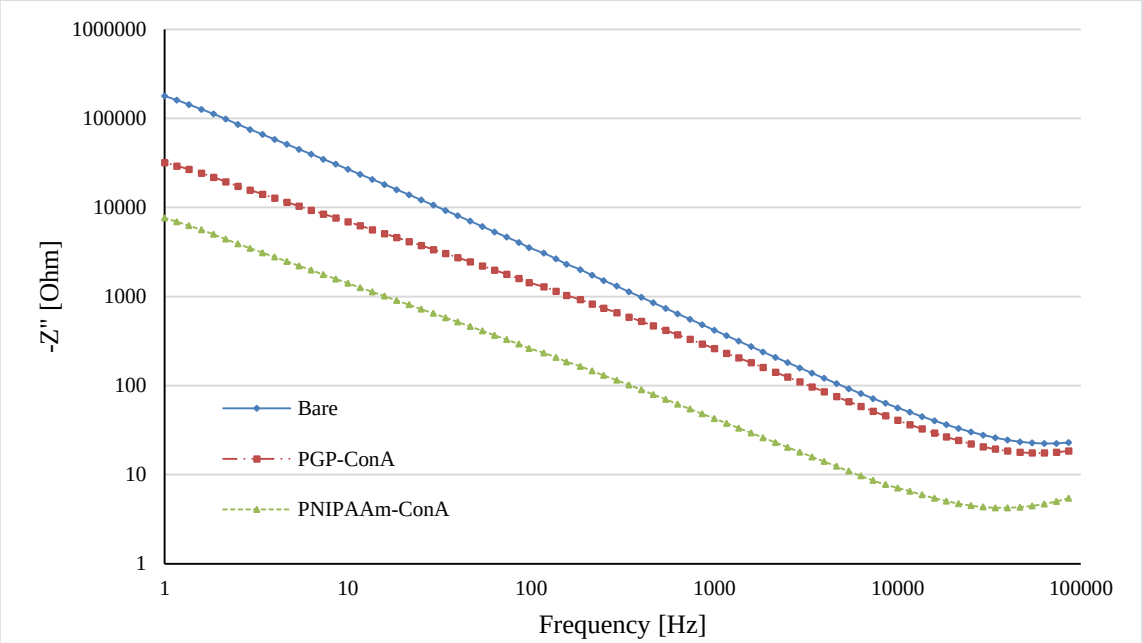

Figure 6.15. Representative Bode plot (imaginary impedance vs. frequency) for Bare, PGP-ConA, and PGP-PNIPAAm-ConA modified electrodes over the frequency range of 1-100,000 Hz. Results represent the average of 3 replicates.

Table 6.4. Parameter estimates from Randles equivalent circuit for Bare, PGP-ConA-modified, and PNIPAAm-ConA-modified electrodes. Results are shown for solution resistance (R_s), Warburg impedance (W), capacitance (C_{dl}), charge transfer resistance (R_{ct}), and error between simulated values and experimental values.

Parameter	Bare	PGP-ConA	PNIPAAm-ConA
R_s [Ω]	$1.950 \times 10^{2} \pm 1.528 \times 10^{-1}$	$1.707 \times 10^{2} \pm 2.082 \times 10^{-1}$	$1.091 \times 10^{2} \pm 1.386 \times 10^{0}$
W [Ω $s^{1/2}$]	$2.104 \times 10^{11} \pm 3.531 \times 10^{11}$	$1.712 \times 10^{-5} \pm 2.109 \times 10^{-6}$	$3.006 \times 10^{10} \pm 5.207 \times 10^{10}$
C_{dl} [μF]	$7.208 \times 10^{-7} \pm 4.545 \times 10^{-9}$	$1.527 \times 10^{-5} \pm 6.907 \times 10^{-7}$	$5.089 \times 10^{-5} \pm 1.131 \times 10^{-5}$
R_{ct} [Ω]	$8.900 \times 10^{11} \pm 9.510 \times 10^{10}$	$2.017 \times 10^{3} \pm 8.169 \times 10^{2}$	$4.427 \times 10^{10} \pm 4.094 \times 10^{10}$
Error	$3.276 \times 10^{-2} \pm 2.854 \times 10^{-4}$	$2.238 \times 10^{-2} \pm 1.029 \times 10^{-3}$	$2.833 \times 10^{-2} \pm 1.599 \times 10^{-3}$

Results represent the average of 3 replicates. Values are shown ± their respective standard deviations.

It was expected that the solution resistance and Warburg impedance would remain relatively constant for all of the electrode treatments as these are both related to the properties of the bulk solution and PBS was the testing solution used for all treatments. Indeed, the solution resistance was relatively constant for all treatments, though the Warburg impedance varied greatly, being particularly low for the PGP-ConA modified electrodes. Moreover, there was also a large variation within the runs for the remaining parameters, including the Warburg impedance, as demonstrated by the resulting large standard deviations. On the other hand, the error for each treatment was small which indicates that the simulated values used by the fitting software were close to the experimental values for each replication, showing a good fit to the equivalent circuitry

The capacitance and charge transfer resistance are related to the dielectric and insulating features at the electrode surface in contact with the electrolyte (L. Yang, Li, & Erf, 2004). As such, the modification of the electrode surface would be expected be reflected in both the charge transfer and capacitance values. Capacitance values fitted were similar between the modified electrodes; both higher than that fitted for the bare electrode tested indicating this parameter predicted by the software would not be the most appropriate to evaluate the modifications made to the electrode surface.

Another important circuit parameter to observe for systems with a redox reaction is the charge transfer resistance (Prodromidis, 2010). Charge transfer resistance was lower for both PGP-ConA and PGP-PNIPAAm-ConA modified electrodes compared to the bare electrode. This matched the expectation for the charge transfer resistance was

to decrease with the addition of conductive electrode coatings (Burrs et al., 2015). It also corresponds with the findings of Burrs et al. (2015), which showed that the lower the ESA value, the higher the respective R_{ct} value. The ESA values for Bare, PGP-ConA, and PGP-PNIPAAm-ConA modified electrodes were 0.018 ± 0.000 cm^2, 0.072 ± 0.000 cm^2, and 0.032 ± 0.004 cm^2, respectively (previously reported in section 6.1.); supporting the direct opposite relationship between ESA and R_{ct} values. Thus, this circuit parameter would be the most suited to evaluate modifications made to the electrode surface.

While this method is accepted widely, it is important to use caution as the same data may be fitted by more than one circuit (Lazcka et al., 2007). A disadvantage to using equivalent circuits is that ideal circuits represent lumped constant properties and therefore the ideal elements used may not be adequate in describing the electrical response detected (Barsoukov & Macdonald, 2005). For these reasons and the inconsistency in the results gathered, i.e., high standard deviation for circuit components, equivalent circuit results were not used in this study to validate the use of modified electrodes to detect *E. coli*.

6.4. Electrochemical Detection

6.4.1. PGP

Electrochemical impedance spectroscopy (EIS) was used to measure the electrochemical response produced by PGP-ConA and PGP-Anti-GroEL antibody biosensors when exposed to *E. coli* K12 at concentrations varying from 10^2-10^8 CFU mL^{-1}. All tests were performed in PBS at a neutral pH with bacteria capture taking place

at 20 °C and sensing at 40 °C in accordance with the findings from section 6.2. The time required for bacteria capture was 15 min and EIS measurement required 2 min to run for a total capture and testing time of 17 min. This was true for all electrode modifications tested in this study.

Figures 6.16. A and B show Bode plots over a frequency range of 1-100,000 Hz for varying bacteria concentrations for PGP-ConA and PGP-antibody sensors, respectively, which relate the testing frequency (Hz) to the imaginary portion of the impedance response, -Z" (Ohms). The insets of the figure are an exploded view of the frequency range for each corresponding capture probe that produced the best linear range over the bacteria concentrations tested. For PGP-ConA, the best frequency to observe a linear relationship between bacteria concentrations was 63090 Hz, while 1 Hz provided the best results for PGP-antibody testing. EIS data displayed in the form of Nyquist plots for PGP-ConA and PGP-antibody is shown in Figures 6.17. A and B, respectively. The Nyquist plots relate the real portion of impedance, Z' (Ohms), to the imaginary portion, -Z" (Ohms) with the frequency increasing from right to left on the plot.

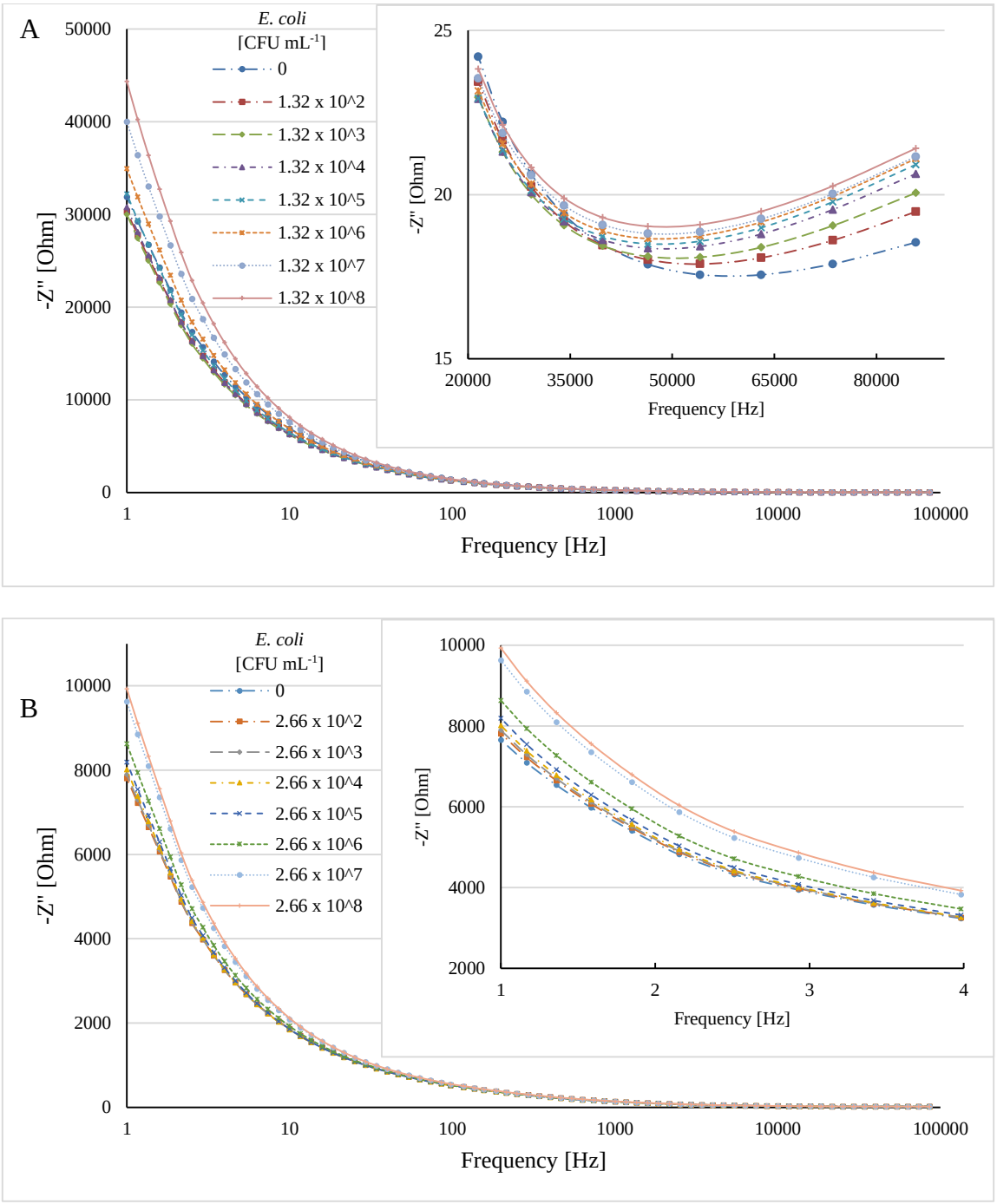

Figure 6.16. Representative Bode plots for A) PGP-ConA modified electrodes with the inset showing exploded view focusing on higher frequencies and B) PGP-Anti-GroEL antibody modified electrodes with the inset showing exploded view focusing on lower frequencies for various concentrations of *E. coli* K12 tested (CFU mL^{-1}). All data represents the average of 3 repetitions.

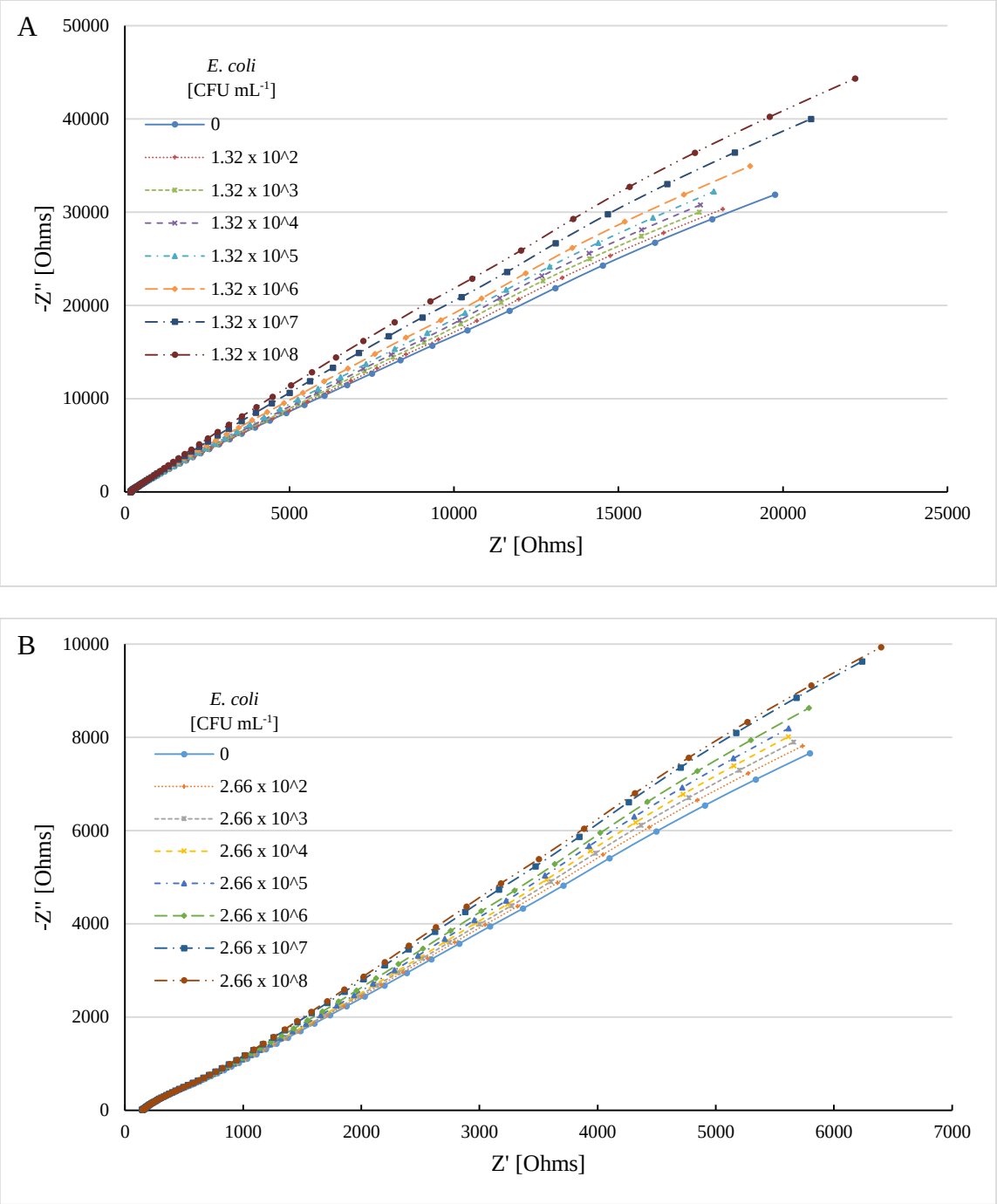

Figure 6.17. Representative Nyquist plots for A) PGP-ConA modified electrodes and B) PGP-Anti-GroEL antibody modified electrodes for various concentrations of *E. coli* K12 tested (CFU mL^{-1}). All data represents the average of 3 repetitions.

Figure 6.18. shows the linear portion of the calibration curves for PGP-ConA and PGP-antibody. Calibration curves were created using data obtained at the optimum frequency determined from the Bode plots for each capture probe. The calibration curves show the relationship between the bacteria concentration tested (CFU mL^{-1}) and the normalized change in the imaginary portion of impedance, -Z" (Ohms), observed. Change in imaginary impedance was calculated as the difference between the –Z" value obtained at each bacteria concentration tested and the –Z" signal output when no bacteria was present; i.e., the baseline. This change in impedance was normalized by dividing by the baseline and then multiplying by 100 as shown in Eq. 6.1 below in order to compare results from various electrode treatments. The imaginary portion of impedance was chosen for use in analysis of the all sensors in this study as it can provide higher sensitivity compared to the real portion of the impedance (Jantra et al., 2011).

$$\Delta - Z''_{normalized} = \frac{\left|\left(-Z''_{sample}\right) - \left(-Z''_{baseline}\right)\right|}{\left(-Z''_{baseline}\right)} x100 \qquad (6.1)$$

The sensitivity and range for each sensor was determined from the linear regions of the calibration curves. Sensitivities for ConA and antibody are listed in Table 6.5. along with the range and lower limit of detection (LOD). Sensitivity was defined as the slope of the linear portion of the calibration curve (Shi et al., 2011; Vanegas et al., 2014). While sensitivity is commonly reported and used as a parameter of performance for biosensors, currently, there is not a dependable protocol to compare sensitivities reported in the literature as calibration curves are not always constructed using the same parameters (Shi et al., 2011). LOD and range of detection are much more reliable parameters to use for performance comparison between biosensors. The LOD was calculated using the 3σ method (Hu et al., 2013; McNaught & Wilkinson, 1997; Vanegas et al., 2014). These methods were used to calculate sensitivity, range of detection, and LOD for all sensors in this study.

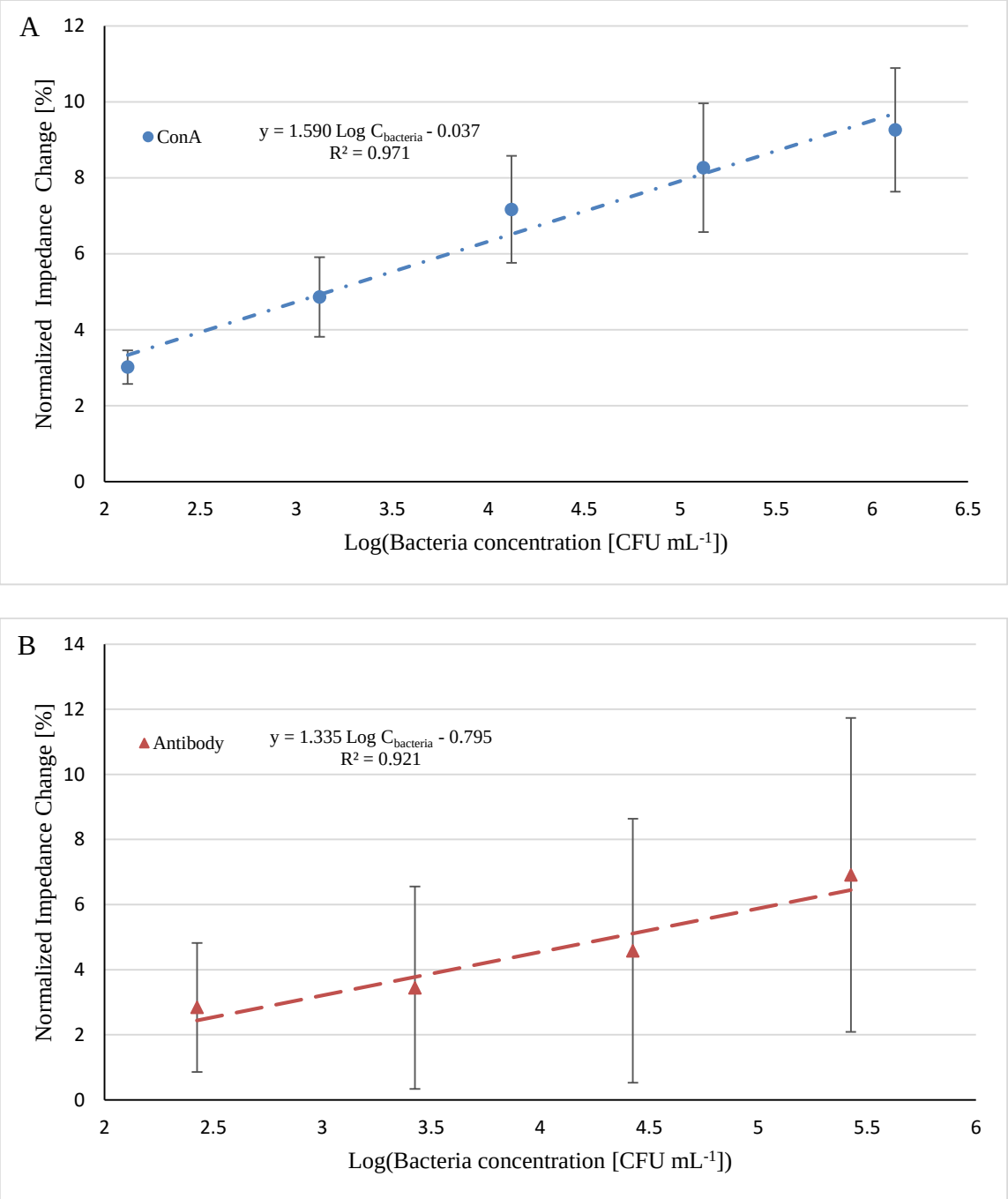

Figure 6.18. Calibration curves for *E. coli* K12 detection in PBS (normalized impedance change (%) vs. log bacteria concentration) for sensors using A) PGP-ConA and B) PGP-Anti-GroEL Antibodies coatings over their respective linear ranges. Curves represent the average of 3 replicates for each capture probe. Equations are displayed to the right of their corresponding electrode treatment. Error bars displayed represent the standard deviation for each data point.

Table 6.5. Performance comparison of ConA and Anti-GroEL Antibody capture probes.

Treatment	Sensitivity $[(\log(CFU\ mL^{-1}))^{-1}]$	R^2	Range $[CFU\ mL^{-1}]$	LOD $[CFU\ mL^{-1}]$
PGP-ConA	$1.590^a \pm 0.115$	0.971	$1.32 \times 10^2 – 1.32 \times 10^6$	$66.877^a \pm 7.993$
PGP-Antibody	$1.335^a \pm 0.307$	0.921	$2.66 \times 10^2 – 2.66 \times 10^5$	$68.000^a \pm 17.580$

Values given are averages of three replicates ± standard deviations. Means that are not followed by a common superscript letter are significantly different ($p < 0.05$).

Results of ANOVA and Tukey HSD testing show there was not a significant difference in sensitivity nor LOD between PGP-ConA and PGP-antibody sensors for the detection of *E. coli* K12. While the sensitivities and LOD's were comparable, the PGP-ConA sensor displayed a larger linear range of detection ($1.32 \times 10^2 – 1.32 \times 10^6$ CFU mL^{-1}) than the PGP-antibody sensor ($2.66 \times 10^2 – 2.66 \times 10^5$ CFU mL^{-1}) indicating that the PGP-ConA sensor is superior in detection of *E. coli* K12 compared to the PGP-antibody sensor. This could signify attachment of the ConA capture probe onto the electrode surface is more efficient than that of the Anti-GroEL antibody even with both capture probes loaded onto the surface at the same concentration (100 nM) using the same attachment procedure. Along with producing similar results to the antibodies, ConA would be advantageous for use in biosensors due to the possibility of washing and reuse, decreased cost of production, and superior shelf-life (Campuzano et al., 2012; Cunningham, 1998; Gamella et al., 2009).

In comparison, the group of Jantra et al.*(2011)*, who also used ConA attached via a 11-MUA self- assembled monolayer and EIS to analyze the response, reported a linear sensitivity range between 12 CFU mL^{-1} and 1.2×10^6 CFU mL^{-1} and an LOD of 12 CFU $mL^{-1}$when detecting *E. coli*. The testing solution used was a carrier buffer at pH 4, which may have played a role in the detection results; moreover it was not specified which *E. coli* strain was used during testing (Jantra et al., 2011). Su and Li (2004) used 16-MUA to attach antibodies for use in a piezoelectric immunosensor and reported a detection range of 10^3-10^8 CFU mL^{-1} and an LOD of 10^3 CFU mL^{-1}. Cyclic voltammetry and quartz crystal microbalance (QCM) were both used for analysis of the

sensor (X.-L. Su & Li, 2004). Superior range and LOD were observed for the PGP-Anti-GroEL antibody sensor used in this study; possibly due to the use of 11-MUA rather than 16-MUA for attachment of the antibodies as well as the use of a PGP base layer to aid in attachment and signal response.

6.4.2. PGP-PNIPAAm-ConA

Electrochemical responses produced by PGP-PNIPAAm-ConA biosensor when exposed to *E. coli* K12 at concentrations varying from 10^2-10^8 CFU mL^{-1} were measured using electrochemical impedance spectroscopy (EIS). Responses were also reported to observe selectivity for PGP-PNIPAAm-ConA modified sensors exposed to equal concentrations ranging from 10^2 CFU mL^{-1} to 10^8 CFU mL^{-1} of *E. coli* K12 and *Salmonella enterica* serovar Enteritidis. *Salmonella* Enteritidis was the bacteria chosen for specificity testing due to its similarity to *E. coli* with both being gram negative and both being known foodborne pathogens (Adams & Moss, 2008). Using a similar gram stain bacterium that is a different species from the target *E. coli* was considered a good test for interference, if any, picked up by the biosensor. All tests were performed in PBS at a neutral pH with bacteria capture taking place at 20 °C and sensing at 40 °C in accordance with the findings from section 6.2.

Figures 6.19. A and B show Bode plots over a frequency range of 1-100,000 Hz for varying bacteria concentrations for PNIPAAm-ConA modified sensors exposed to *E. coli* alone and *E.coli* together with *Salmonella*, respectively. The Bode plots relate the testing frequency (Hz) to the imaginary portion of the impedance response, -*Z*" (Ohms). The insets of the figure are an exploded view of the frequency range for each

corresponding testing scenario that produced the best linear range of impedance change over the bacteria concentrations tested. For PNIPAAm-ConA modified sensors exposed to *E. coli* only and *E. coli* along with *Salmonella*, the best frequency to observe a linear relationship between bacteria concentrations and impedance change was 1 Hz. EIS data displayed in the form of Nyquist plots for sensors tested for sensitivity (*E. coli*) and selectivity (*E. coli* and *Salmonella*) are shown in Figures 6.20. A and B, respectively. The Nyquist plots relate the real portion of impedance, Z' (Ohms), to the imaginary portion, -Z" (Ohms).

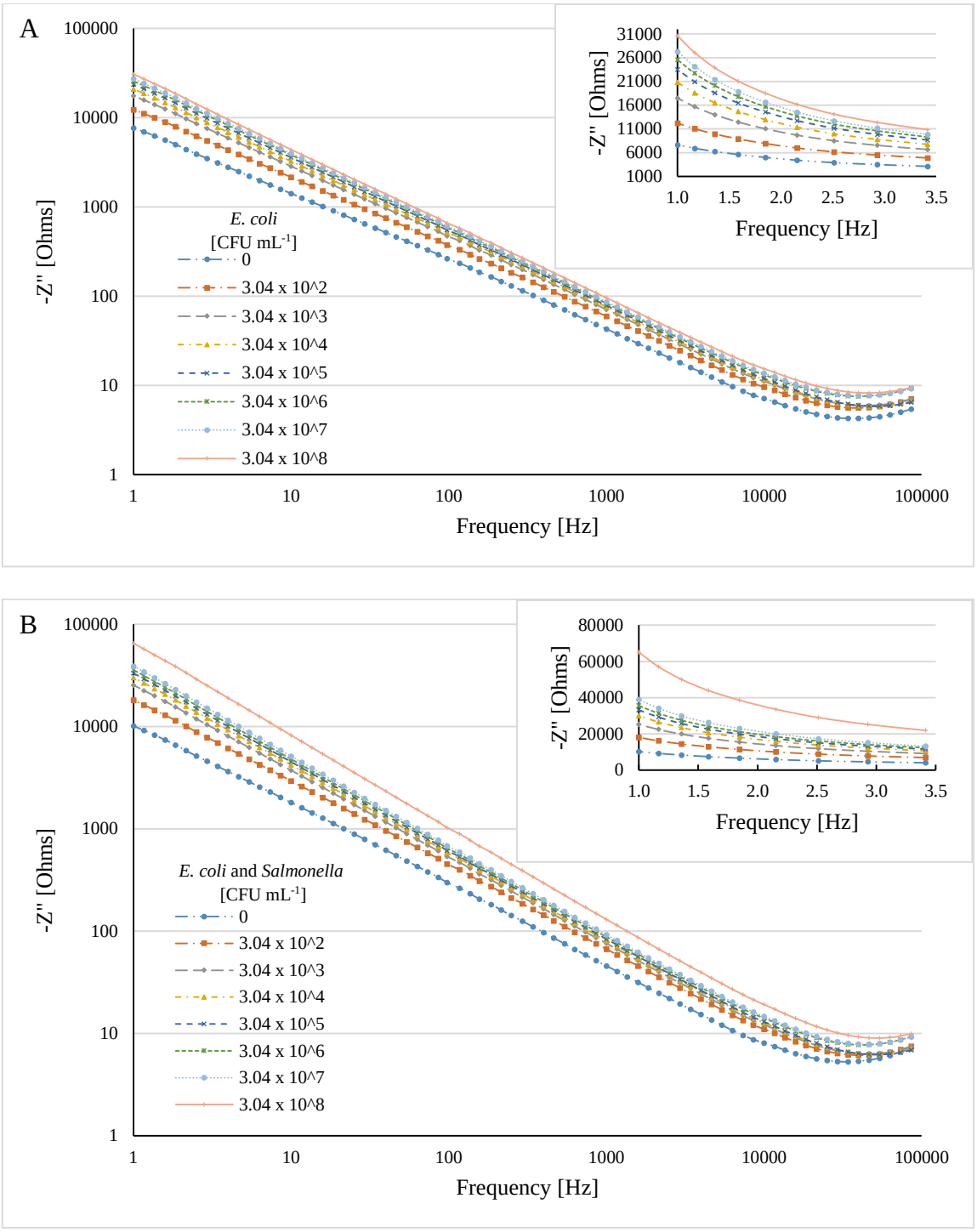

Figure 6.19. Representative Bode plots for PNIPAAm-ConA modified electrodes over the frequency range of 1-100,000 Hz exposed to A) *E. coli* K12 (CFU mL^{-1}) and B) *E. coli* K12 and *Salmonella* Enteritidis (CFU mL^{-1}) in PBS. Insets show exploded view over the frequency range from 1-3.5 Hz. All data represents the average of 3 repetitions.

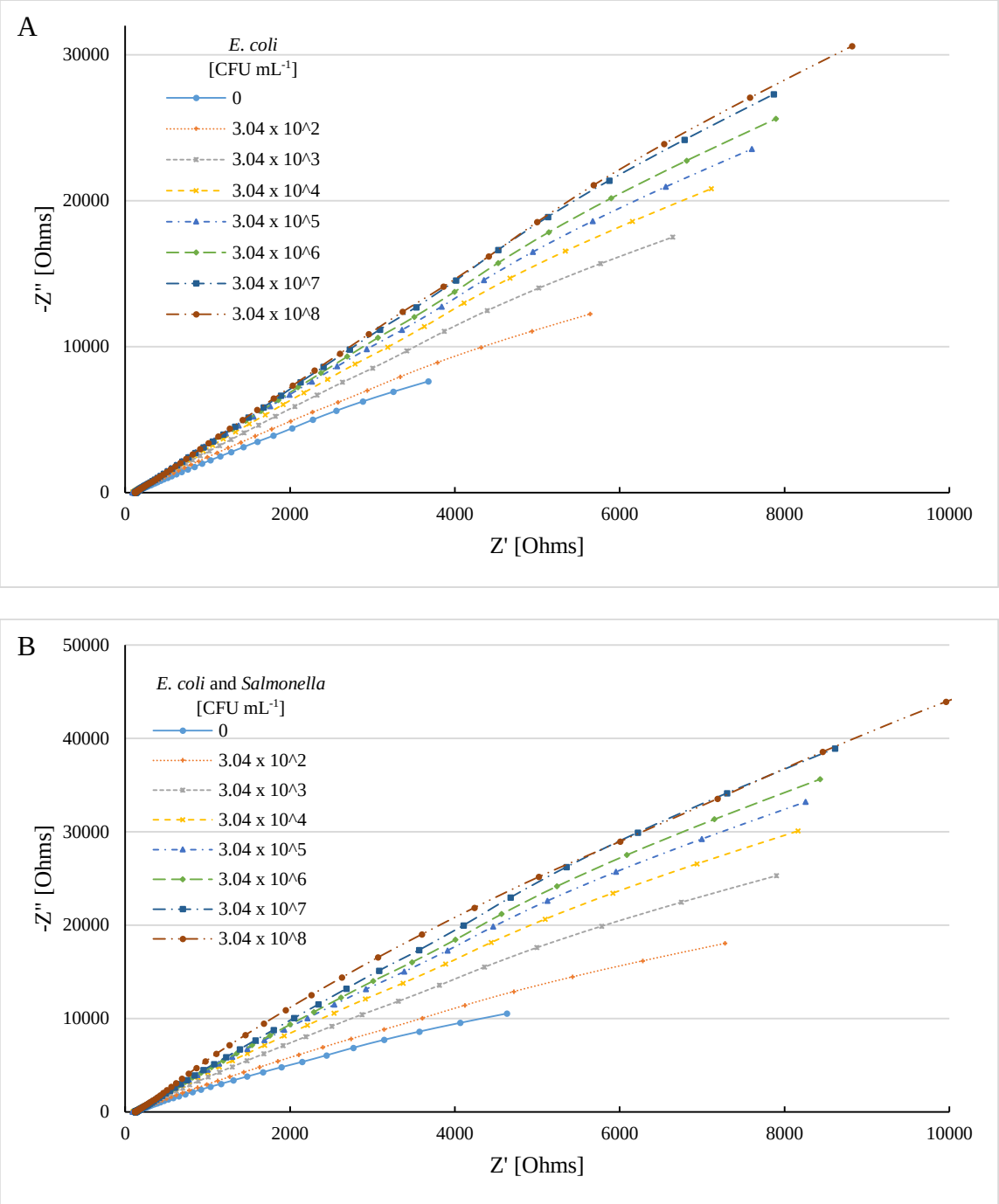

Figure 6.20. Representative Nyquist plots for A) PNIPAAm-ConA modified electrodes exposed to *E. coli* K12 (CFU mL^{-1}) and B) PNIPAAm-ConA modified electrodes exposed to equal concentrations (CFU mL^{-1}) of *E. coli* K12 and *Salmonella* Enteritidis in PBS over the frequency range from 1 – 100,000 Hz. All data represents the average of 3 repetitions.

Figures 6.21. A and B show the linear portion of the calibration curves for PNIPAAm-ConA electrodes with exposure to *E. coli* alone and *E. coli* with *Salmonella*, respectively. Calibration curves were created using data obtained at the optimum frequency (1 Hz) determined from the Bode plots for each testing scenario. The calibration curves show the relationship between the bacteria concentration tested (CFU mL^{-1}) and the normalized change in the imaginary portion of impedance, -Z" (Ohms), observed. The normalized change in imaginary impedance was calculated using Equation 6.1. This value was normalized in order to compare results from various electrode treatments.

The sensitivity and range for each testing scenario was determined from the linear regions of the calibration curves. Sensitivities and R^2 for PNIPAAm-ConA sensors for both testing scenarios are listed in Table 6.6. along with the range and lower limit of detection (LOD).

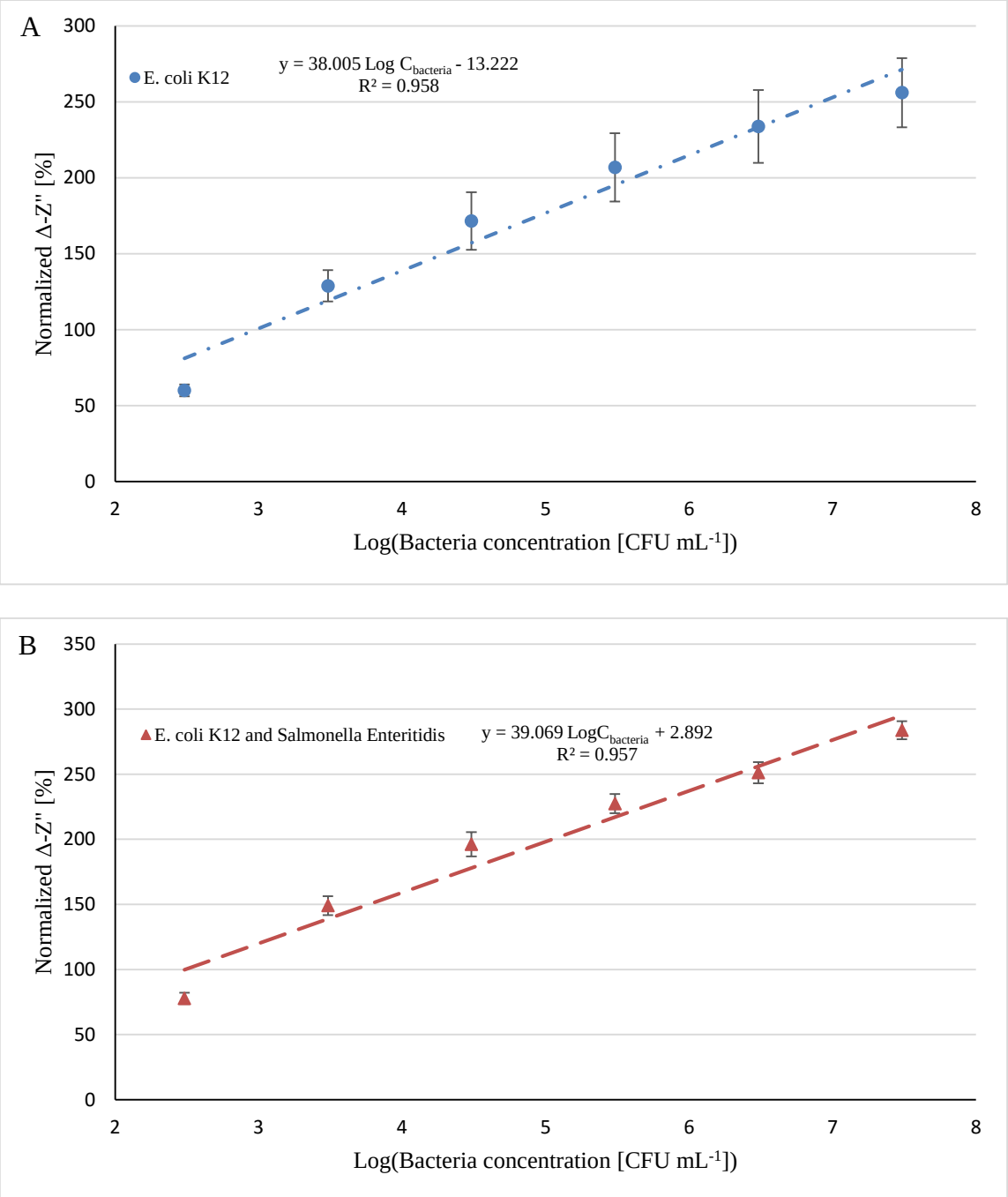

Figure 6.21. Calibration curves (normalized impedance change vs. log bacteria concentration) for PNIPAAm-ConA sensors exposed to A) *E. coli* K12 and B) *E. coli* K12 and *Salmonella* Enteritidis over their respective linear ranges. Curves represent the average of 3 replicates for each capture probe. Equations are displayed to the right of their corresponding testing scenario. Error bars displayed represent the standard deviation for each data point.

Table 6.6. Performance comparison of PNIPAAm-ConA modified electrodes exposed to *E. coli* K12 and *E. coli* K12 with *Salmonella* Enteritidis.

Bacteria Exposure	Sensitivity $[(\log(CFU\ mL^{-1}))^{-1}]$	R^2	Range $[CFU\ mL^{-1}]$	LOD $[CFU\ mL^{-1}]$
E. coli K12	$38.005^a \pm 2.330$	0.958	$3.04 \times 10^2 - 3.04 \times 10^7$	$3.467^a \pm 0.297$
E. coli K12 and *Salmonella* Enteritidis	$39.069^a \pm 2.208$	0.957	$3.04 \times 10^2 - 3.04 \times 10^7$	$2.947^a \pm 0.166$

Values given are averages of three replicates ± standard deviations. Means that are not followed by a common superscript letter are significantly different ($p < 0.05$).

Results of ANOVA and Tukey HSD testing show there was not a significant difference in sensitivity nor LOD between PGP-PNIPAAm-ConA sensors exposed to *E. coli* K12 or to *E. coli* K12 with *Salmonella* Enteritidis. The linear range of detection ($3.04 \times 10^2 – 1.32 \times 10^7$ CFU mL^{-1}) was the same under both testing conditions. The PGP-PNIPAAm-ConA sensor performed similarly when exposed to *E. coli* K12 or to *E. coli* K12 with *Salmonella* Enteritidis indicating that the sensor is both sensitive and specific to *E. coli*. The presence of *Salmonella* Enteritidis in the testing solution did not cause significant interference suggesting there was no cross reaction between the PNIPAAm-ConA sensor and the *Salmonella* Enteritidis (Li et al., 2012). *E. coli* and *Salmonella* contain lipopolysaccharides (LPS) on their cell membranes and the LPS in *E. coli* is capped by an O-antigen consisting of glucose, to which the ConA binds (Adams & Moss, 2008; Lu et al., 2009). The specific ConA binding site known for *E. coli* is G_{M1} ganglioside (Haseley, 2002). While *E. coli* and *Salmonella* are both gram-negative enterobacteria with many similarities, they differ in sugar combining sites (Firon, Ofek, & Sharon, 1984). This difference in combining sites together with the results observed in this study suggest ConA is specific to the membrane sugars sequence and composition in *E. coli* and not those in *Salmonella*.

6.4.3. ConA and Antibody Analysis in Vegetable Broth

Electrochemical responses produced by PGP-PNIPAAm-ConA and PGP-PNIPAAm-Anti-GroEL antibody when exposed to *E. coli* O157:H7 at concentrations varying from 10^2-10^8 CFU mL^{-1} were measured using electrochemical impedance spectroscopy (EIS). The PGP-PNIPAAm modification was chosen over PGP alone

based on the results of the PGP-PNIPAAm-ConA testing in PBS, outlined in section 6.3.2., being superior to PGP-ConA results observed in section 6.3.1. All tests were performed in commercially sterile vegetable broth with bacteria capture taking place at 20 °C and sensing at 40 °C in accordance with the findings from section 6.2. The vegetable broth (H-E-B brand) was made of water, vegetable flavor concentrate, cooked vegetables (carrot, onion, celery), tomato paste, yeast extract, sea salt, sugar, molasses, onion powder, potato flour, natural flavor, canola oil, cane sugar, and sea salt (H-E-B, 2015). Vegetable broth was chosen as it is a complex system made up of foods with the potential for contamination by foodborne pathogens. It is also representative of a solution that might be made using food samples dispersed in aqueous solution that may cause interference with the electrochemical response.

Figures 6.22. A and B show Bode plots over a frequency range of 1-100,000 Hz for varying bacteria concentrations for PNIPAAm-ConA and PNIPAAm-Anti-GroEL antibody modified sensors, respectively. The Bode plots relate the testing frequency (Hz) to the imaginary portion of the impedance response, -Z" (Ohms). The insets of the figure are an exploded view of the frequency range for each corresponding sensor modification that produced the best linear range over the bacteria concentrations tested. For both PNIPAAm-ConA and PNIPAAm-Anti-GroEL antibody modified sensors, the best frequency to observe a linear relationship between bacteria concentrations was 2510 Hz. EIS data displayed in the form of Nyquist plots for both sensor modifications are shown in Figures 6.23. A and B, respectively. The Nyquist plots relate the real portion

of impedance, Z' (Ohms), to the imaginary portion, -Z" (Ohms) with frequency increasing from right to left on the plot.

Figures 6.24. A and B show the calibration curves for PNIPAAm-ConA and PNIPAAm-Anti-GroEL antibody electrodes, respectively, with exposure to *E. coli* O157:H7. Calibration curves were created using data obtained at the optimum frequency (2510 Hz) determined from the Bode plots for each testing scenario. The calibration curves show the relationship between the bacteria concentration tested (CFU mL^{-1}) and the normalized change in the imaginary portion of impedance, -Z" (Ohms), observed. The normalized change in imaginary impedance was calculated using Equation 6.1. This value was normalized in order to compare results from various electrode treatments.

The sensitivity and range for each testing scenario was determined from the linear regions of the calibration curves. Sensitivities for PNIPAAm-ConA and PNIPAAm-antibody sensors are listed in Table 6.7. along with the range and lower limit of detection (LOD).

Results of ANOVA and Tukey HSD testing show there was not a significant difference in sensitivity between PGP-PNIPAAm-ConA and PGP-PNIPAAm-Anti-GroEL antibody sensors exposed to *E. coli* O157:H7. The linear range of detection for PNIPAAm-ConA ($2.64 \times 10^2 – 2.64 \times 10^6$ CFU.mL^{-1}) was lower than the range of detection for PNIPAAm-antibody ($1.47 \times 10^2 – 1.47 \times 10^7$ CFU.mL^{-1}). The LOD for PNIPAAm-ConA (39.06 ± 3.382 CFU.mL^{-1}) was significantly different ($p < 0.05$) from the PNIPAAm-antibody (21.850 ± 3.459 CFU.mL^{-1}). The similarity in sensitivity results

between the PNIPAAm-ConA and PNIPAAm-antibody sensors indicated both are capable of detecting *E. coli* O157:H7 in a complex system. The LOD values were not similar ($p > 0.05$), though they were on the same order of magnitude, which aligns with the assessment that both are capable of *E. coli* O157:H7 detection. For PNIPAAm-ConA modified electrodes, the linear range of detection may have been smaller than that for PNIPAAm-antibody sensors because of interactions between sugars present in the broth from the added sugar, molasses, or other ingredients and the ConA binding site if these sugars were similar to those present on the *E. coli* binding site. The lipopolysaccharide (LPS) on the cell membrane of *E. coli*, which is capped by an O-antigen consisting of glucose, is the binding site for ConA (Adams & Moss, 2008; Lu et al., 2009). ConA is also known to bind to other carbohydrate components such as mannose (T. K. Chowdhury & Weiss, 1975; Lu et al., 2009). This may also explain the superior, though not significantly different, sensitivity and LOD observed for the PNIPAAm-antibody sensor.

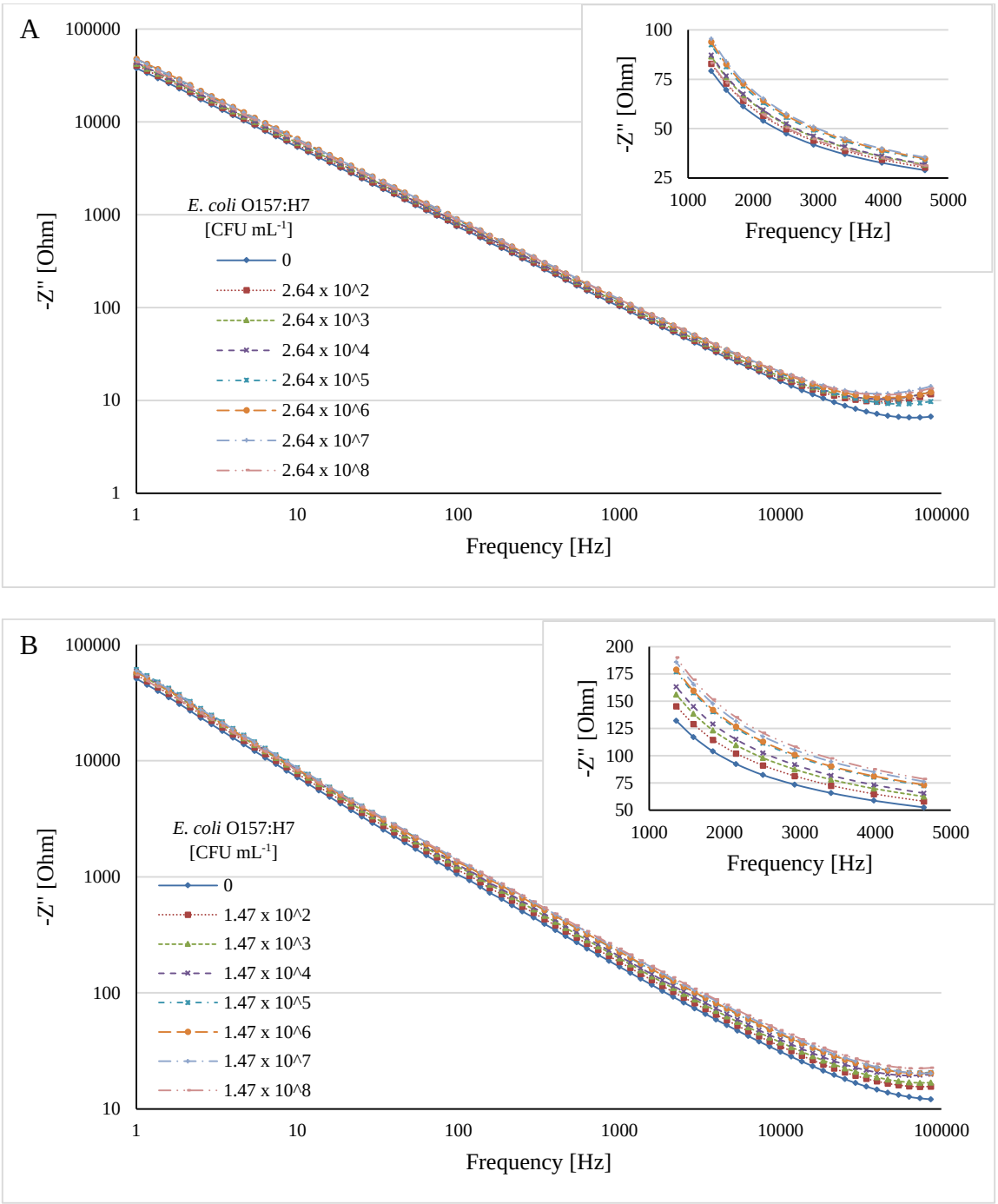

Figure 6.22. Representative Bode plots over the frequency range of 1-100,000 Hz for A) PNIPAAm-ConA and B) PNIPAAm-Anti-GroEL antibody modified electrodes exposed to various concentrations of *E. coli* O157:H7 (CFU mL^{-1}). Insets show the exploded view over the frequency range of 1350 – 4650 Hz. All data represents the average of 3 repetitions.

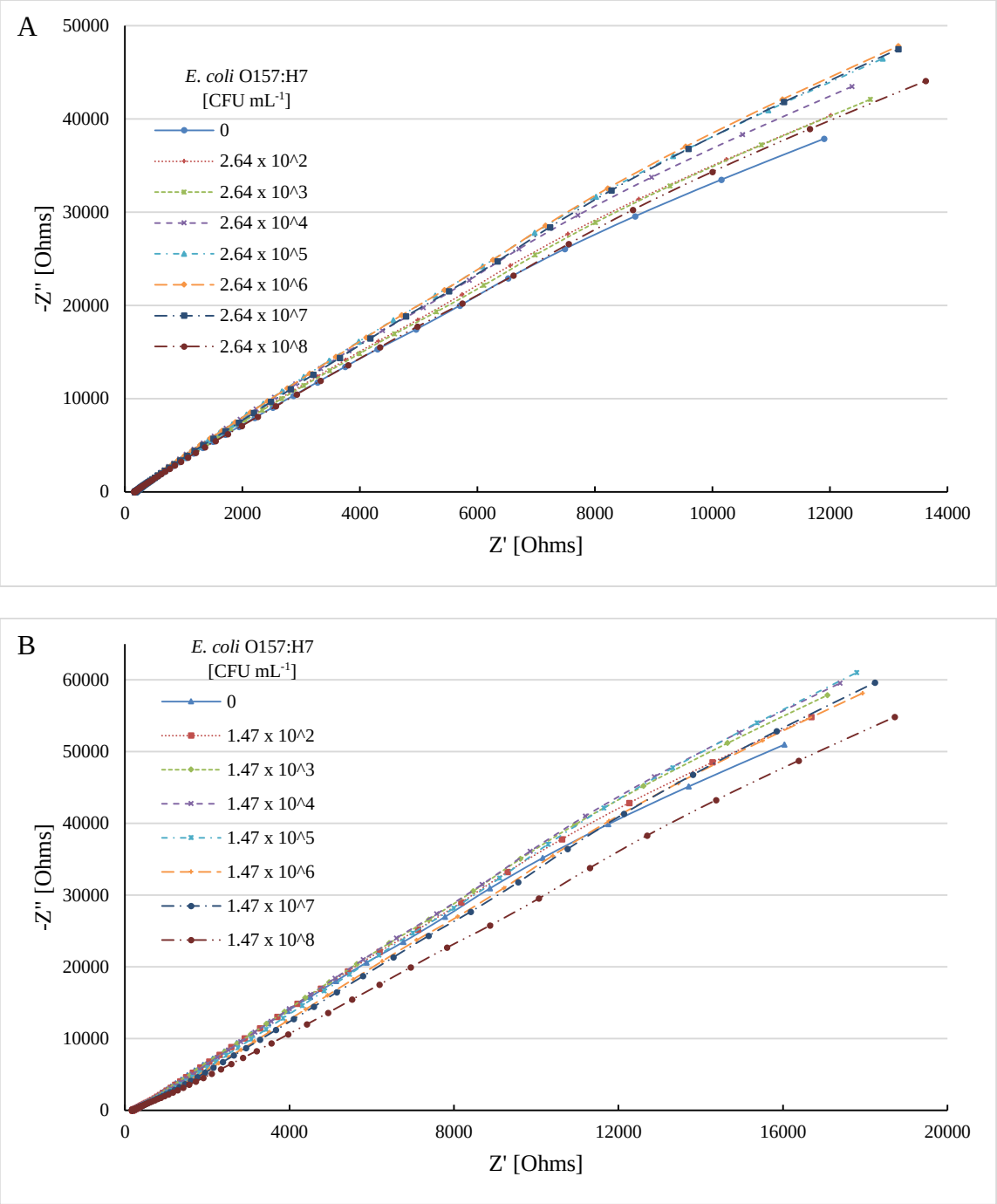

Figure 6.23. Representative Nyquist plots for A) PNIPAAm-ConA modified electrodes and B) PNIPAAm-Anti-GroEL antibody modified electrodes exposed to various concentration of *E. coli* O157:H7 (CFU mL^{-1}). Curves represent the average of 3 replicates.

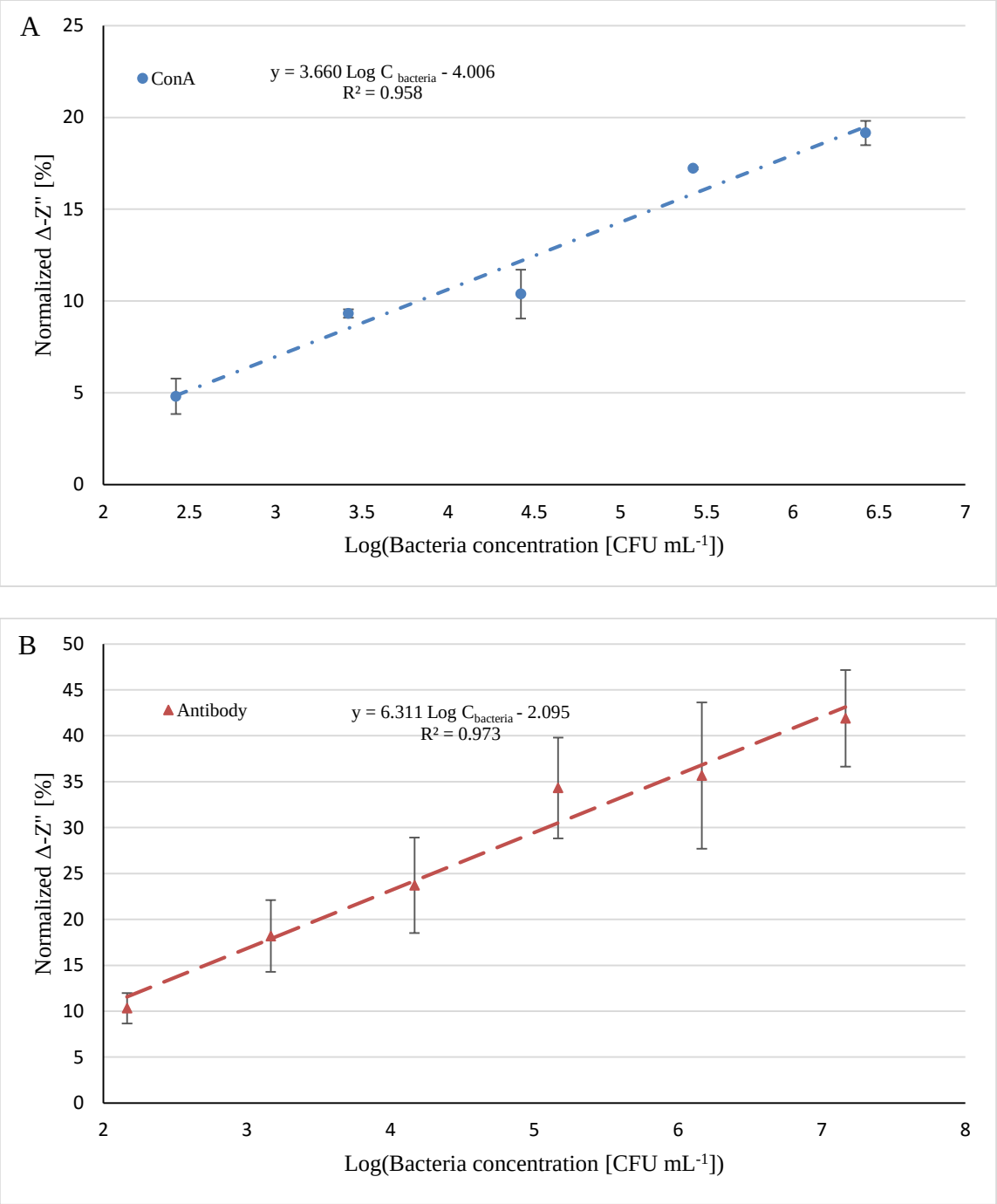

Figure 6.24. Calibration curves for A) PNIPAAm-ConA and B) PNIPAAm-Anti-GroEL antibody modified electrodes exposed to *E. coli* O157:H7 over their respective linear ranges. Curves represent the average of 3 replicates for each capture probe. Equations are displayed to the right of their corresponding electrode modification. Error bars displayed represent the standard deviation for each data point.

Table 6.7. Performance comparison of PNIPAAm-ConA and PNIPAAm-Anti-GroEL antibody modified electrodes exposed *E. coli* O157:H7.

Treatment	Sensitivity $[(\log(CFU\ mL^{-1}))^{-1}]$	R^2	Range $[CFU\ mL^{-1}]$	LOD $[CFU\ mL^{-1}]$
PNIPAAm-ConA	$3.660^{a} \pm 0.264$	0.958	$2.64 \times 10^{2} – 2.64 \times 10^{6}$	$39.06^{b} \pm 3.382$
PNIPAAm-antibody	$6.311^{a} \pm 0.370$	0.973	$1.47 \times 10^{2} – 1.47 \times 10^{7}$	$21.850^{a} \pm 3.459$

Values given are averages of three replicates ± standard deviations. Means that are not followed by a common superscript letter are significantly different ($p < 0.05$).

6.5. SEM Image Analysis

The morphology of the electrode surface after coating with PGP and PGP-PNIPAAm was observed through field emission scanning electron microscopy (SEM) images. Figures 6.25. A and B show the surface characteristics of the "sandwich" platinum-graphene-platinum (PGP) coating on the surface of the Pt/Ir electrode at 5,000 and 10,000 times magnification, respectively. In addition to the PGP structures, scratches on the electrode surface are also visible in Figure 6.25., most likely from repeated polishing between surface modifications.

Comparison to the SEM image of the PGP modification by Vanegas et al. (2014), seen in Figure 6.26., shows the difference in PGP structure size as well as distribution on the electrode surface. The nanoplatinum and reduced graphene structures, approximately 0.5-1 μm in diameter, from this study were on the micro- rather than nano-scale and the overall coating was sporadic compared to the homogeneous surface reported by Vanegas et al. (2014). The morphological differences in these conductive coatings support the findings observed in section 6.1.1. where the ESA values for PGP coatings in this study were found to be lower than those reported by both Burrs et al.(2015) and Vanegas et al. (2014). Also noted in section 6.1.1., ESA values for PGP coatings were lower, though not significantly, than the ESA values for PGP-PNIPAAm coatings.

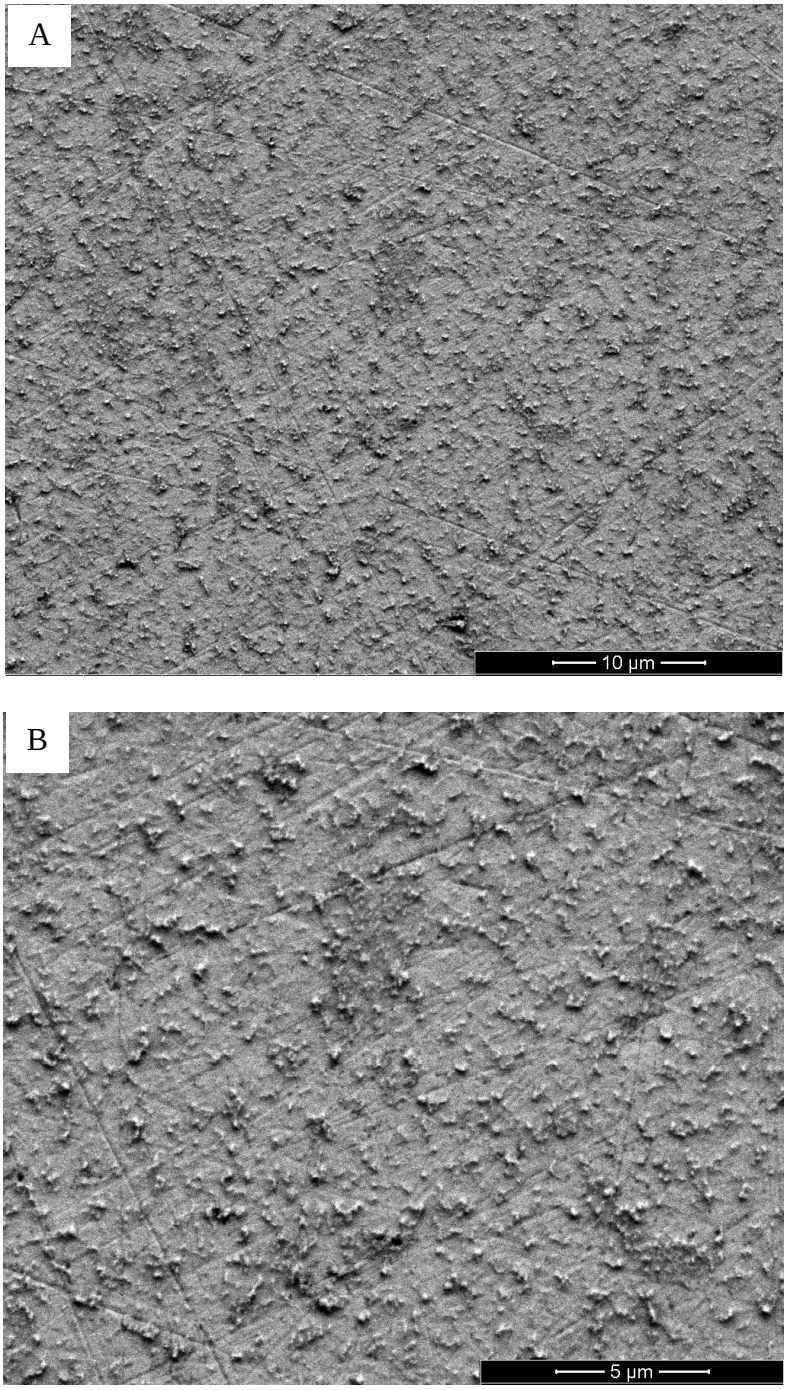

Figure 6.25. SEM image for PGP-modified electrode at A) 5,000 times and B) 10,000 times magnification.

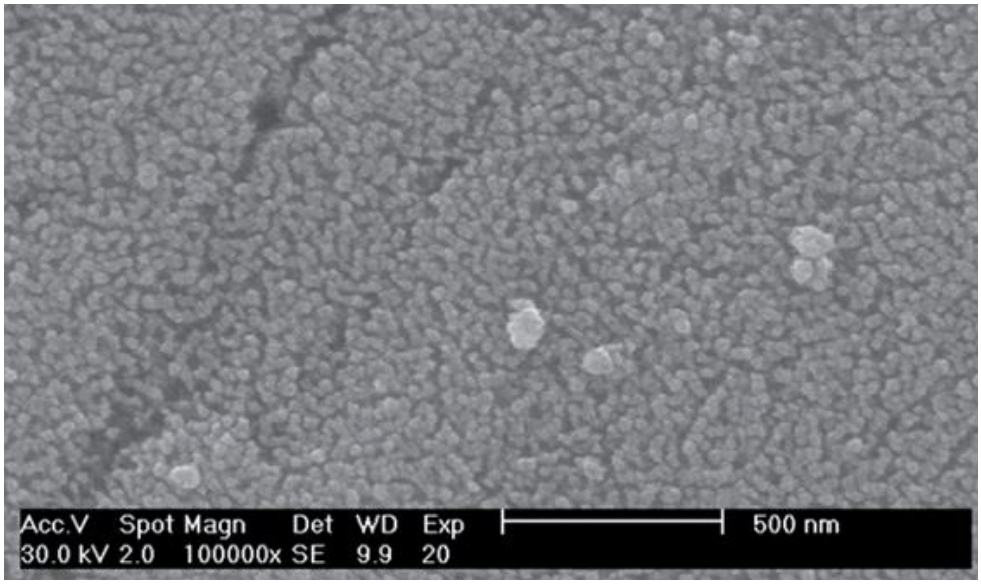

Figure 6.26. Representative SEM image of PGP sandwich surface modification at 100,000 times magnification adapted from Vanegas et al. (2014).

Figures 6.27. A and B show the surface morphology observed for PGP-PNIPAAm modified electrodes at 5,000 and 10,000 times magnification, respectively. PGP-PNIPAAm appears to coat the electrode surface in individual brush-like structures that cluster together and form a heterogeneous layer across the electrode surface. The PNIPAAm brushes, like those of the PGP clusters shown in Figure 6.25., are on the micro-scale (about 1 μm diameter), though the brushes are much more evenly distributed and cover more of the electrode surface than PGP clusters alone. Thus, it can be said the ESA values (reported in section 6.1.) were directly linked to the surface coverage; i.e., increase in surface area from the PGP-PNIPAAm brushes.

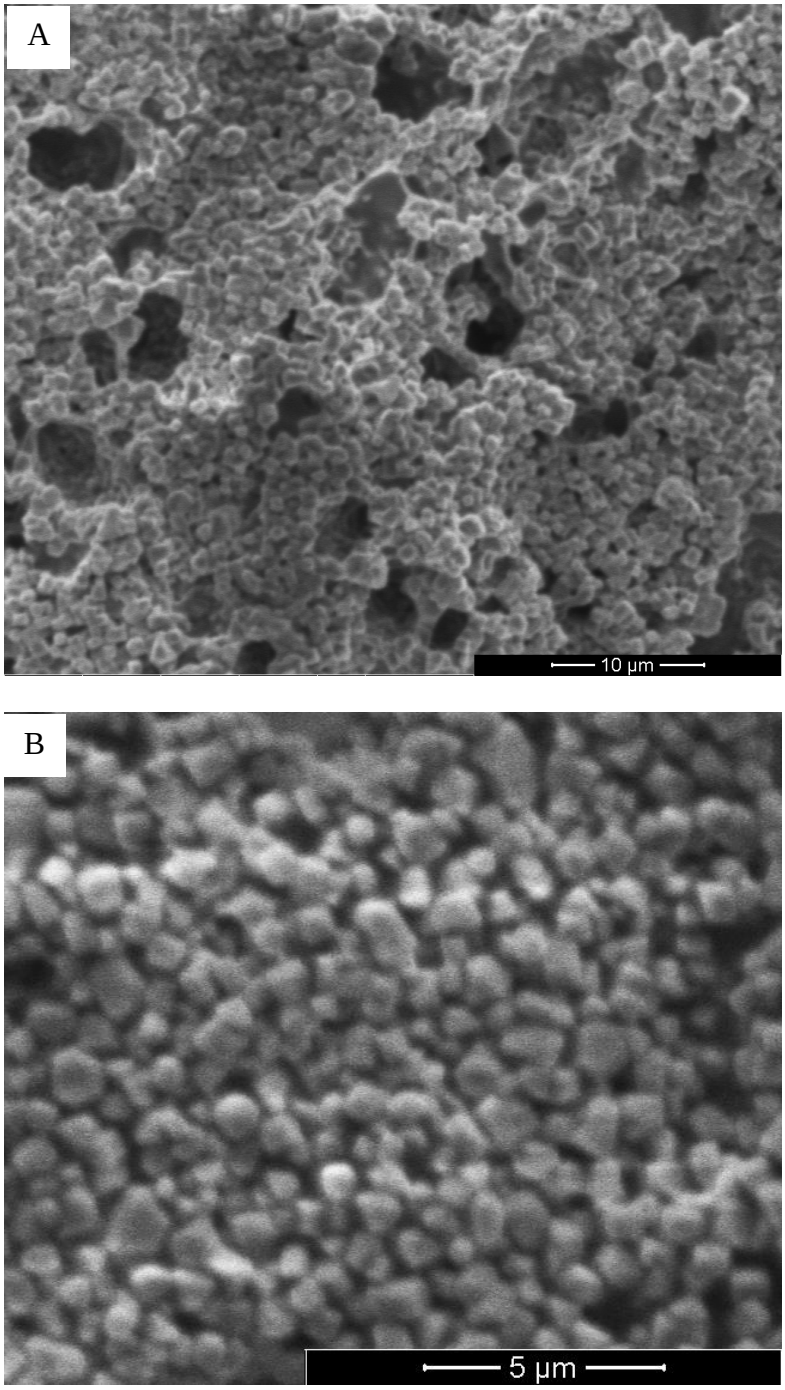

Figure 6.27. SEM image for PGP-PNIPAAm-modified electrode at A) 5,000 times and B) 10,000 times magnification.

The correlation between structures observed in the SEM images and the ESA values reported both in this study and by Burrs et al. (2015) and Vanegas et al. (2014) suggest that nano-scale structures are desirable for achieving higher ESA values compared to micro-scale structures. Differences in coating procedures cited in section 6.1.1. are most likely the reason for the morphological differences and structure sizes observed in the SEM images. When fabricating nanoparticles, size, size distribution, and shape control are all necessary for the optimization of electroactivity of the sensor (Kloke, von Stetten, Zengerle, & Kerzenmacher, 2011). Particles too large or small in diameter can negatively affect the catalytic activity of the sensor and uneven distribution of particle size across the surface can make it difficult to control sensor parameters and achieve reliable results when attaching capture probes and detecting bacteria (Kloke et al., 2011). Furthermore, PNIPAAm has been shown to be desirable as an electrode coating due to its stimuli-responsive behavior and ease of manipulation for any further attachment necessary (Ju et al., 2001; Leal et al., 2013; Lee et al., 2004). Its response to stimuli gives control over electron transfer through manipulation of the surface morphology as shown in the ESA values calculated in section 6.2.1. with regard to actuation.

The group of Burrs et al. (2015) reported PGP-PNIPAAm coatings on a nanoscale based on images from scanning white light interferometry (SWLI). Similarly to the PGP structures, the micro-scale observed in this study compared to the nano-scale may explain the dissimilarity between ESA values, discussed in section 6.1.1., observed in this study and those reported by Burrs et al. (2015). The higher ESA values reported

by Burrs et al. (2015) could be attributed to the uniformity provided by the conductive composite structures at the nano-scale where the unevenly distributed and larger structures at the micro-scale in this study likely contributed negatively to the electrochemical interactions during EIS and CV testing (Kloke et al., 2011).

In a study by Zhao et al. (2012), nano-composite films made up of PNIPAAm and multiwalled carbon nanotubes were reported to exhibit high conductivity and electrocatalytic activity even though they were estimated to be around 6 μm thick. While configured as a film rather than brushes as with this study, the micro-scale of the composite material still exhibiting favorable electroactive properties supports the use of micro-scale PGP-PNIPAAm brushes in the detection of bacteria in this study (Zhao et al., 2012).

6.6. Comparison to Literature

Results from all sensor coating and testing scenarios explored in this study are outlined in Table 6.8. Statistical analysis by ANOVA and Tukey HSD of performance parameters (sensitivity and LOD) revealed significant differences among the treatments analyzed. The highest sensitivity and lowest LOD values were observed for PGP-PNIPAAm-ConA sensors tested in PBS, conversely, PGP coatings for both ConA and Anti-GroEL antibodies produced the lowest sensitivity and highest LOD. Detection time for all treatments in this study was 17 min.

The sensor platform of PGP-PNIPAAm produced better LOD and sensitivity results than PGP alone even when tested in vegetable broth suggesting it is superior for detection of *E. coli* and future studies and improvement should be focused on the use of PGP-PNIPAAm platform. Manipulation of the PGP-PNIPAAm brush size and configuration as discussed in section 6.5. could be used to improve the electrochemical response produced in more complex testing media such as broth.

Table 6.8. Comparison of ConA and Anti-GroEL modified electrodes tested in this study for detection of *E. coli* spp.

Treatment	Media	Bacteria	Sensitivity [$(\log(CFU\ mL^{-1}))^{-1}$]	Range [$CFU\ mL^{-1}$]	LOD [$CFU\ mL^{-1}$]
PGP-ConA	PBS	*E. coli* K12	$1.590^{a} \pm 0.115$	$1.32 \times 10^{2} – 1.32 \times 10^{6}$	$66.877^{d} \pm 7.993$
PGP-Antibody	PBS	*E. coli* K12	$1.335^{a} \pm 0.307$	$2.66 \times 10^{2} – 2.66 \times 10^{5}$	$68.000^{d} \pm 17.580$
PNIPAAm-ConA	PBS	*E. coli* K12	$38.005^{c} \pm 2.330$	$3.04 \times 10^{2} – 3.04 \times 10^{7}$	$3.467^{a} \pm 0.297$
PNIPAAm-ConA	PBS	*E. coli* K12 and *Salmonella* Enteritidis	$39.069^{c} \pm 2.208$	$3.04 \times 10^{2} – 3.04 \times 10^{7}$	$2.947^{a} \pm 0.166$
PNIPAAm-ConA	Broth	*E. coli* O157:H7	$3.660^{a,b} \pm 0.264$	$2.64 \times 10^{2} – 2.64 \times 10^{6}$	$39.06^{c} \pm 3.382$
PNIPAAm-Antibody	Broth	*E. coli* O157:H7	$6.311^{b} \pm 0.370$	$1.47 \times 10^{2} – 1.47 \times 10^{7}$	$21.850^{b} \pm 3.459$

Values given are averages of three replicates ± standard deviations. Means that are not followed by a common superscript letter are significantly different ($p < 0.05$).

Table 6.9. is a compilation of various existing sensors being used for the detection of *E. coli* in various testing media. Performance parameter results from sensors used in this study were shown to be comparable to those from the literature. All sensors used in the study required 15 minutes to capture bacteria and 2 minutes to perform EIS, which is a lower time for detection than all times reported in the literature with the exception of the sensor used by Radke and Alocilja (2005) that reported 10 min. Similarly, the LOD values for sensing *E. coli* in broth were on the same order of magnitude of the lowest reported (10 CFU mL^{-1}) by Joung et al. (2013). In addition, PGP-PNIPAAm-ConA sensor tested in PBS was superior in terms of LOD (3.467 ± 0.297 CFU mL^{-1}) to all LOD values reported in Table 6.9.

Differences between testing media reported in the literature and this study further validate the use of PGP-PNIPAAm-ConA for the detection of *E. coli* both in PBS and the more complex solution of vegetable broth. Several studies used more complex mediums such as whole milk, lettuce wash water, and ground beef, but did not achieve LODs as low as those reported using PGP-PNIPAAm-ConA (Joung et al., 2013; Radke & Alocilja, 2005; Varshney & Li, 2007). Even though the vegetable broth used in this study was processed, the complexity due to the ingredients indicate the ConA and antibody sensors would work in complex solutions such as wash water from produce and other aqueous suspensions of food samples. Another advantage of the PGP-PNIPAAm-ConA sensor used for detection is there was no need for bacteria purification or concentration steps before analysis as with the study by Chowdhury et al. (2012). This

is favorable for industry use to reduce the number of steps required and the overall detection time.

While PGP-PNIPAAm proved to be the superior platform used for detection in this study, PGP alone with ConA and antibody compared to the best sensors reported in the literature. In terms of LOD and detection time, PGP sensors outperformed the majority of sensors used for comparison. Moreover, the linear range of detection was competitive with the sensors from the literature (Table 6.9.).

Table 6.9. Comparison of various biosensors from the literature for detection of *E. coli* O157:H7.

Capture Probe	Detection Method	Media	Range [CFU mL^{-1}]	LOD [CFU mL^{-1}]	Detection Time [min]	Reference
Antibody	Impedimetric	Phosphate Citrate Buffer	10^2 - 10^7	10^2	NR	Chowdhury et al. (2012)
ConA*	Impedimetric	Carrier Buffer	12-1.2 x 10^6	12	< 20	Jantra et al. (2011)
Antibody	Impedimetric	PBS	10-10^5	10	NR	Joung et al. (2013)
Antibody	Impedimetric	Whole Milk	NR	83	NR	Joung et al. (2013)
Antibody	Amperometric	PBS	4.12 x 10^2-12 x 10^5	250	< 45	Li et al. (2012)
ConA	Remote-query magnetoelastic	Water	60-6.1 x 10^9	60	180	Lu et al. (2009)
Antibody	Impedimetric	Lettuce Wash Water	10^4-10^7	10^4	10	Radke & Alocilja (2005)
Antibody	Piezoelectric	1:1 ratio of 10 mM $Fe(SCN)_6^{3-/4-}$ and PBS	10^3-10^8	10^3	30-50	Su & Li (2004)
Antibody	Impedimetric	Ground Beef	8.0 x 10^5-8.0 x 10^7	8.0 x 10^5	35	Varshney & Li (2007)
Antibody	Impedimetric	1:1 ratio of 10 mM $[Fe(CN)_6]^{3-/4-}$ and PBS	10^5-10^8	10^6	NR	Yang et al. (2004)

NR denotes values not reported

**E. coli* strain not specified in literature

7. FUTURE RECOMMENDATIONS

Recommendations for future research on real-time detection of *E. coli* through the use of biosensors functionalized with lectin and carbon-hydrogel nanostructures include:

- Refine the procedure used for PGP coating of electrodes through better control over spin coating speeds and ultrasonication of graphene oxide to improve PNIPAAm attachment to the surface and increase the ESA, thus improving electrochemical response and, consequently, the sensitivity of the sensor.
- Test the effect of the addition of mannose on the adhesion and capture efficiency of ConA to *E. coli* to improve sensor sensitivity and selectivity.
- Study the specificity of ConA to *E. coli* in other, more complex testing solutions such as different types of food and water samples to validate the use of the sensor over a wide range of food systems varying in composition and testing condition (i.e.; pH).
- Study the specificity of ConA to *E. coli* against other types of bacteria, both similar and dissimilar to *E. coli* in type and structure, as well as other interferences in order to test for false positives and false negatives to validate the reliability of the sensor.
- Explore the use of other lectins as capture probes for *E. coli* and other bacteria using the same PNIPAAm and PGP nanostructures to optimize the sensor sensitivity and specificity and range of application.

- Test the effects of various PNIPAAm nanobrush size, thickness, and configuration to increase ESA and optimize PNIPAAm nanobrush coating for improved bacteria capture efficiency.
- Determine sensor performance with different sample types and collection techniques such as swab, broth, and slurry to validate sensor performance in various sample mediums and the effect they have on bacteria capture and sensitivity.
- Test the effect of different capture probe crosslinking attachments on sensor performance to improve sensitivity and optimize robustness of the sensor for reuse.
- Design experiments to evaluate sensor shelf-life and optimize storage conditions for best sensor performance and cost efficiency.
- Test sensor reusability and the effect of different washing techniques for bacteria removal post detection on sensor performance and reliability related to the sensor platform integrity after washing steps on subsequent bacteria capture and detection.
- Optimize the total time required for bacteria detection by experimenting with various bacteria capture times and EIS testing.
- Explore the attachment of multiple capture probes on one sensor surface to create a multiplex sensor capable of detecting and differentiating among different bacteria present.
- Work to miniaturize the system in order to improve portability and accessibility for use in varying environments, especially within the food industry.

8. CONCLUSIONS

Current detection methods for foodborne pathogens such as culture and colony counting, ELISA, and PCR require training and are time consuming. As foodborne pathogens are a constant concern in the food industry for purposes of food safety, public health, and food quality, there is a need for a rapid, reliable, and cost effective detection method. A biosensor using Concanavalin A (ConA) lectin and carbon-hydrogel nanostructures was designed and built for the real-time detection of *Escherichia coli* in a buffer solution (PBS) as well as a real-world scenario simulated by a complex vegetable broth. The use of thermo-responsive polymer brush interfaces in combination with hybrid PGP nanostructures were shown to enhance the capture of target *E. coli* bacteria and transduction of electrochemical outputs as the acquisition signal. The interactions between ConA lectin and O-antigens on *E. coli* membrane resulted in sensor performance (time of detection, range of detection, lower detection limit (LOD), and sensitivity) comparable to that using an antibody for bacteria capture. All sensors used in the study required 15 minutes to capture bacteria and 2 minutes to perform EIS.

The specific results and conclusions from this study are as follows:

- Electroactive surface area (ESA) in cm^2 was evaluated for bare (0.018 ± 0.000), PGP (0.028 ± 0.002), and PGP-PNIPAAm (0.03 ± 0.004) modified electrodes. Resulting ESA values for modified electrodes were significantly higher ($p < 0.05$) than bare electrodes as determined by ANOVA and Tukey HSD. The addition of nanoparticles such as hybrid-hydrogel structures increases the elecrocatalytic activity of the sensor surface, which translates to an increase in ESA values. As a high ESA

value is desirable for electrochemical analysis, PGP and PGP-PNIPAAm coated electrodes were chosen for further development of the biosensor.

- The optimum loading concentration of ConA was determined to be 100 nM for both PGP and PGP-PNIPAAm modified electrodes based on the ESA results acquired from CV testing for several different loading concentrations. This concentration was used throughout the rest of the study for sensors using ConA for detection of *E. coli*.
- The optimum loading concentration for Anti-GroEL antibody, determined for each type of electrode coating (PGP and PGP-PNIPAAm) for comparison with ConA sensor performance, was found to be 50 nM and 100 nM, respectively. Similarly to ConA loading optimization, antibody loading was optimized based on results from ESA calculations.
- Testing conditions for the capture and detection of *E. coli* were determined for the stimuli-responsive polymer, PNIPAAm, based on ESA and bacteria capture results from actuation testing above and below the LCST. Optimum conditions for testing were to capture bacteria at 20 °C when PNIPAAm nanobrushes were expanded and sense at 40 °C when the brushes were collapsed. Expanded brushes allowed ConA to more easily attach to bacteria, while the shrunken state aided in electrochemical response.
- Sensor performance for the detection of *E. coli* K12 was evaluated in PBS for both PGP-ConA and PGP-Anti-GroEL antibodies. Performance parameters including sensitivity and LOD were found to be similar ($p > 0.05$) between the two capture probes. Sensitivities were reported as 1.590 ± 0.115 and 1.335 ± 0.307 (log(CFU

$mL^{-1}))^{-1}$), for ConA and antibody, respectively. The LOD for ConA and antibody were 66.877 ± 7.993 and 68.000 ± 17.580 CFU mL^{-1}, respectively. The use of ConA did result in a wider range of detection ($1.32 \times 10^2 – 1.32 \times 10^6$ CFU mL^{-1}) compared to the antibody ($2.66 \times 10^2 – 2.66 \times 10^5$ CFU mL^{-1}) possibly signifying more efficient attachment of ConA to the electrode surface than antibody when loaded at the same concentration (100 nM). These results indicate ConA is comparable to using antibodies for *E. coli* detection and superior based on the range of detection, possibility for reuse, superior shelf-life and decreased cost of production.

- Performance parameters were evaluated for PGP-PNIPAAm-ConA and also included a test for specificity with *E. coli* K12 and *Salmonella* Enteritidis present in the PBS test solution. All parameters (sensitivity, R^2, range of detection, and LOD) were found to be similar ($p > 0.05$) between the sensors testing using only *E. coli* and those with *Salmonella* also present. The LOD (CFU mL^{-1}) with only *E. coli* present was 3.467 ± 0.297 and when both bacteria were present the LOD was 2.947 ± 0.166. Sensitivities ($(\log(\text{CFU } mL^{-1}))^{-1}$) with *E. coli* present and with both *E. coli* and *Salmonella* were reported as 38.005 ± 2.330 and 39.069 ± 2.208, respectively. The linear range for both testing scenarios was $3.04 \times 10^2 – 3.04 \times 10^7$ CFU mL^{-1}. The PNIPAAm-ConA sensor design proved superior to the PGP sensors, particularly with regard to the LOD achieved. Specificity to *E. coli* with *Salmonella* present was important in evaluating the success of the sensor and comparison to preexisting sensors. Similar results by the sensor exposed to *E. coli* and *E. coli* with *Salmonella*

indicated there was no cross reaction between ConA and *Salmonella*, therefore the sensor was both sensitive and specific to *E. coli*.

- With proof of concept for PNIPAAm-ConA in PBS, it was then tested in vegetable broth spiked with *E. coli* O157:H7 to simulate a real-world, complex sample in the presence of a foodborne pathogen. PNIPAAm-antibody was also tested in broth with *E. coli* for comparison. Sensitivities $(\log(\text{CFU mL}^{-1}))^{-1}$ for PNIPAAm-ConA and PNIPAAm-antibody were 3.660 ± 0.264 and 6.311 ± 0.370, respectively. The LOD (CFU mL^{-1}) for PNIPAAm-ConA was 39.06 ± 3.382 and 21.850 ± 3.459 for PNIPAAm-antibody. Sensitivity results for both sensors were similar ($p > 0.05$), though the antibody showed a wider range of detection ($1.47 \times 10^2 – 1.47 \times 10^7$ CFU mL^{-1}) compared to the ConA ($2.64 \times 10^2 – 2.64 \times 10^6$ CFU mL^{-1}) and significantly lower ($p < 0.05$) LOD.

These results indicated both PNIPAAm-ConA and PNIPAAm-antibody sensors are capable of detecting *E. coli* O157:H7 in a complex system. Due to advantages such as cost of production, shelf-life, and possibility for reuse in addition to performance results being similar to those by antibody, ConA can be said to be the desirable option for detection of *E. coli*.

Evaluation of performance of PGP and PGP-PNIPAAm coatings for use in a biosensor using ConA or antibody to detect *E. coli* indicated PGP-PNIPAAm was significantly better than PGP alone for capture and detection. Compared to values reported in the literature, PGP-PNIPAAm as a platform for both ConA and antibodies produced superior performance results when detecting *E. coli* in a stable media such as

PBS. PGP alone with ConA and antibody was also comparable to the best sensors reported in the literature and in terms of LOD and detection time, PGP sensors outperformed the majority of sensors used for comparison. In the complex media tested, PGP-PNIPAAm with either ConA or antibody were comparable to sensors reported in literature for *E.coli* detection in both complex and simple testing solutions. The advantages of ConA over antibodies in terms of production, cost, and shelf-life combined with comparable results to other biosensors make PGP-PNIPAAm-ConA a potential and attractive alternative solution to current detection methods used in the food industry and by government agencies. Further validation studies with other food products and interferents would be needed to replace the current methods with this biosensor.

REFERENCES

Abu-Rabeah, K., Ashkenazi, A., Marks, R. S., Atias, D., & Amir, L. (2009). Highly sensitive amperometric immunosensor for the detection of Escherichia coli. *Biosensors and Bioelectronics, 24*(12), 3461-3466. doi:10.1016/j.bios.2009.04.042

Adams, M. R., & Moss, M. O. (2008). *Food microbiology*: Cambridge, UK : RSC Publishing, c2008. 3rd ed.

Ahirwar, R., & Nahar, P. (2015). Development of an aptamer-affinity chromatography for efficient single step purification of Concanavalin A from Canavalia ensiformis. *Journal of Chromatography B: Analytical Technologies in the Biomedical & Life Sciences, 997*, 105-109. doi:10.1016/j.jchromb.2015.06.003

Amano, Y., & Quan, C. (2005). Detection of influenza virus: traditional approaches and development of biosensors. *Analytical & Bioanalytical Chemistry, 381*(1), 156-164. doi:10.1007/s00216-004-2927-0

Arora, P., Sindhu, A., Dilbaghi, N., & Chaudhury, A. (2011). Review: Biosensors as innovative tools for the detection of food borne pathogens. *Biosensors and Bioelectronics, 28*, 1-12. doi:10.1016/j.bios.2011.06.002

Audfray, A., Varrot, A., Imberty, A., Claudinon, J., Römer, W., Abounit, S., . . . Wimmerová, M. (2012). Fucose-binding lectin from opportunistic pathogen Burkholderia ambifaria binds to both plant and human oligosaccharidic epitopes. *Journal of Biological Chemistry, 287*(6), 4335-4347. doi:10.1074/jbc.M111.314831

Babacan, S., Pivarnik, P., Letcher, S., & Rand, A. (2002). Piezoelectric Flow Injection Analysis Biosensor for the Detection of Salmonella Typhimurium. *Journal of Food Science, 67*(1), 314-320. Retrieved from http://lib-ezproxy.tamu.edu:2048/login?url=http://search.ebscohost.com/login.aspx?direct=true&db=eih&AN=29326624&site=eds-live

Barsoukov, E., & Macdonald, J. R. (2005). *Impedance spectroscopy. [electronic resource] : theory, experiment, and applications*: Hoboken, N.J. : Wiley-Interscience, c2005. 2nd ed. / edited by Evgenij Barsoukov, J. Ross Macdonald.

Bomans, K., Lang, A., Roedl, V., Adolf, L., Kyriosoglou, K., Diepold, K., . . . Bulau, P. (2013). Identification and monitoring of host cell proteins by mass spectrometry combined with high performance immunochemistry testing. *Plos One, 8*(11), e81639-e81639. doi:10.1371/journal.pone.0081639

Burrs, S. L., Vanegas, D. C., Bhargava, M., Mechulan, N., McLamore, E. S., Hendershot, P., . . . Gomes, C. (2015). A comparative study of graphene-hydrogel hybrid bionanocomposites for biosensing. *Analyst, 140*(5), 1466-1476. doi:10.1039/c4an01788a

Cambi, A., Koopman, M., & Figdor, C. G. (2005). How C-type lectins detect pathogens. *Cellular Microbiology, 7*(4), 481-488. Retrieved from http://lib-ezproxy.tamu.edu:2048/login?url=http://search.ebscohost.com/login.aspx?direct=true&db=mdc&AN=15760448&site=eds-live http://onlinelibrary.wiley.com/store/10.1111/j.1462-5822.2005.00506.x/asset/j.1462-5822.2005.00506.x.pdf?v=1&t=if4derod&s=4ea0d9a12a3295e2e77c179e9f7e0596880b3941

Campuzano, S., Orozco, J., Kagan, D., Guix, M., Gao, W., Sattayasamitsathit, S., . . . Merkoçi, A. (2012). Bacterial isolation by lectin-modified microengines. *Nano Letters, 12*(1), 396-401. doi:10.1021/nl203717q

Carraro, C., Maboudian, R., & Magagnin, L. (2007). Metallization and nanostructuring of semiconductor surfaces by galvanic displacement processes. *Surface Science Reports, 62*(12), 499-525. doi:http://dx.doi.org/10.1016/j.surfrep.2007.08.002

CDC. (2012). Multistate Outbreak of *E. coli* O157:H7 Infections Linked to Romaine Lettuce (Final Update). Retrieved from http://www.cdc.gov/ecoli/2011/romaine-lettace-3-23-12.html

CDC. (2013a). Foodborne Outbreak Tracking and Reporting. Retrieved from http://www.cdc.gov/foodsafety/fdoss/overview/index.html

CDC. (2013b). Multistate Outbreak of Shiga toxin-producing *Escherichia coli* O157:H7 Infections Linked to Ready-to-Eat Salads (Final Update). Retrieved from http://www.cdc.gov/ecoli/2013/O157H7-11-13/index.html

CDC. (2013c). Surveillance for foodborne disease outbreaks--United States, 2009-2010. *MMWR. Morbidity And Mortality Weekly Report, 62*(3), 41-47. Retrieved from http://lib-ezproxy.tamu.edu:2048/login?url=http://search.ebscohost.com/login.aspx?direct=true&db=mdc&AN=23344696&site=eds-live

CDC. (2014a). CDC Estimates of Foodborne Illness in the United States; CDC 2011 Estimates: Findings. Retrieved from http://www.cdc.gov/foodborneburden/2011-foodborne-estimates.html

CDC. (2014b). E. coli Infection and Food Safety. Retrieved from http://www.cdc.gov/features/ecoliinfection/index.html

CDC. (2014c). Multistate Outbreak of Shiga toxin-producing *Escherichia coli* O157:H7 Infections Linked to Ground Beef (Final Update). Retrieved from http://www.cdc.gov/ecoli/2014/O157H7-05-14/index.html

CDC. (2014d). Reports of Selected *E. coli* Outbreak Investigations. Retrieved from http://www.cdc.gov/ecoli/outbreaks.html

CDC. (2015). Preliminary Incidence and Trends of Infection with Pathogens Transmitted Commonly Through Food- Foodborne Diseases Active Surveillance Network, 10 U.S. Sites, 2006-2014. Retrieved from http://www.cdc.gov/mmwr/preview/mmwrhtml/mm6418a4.htm

Chandrasekar, M. S., & Pushpavanam, M. (2008). Pulse and pulse reverse plating—Conceptual, advantages and applications. *Electrochimica Acta, 53*(8), 3313-3322. doi:http://dx.doi.org/10.1016/j.electacta.2007.11.054

Chen, X., Li, N., Eckhard, K., Stoica, L., Xia, W., Assmann, J., . . . Schuhmann, W. (2007). Pulsed electrodeposition of Pt nanoclusters on carbon nanotubes modified carbon materials using diffusion restricting viscous electrolytes. *Electrochemistry Communications, 9*(6), 1348-1354. doi:http://dx.doi.org/10.1016/j.elecom.2007.01.034

Choi, E.-Y., Han, T. H., Hong, J., Kim, J. E., Lee, S. H., Kim, H. W., & Kim, S. O. (2010). Noncovalent functionalization of graphene with end-functional polymers. *Journal of Materials Chemistry, 20*(10), 1907-1912. doi:10.1039/B919074K

Chowdhury, A. D., De, A., Chaudhuri, C. R., Bandyopadhyay, K., & Sen, P. (2012). Label free polyaniline based impedimetric biosensor for detection of E. coli O157:H7 Bacteria. *Sensors & Actuators: B. Chemical, 171-172*, 916-923. doi:10.1016/j.snb.2012.06.004

Chowdhury, T. K., & Weiss, A. K. (1975). *Concanavalin A*: Boston, MA : Springer US, 1975.

Claussen, J. C., Franklin, A. D., ul Haque, A., Porterfield, D. M., & Fisher, T. S. (2009). Electrochemical Biosensor of Nanocube-Augmented Carbon Nanotube Networks. *ACS Nano, 3*(1), 37-44. doi:10.1021/nn800682m

Claussen, J. C., Kumar, A., Jaroch, D. B., Khawaja, M. H., Hibbard, A. B., Porterfield, D. M., & Fisher, T. S. (2012). Nanostructuring Platinum Nanoparticles on Multilayered Graphene Petal Nanosheets for Electrochemical Biosensing.

Advanced Functional Materials, 22(16), 3399-3405. doi:10.1002/adfm.201200551

Claussen, J. C., Wickner, M. M., Fisher, T. S., & Porterfield, D. M. (2011). Transforming the Fabrication and Biofunctionalization of Gold Nanoelectrode Arrays into Versatile Electrochemical Glucose Biosensors. *ACS Applied Materials & Interfaces, 3*(5), 1765-1770. doi:10.1021/am200299h

Coleman, E. J., & Co, A. C. (2014). Galvanic displacement of Pt on nanoporous copper: An alternative synthetic route for obtaining robust and reliable oxygen reduction activity. *Journal of Catalysis, 316,* 191-200. doi:http://dx.doi.org/10.1016/j.jcat.2014.05.012

Cunningham, A. J. (1998). *Introduction to bioanalytical sensors*: New York : Wiley, [1998].

Daniels, J., & Pourmand, N. (2007). Label-free impedance biosensors: Opportunities and challenges. *Electroanalysis, 19*(12), 1239-1257.

Deisingh, A. K., & Thompson, M. (2004). Strategies for the detection of Escherichia coli O157:H7 in foods. *Journal of applied microbiology*. Retrieved from http://lib-ezproxy.tamu.edu:2048/login?url=http://search.ebscohost.com/login.aspx?direct=true&db=edsagr&AN=edsagr.US201300998429&site=eds-live

Devi, R., Yadav, S., & Pundir, C. S. (2011). Electrochemical detection of xanthine in fish meat by xanthine oxidase immobilized on carboxylated multiwalled carbon nanotubes/polyaniline composite film. *Biochemical Engineering Journal, 58-59*(1), 148-153. doi:10.1016/j.bej.2011.09.008

Duncan, T. V. (2011). Applications of nanotechnology in food packaging and food safety: Barrier materials, antimicrobials and sensors. *Journal of Colloid and Interface Science, 363*(1), 1-24. doi:10.1016/j.jcis.2011.07.017

Eddie Ip, W. K., Takahashi, K., Alan Ezekowitz, R., & Stuart, L. M. (2009). Mannose-binding lectin and innate immunity. *Immunological reviews*(1). Retrieved from http://lib-ezproxy.tamu.edu:2048/login?url=http://search.ebscohost.com/login.aspx?direct=true&db=edsagr&AN=edsagr.US201301649739&site=eds-live

FDA. (2012). *Bad Bug Book, Foodborne Pathogenic Microorganisms and Natural Toxins. Second Edition.* (Second ed.): [Washington, D.C.?] : U.S. Food & Drug Administration, Center for Food Safety & Applied Nutrition.

FDA. (2015). Prevention as Cornerstone of FDA Food Safety Modernization Act. Retrieved from http://www.fda.gov/Food/GuidanceRegulation/FSMA/ucm256826.htm

Feng, P., Weagant, S. D., & Jinneman, K. (2011). Bacteriological Analytical Manual: Chapter 4A Diarrheagenic *Escherichia coli*. Retrieved from http://www.fda.gov/Food/FoodScienceResearch/LaboratoryMethods/ucm070080.htm

Firon, N., Ofek, I., & Sharon, N. (1984). Carbohydrate-binding sites of the mannose-specific fimbrial lectins of Enterobacteria. *Infection and Immunity, 43*(3), 1088-1091. Retrieved from http://lib-ezproxy.tamu.edu:2048/login?url=http://search.ebscohost.com/login.aspx?direct=true&db=edselc&AN=edselc.2-52.0-0021345727&site=eds-live http://iai.asm.org/content/43/3/1088.full.pdf

Funk & Wagnalls new world encyclopedia. (2015). Retrieved from cat03318a database Retrieved from http://lib-ezproxy.tamu.edu:2048/login?url=http://search.ebscohost.com/login.aspx?direct=true&db=cat03318a&AN=tamug.2176658&site=eds-live http://lib-ezproxy.tamu.edu:2048/login?url=http://coral.library.tamu.edu/resourcelink.php?resource=2033

Gamella, M., Campuzano, S., Parrado, C., Reviejo, A. J., & Pingarrón, J. M. (2009). Microorganisms recognition and quantification by lectin adsorptive affinity impedance. *Talanta, 78*, 1303-1309. doi:10.1016/j.talanta.2009.01.059

Geng, P., Zhang, X., Meng, W., Wang, Q., Zhang, W., Jin, L., . . . Wu, Z. (2008). Self-assembled monolayers-based immunosensor for detection of Escherichia coli using electrochemical impedance spectroscopy. *Electrochimica Acta, 53*, 4663-4668. doi:10.1016/j.electacta.2008.01.037

Ghazarian, H., Idoni, B., & Oppenheimer, S. B. (2011). Review: A glycobiology review: Carbohydrates, lectins and implications in cancer therapeutics. *Acta Histochemica, 113*, 236-247. doi:10.1016/j.acthis.2010.02.004

Gil, E. S., & Hudson, S. M. (2004). Stimuli-reponsive polymers and their bioconjugates. *Progress in Polymer Science, 29*, 1173-1222. doi:10.1016/j.progpolymsci.2004.08.003

Grieshaber, D., MacKenzie, R., Voros, J., & Reimhult, E. (2008). Electrochemical biosensors - Sensor principles and architectures. *Sensors, 8*(3), 1400-1458.

H-E-B. (2015). H-E-B Vegetable Broth. Retrieved from https://www.heb.com/product-detail/h-e-b-vegetable-broth/1605840

Haseley, S. R. (2002). Carbohydrate recognition: A nascent technology for the detection of bioanalytes. *Analytica Chimica Acta, 457*(1), 39-45. doi:10.1016/S0003-2670(01)01329-0

Hill, L. E., & Gomes, C. L. (2014). Characterization of temperature and pH-responsive poly-N-isopropylacrylamide-co-polymer nanoparticles for the release of antimicrobials. *Materials Research Express, 1*(3), 035405. Retrieved from http://stacks.iop.org/2053-1591/1/i=3/a=035405

Hu, Y., Zuo, P., & Ye, B. C. (2013). Label-free electrochemical impedance spectroscopy biosensor for direct detection of cancer cells based on the interaction between carbohydrate and lectin. *Biosensors and Bioelectronics, 43*(1), 79-83. doi:10.1016/j.bios.2012.11.028

Ivnitski, D., Abdel-Hamid, I., Atanasov, P., & Wilkins, E. (1999). Review: Biosensors for detection of pathogenic bacteria. *Biosensors and Bioelectronics, 14*, 599-624. doi:10.1016/S0956-5663(99)00039-1

Jantra, J., Kanatharana, P., Asawatreratanakul, P., Thavarungkul, P., Hedstrom, M., & Mattiasson, B. (2011). Real-time label-free affinity biosensors for enumeration of total bacteria based on immobilized concanavalin A. *Journal of Environmental Science and Health - Part A Toxic/Hazardous Substances and Environmental Engineering, 46*(13), 1450-1460. doi:10.1080/10934529.2011.609022

Jayasena, S. D. (1999). Aptamers: An Emerging Class of Molecules That Rival Antibodies in Diagnostics. *Clinical Chemistry, 45*(9), 22.

Joung, C.-K., Kim, H.-N., Lim, M.-C., Jeon, T.-J., Kim, H.-Y., & Kim, Y.-R. (2013). A nanoporous membrane-based impedimetric immunosensor for label-free detection of pathogenic bacteria in whole milk. *Biosensors and Bioelectronics, 44*, 210-215. doi:10.1016/j.bios.2013.01.024

Ju, H. K., Kim, S. Y., & Lee, Y. M. (2001). pH/temperature-responsive behaviors of semi-IPN and comb-type graft hydrogels composed of alginate and poly(N-isopropylacrylamide). *Polymer, 42*(16), 6851-6857. doi:10.1016/S0032-3861(01)00143-4

Kärkkäinen, R. M., Drasbek, M. R., McDowall, I., Smith, C. J., Young, N. W. G., & Bonwick, G. A. (2011). Aptamers for safety and quality assurance in the food industry: detection of pathogens. *International Journal of Food Science & Technology, 46*(3), 445-454. doi:10.1111/j.1365-2621.2010.02470.x

Kim, S. (2000). Thermo- and pH-responsive behaviors of graft copolymer and blend based on chitosan and N-isopropylacrylamide. *Journal of Applied Polymer Science, 78*(7), 1381-1391. Retrieved from http://linkresolver.tamu.edu:9003/tamu?ctx_ver=Z39.88-2004&ctx_enc=info%3Aofi%2Fenc%3AUTF-8&ctx_tim=2015-05-28T16%3A43%3A25IST&url_ver=Z39.88-2004&url_ctx_fmt=infofi%2Ffmt%3Akev%3Amtx%3Actx&rfr_id=info%3Asid%2Fprimo.exlibrisgroup.com%3Aprimo3-Article-wos&rft_val_fmt=info%3Aofi%2Ffmt%3Akev%3Amtx%3Ajournal&rft.genre=article&rft.atitle=Thermo-%20and%20pH-responsive%20behaviors%20of%20graft%20copolymer%20and%20blend%20based%20on%20chitosan%20and%20N-isopropylacrylamide&rft.jtitle=Journal%20Of%20Applied%20Polymer%20Science&rft.btitle=&rft.aulast=Kim&rft.auinit=&rft.auinit1=&rft.auinitm=&rft.ausuffix=&rft.au=Kim%2C%20Sy&rft.aucorp=&rft.date=20001114&rft.volume=78&rft.issue=7&rft.part=&rft.quarter=&rft.ssn=&rft.spage=1381&rft.epage=1391&rft.pages=1381-1391&rft.artnum=&rft.issn=0021-8995&rft.eissn=&rft.isbn=&rft.sici=&rft.coden=&rft_id=info%3Adoi%3A&rft_id=info%3Aoai%2F&rft.object_id=&rft_dat=%3Cwos%3E000089532400009%3C%2Fwos%3E&rft.eisbn=

Kloke, A., von Stetten, F., Zengerle, R., & Kerzenmacher, S. (2011). Strategies for the Fabrication of Porous Platinum Electrodes. *Advanced Materials, 23*(43), 4976-5008. doi:10.1002/adma.201102182

Lazcka, O., Campo, F. J. D., & Muñoz, F. X. (2007). Review: Pathogen detection: A perspective of traditional methods and biosensors. *Biosensors and Bioelectronics, 22*, 1205-1217. doi:10.1016/j.bios.2006.06.036

Leal, D., De Borggraeve, W., Encinas, M. V., Matsuhiro, B., & Müller, R. (2013). Preparation and characterization of hydrogels based on homopolymeric fractions of sodium alginate and PNIPAAm. *Carbohydrate Polymers, 92*, 157-166. doi:10.1016/j.carbpol.2012.09.031

Lee, S. B., Ha, D. I., Cho, S. K., Lee, Y. M., & Kim, S. J. (2004). Temperature/pH-Sensitive Comb-Type Graft Hydrogels Composed of Chitosan and Poly(N-isopropylacrylamide). *Journal of Applied Polymer Science, 92*(4), 2612-2620. doi:10.1002/app.20265

Li, Y., Cheng, P., Fang, L., Deng, J., Zheng, J., Gong, J., & Liang, W. (2012). Amperometric immunosensor for the detection of Escherichia coli O157:H7 in food specimens. *Analytical Biochemistry, 421*(1), 227-233. doi:10.1016/j.ab.2011.10.049

Lipman, N. S., Jackson, L. R., Trudel, L. J., & Weis-Garcia, F. (2005). Monoclonal versus polyclonal antibodies: distinguishing characteristics, applications, and information resources. *ILAR journal*(3). Retrieved from http://lib-ezproxy.tamu.edu:2048/login?url=http://search.ebscohost.com/login.aspx?direct=true&db=edsagr&AN=edsagr.US201301006966&site=eds-live

Liu, Y., Meng, S., Mu, L., Jin, G., Zhong, W., & Kong, J. (2008). Novel renewable immunosensors based on temperature-sensitive PNIPAAm bioconjugates. *Biosensors and Bioelectronics, 24*, 710-715. doi:10.1016/j.bios.2008.06.041

Lokuge, I., Wang, X., & Bohn, P. W. (2007). Temperature-controlled flow switching in nanocapillary array membranes mediated by poly(N-isopropylacrylamide) polymer brushes grafted by atom transfer radical polymerization. *Langmuir, 23*(1), 305-311. doi:10.1021/la060813m

Lu, Q., Lin, H., Ge, S., Luo, S., Cai, Q., & Grimes, C. A. (2009). Wireless, remote-query, and high sensitivity Escherichia coli O157:H7 biosensor based on the recognition action of concanavalin A. *Analytical Chemistry, 81*(14), 5846-5850. doi:10.1021/ac9008572

McLamore, E. S., Shi, J., Jaroch, D., Claussen, J. C., Uchida, A., Jiang, Y., . . . Porterfield, D. M. (2011). A self referencing platinum nanoparticle decorated enzyme-based microbiosensor for real time measurement of physiological glucose transport. *Biosensors and Bioelectronics, 26*, 2237-2245. doi:10.1016/j.bios.2010.09.041

McNaught, A. D., & Wilkinson, A. (1997). *Compendium of chemical terminology : IUPAC recommendations*: Oxford [Oxfordshire] ; Malden, MA : Blackwell Science, 1997. 2nd ed.

Mendes, P. M. (2008). Stimuli-responsive surfaces for bio-applications. *Chemical Society Reviews, 37*(11), 2512-2529. doi:10.1039/B714635N

Miller, J. R. C., & Andre, R. (2014). Quantitative polymerase chain reaction. *British Journal Of Hospital Medicine (London, England: 2005), 75*(12), C188-C192. doi:10.12968/hmed.2014.75.Sup12.C188

Minko, S. (2006). Responsive Polymer Brushes. *Journal of Macromolecular Science: Polymer Reviews, 46*(4), 397. Retrieved from http://lib-ezproxy.tamu.edu:2048/login?url=http://search.ebscohost.com/login.aspx?direct=true&db=edb&AN=75319919&site=eds-live

Nasir, S., Ali, M., & Ensinger, W. (2012). Thermally controlled permeation of ionic molecules through synthetic nanopores functionalized with amine-terminated polymer brushes. *Nanotechnology, 23*(22). doi:10.1088/0957-4484/23/22/225502

Nayak, M., Kotian, A., Marathe, S., & Chakravortty, D. (2009). Review: Detection of microorganisms using biosensors—A smarter way towards detection techniques. *Biosensors and Bioelectronics, 25*, 661-667. doi:10.1016/j.bios.2009.08.037

Nilsson, C. L. E. (2007). *Lectins: Analytical Technologies* C. L. Nilsson (Ed.) Retrieved from cat03318a database Retrieved from http://lib-ezproxy.tamu.edu:2048/login?url=http://www.sciencedirect.com/science/book/9780444530776

North, J. R. (1985). Immunosensors: Antibody-based biosensors. *Trends in Biotechnology, 3*(7), 180-186. doi:10.1016/0167-7799(85)90119-2

Pejcic, B., De Marco, R., & Parkinson, G. (2006). The role of biosensors in the detection of emerging infectious diseases. *Analyst, 131*(10), 1079-1090.

Penner, R. M. (2002). Mesoscopic Metal Particles and Wires by Electrodeposition. *The Journal of Physical Chemistry B, 106*(13), 3339-3353. doi:10.1021/jp013219o

Pöhlmann, C., Wang, Y., Humenik, M., Heidenreich, B., Gareis, M., & Sprinzl, M. (2009). Rapid, specific and sensitive electrochemical detection of foodborne bacteria. *Biosensors and Bioelectronics, 24*, 2766-2771. doi:10.1016/j.bios.2009.01.042

Prodromidis, M. I. (2010). Review article: Impedimetric immunosensors—A review. *Electrochimica Acta, 55*, 4227-4233. doi:10.1016/j.electacta.2009.01.081

Radke, S. M., & Alocilja, E. C. (2005). A high density microelectrode array biosensor for detection of E. coli O157:H7. *Biosensors and Bioelectronics, 20*(8), 1662-1667. doi:http://dx.doi.org/10.1016/j.bios.2004.07.021

Safina, G., van Lier, M., & Danielsson, B. (2008). Flow-injection assay of the pathogenic bacteria using lectin-based quartz crystal microbalance biosensor. *Talanta, 77*(2), 468-472. doi:10.1016/j.talanta.2008.03.033

Scientific, T. Procedure for EDC/NHS crosslinking of carboxylates with primary amines. Retrieved from http://www.piercenet.com/instructions/2160650.pdf

Shen, Z., Hou, N., Jin, M., Qiu, Z., Wang, J., Zhang, B., . . . Zhou, D. (2014). A novel enzyme-linked immunosorbent assay for detection of Escherichia coli O157:H7

using immunomagnetic and beacon gold nanoparticles. *Gut Pathogens, 6*(1). doi:10.1186/1757-4749-6-14

Shen, Z., Xiao, C., Zeng, X., Huang, M., Zhang, Y., & Wang, P. G. (2007). Nonlabeled quartz crystal microbalance biosensor for bacterial detection using carbohydrate and lectin recognitions. *Analytical Chemistry, 79*(6), 2312-2319. doi:10.1021/ac061986j

Shi, J., Jaroch, D., Rickus, J. L., Marshall Porterfield, D., Claussen, J. C., Ul Haque, A., . . . Calvo-Marzal, P. (2011). A comparative study of enzyme immobilization strategies for multi-walled carbon nanotube glucose biosensors. *Nanotechnology, 22*(35). doi:10.1088/0957-4484/22/35/355502

Shi, J., Marshall Porterfield, D., Zhang, H., Stanciu, L. A., Snyder, A., Wang, M. X., & Xie, J. (2012). An aqueous media based approach for the preparation of a biosensor platform composed of graphene oxide and Pt-black. *Biosensors and Bioelectronics, 38*(1), 314-320. doi:10.1016/j.bios.2012.06.007

Skládal, P., Kovář, D., Krajíček, V., Krajíček, V., Přibyl, J., & Švábenská, E. (2013). Electrochemical immunosensors for detection of microorganisms. *International Journal of Electrochemical Science, 8*(2), 1635-1649. Retrieved from http://lib-ezproxy.tamu.edu:2048/login?url=http://search.ebscohost.com/login.aspx?direct=true&db=edselc&AN=edselc.2-52.0-84873537154&site=eds-live

Su, X.-L., & Li, Y. (2004). A self-assembled monolayer-based piezoelectric immunosensor for rapid detection of Escherichia coli O157:H7. *Biosensors and Bioelectronics, 19*, 563-574. doi:10.1016/S0956-5663(03)00254-9

Su, X., Ren, J., Meng, X., Ren, X., & Tang, F. (2013). A novel platform for enhanced biosensing based on the synergy effects of electrospun polymer nanofibers and graphene oxides. *Analyst, 138*(5), 1459-1466. doi:10.1039/c2an36663k

Subramanian, A., Irudayaraj, J., & Ryan, T. (2006). A mixed self-assembled monolayer-based surface plasmon immunosensor for detection of E. coli O157:H7. *Biosensors and Bioelectronics, 21*, 998-1006. doi:10.1016/j.bios.2005.03.007

Tarabees, R. Z., Hassanin, Z. H., El Rahman, A., & El Bagoury, M. (2015). Polymerase Chain Reaction (PCR): An Alternative Rapid Method for Detection of Some Microbial Contamination of Meat Products. *Alexandria Journal for Veterinary Sciences, 45*, 91-98. doi:10.5455/ajvs.177446

Trilling, A., Beekwilder, J., & Zuilhof, H. (2013). Antibody orientation on biosensor surfaces: a minireview. *Analyst, 138*(6), 1619-1627.

Vanegas, D. C., Taguchi, M., Chaturvedi, P., Burrs, S., McLamore, E. S., Tan, M., & Yamaguchi, H. (2014). A comparative study of carbon-platinum hybrid nanostructure architecture for amperometric biosensing. *Analyst, 139*(3), 660-667. doi:10.1039/c3an01718d

Varshney, M., & Li, Y. (2007). Interdigitated array microelectrode based impedance biosensor coupled with magnetic nanoparticle–antibody conjugates for detection of Escherichia coli O157:H7 in food samples. *Biosensors and Bioelectronics, 22*, 2408-2414. doi:10.1016/j.bios.2006.08.030

Varshney, M., & Li, Y. (2008). Double interdigitated array microelectrode-based impedance biosensor for detection of viable Escherichia coli O157:H7 in growth medium. *Talanta, 74*, 518-525. doi:10.1016/j.talanta.2007.06.027

Varshney, M., & Li, Y. (2009). Review: Interdigitated array microelectrodes based impedance biosensors for detection of bacterial cells. *Biosensors and Bioelectronics, 24*, 2951-2960. doi:10.1016/j.bios.2008.10.001

Vidal, J. C., Bonel, L., Ezquerra, A., Hernández, S., Bertolín, J. R., Cubel, C., & Castillo, J. R. (2013). Electrochemical affinity biosensors for detection of mycotoxins: A review. *Biosensors and Bioelectronics, 49*, 146-158. doi:10.1016/j.bios.2013.05.008

Wan, Y., Zhang, D., & Hou, B. (2009). Monitoring microbial populations of sulfate-reducing bacteria using an impedimetric immunosensor based on agglutination assay. *Talanta, 80*(1), 218-223. doi:10.1016/j.talanta.2009.06.057

Wang, J. (2001). Glucose biosensors: 40 years of advances and challenges. *Electroanalysis, 13*(12), 983-988.

Wang, N., He, M., & Shi, H.-C. (2007). Novel indirect enzyme-linked immunosorbent assay (ELISA) method to detect Total E. coli in water environment. *Analytica Chimica Acta, 590*, 224-231. doi:10.1016/j.aca.2007.03.041

WHO. (2011). Enterohaemorrhagic Escherichia coli (EHEC). Retrieved from http://www.who.int/mediacentre/factsheets/fs125/en/

Xu, S. (2012). Electromechanical biosensors for pathogen detection. *Microchimica Acta, 178*(3/4), 245-260. doi:10.1007/s00604-012-0831-4

Yang, L., Li, Y., & Erf, G. F. (2004). Interdigitated Array Microelectrode-Based Electrochemical Impedance Immunosensor for Detection of Escherichia coli O157:H7. *Analytical Chemistry, 76*(4), 1107-1113. doi:10.1021/ac0352575

Yang, X., Shi, X.-W., Liu, Y., Bentley, W. E., & Payne, G. F. (2009). Orthogonal Enzymatic Reactions for the Assembly of Proteins at Electrode Addresses. *Langmuir, 25*(1), 338-344. doi:10.1021/la802618q

Yin, Z., Zhang, J., Jiang, L. P., & Zhu, J. J. (2009). Thermosensitive behavior of poly(N-isopropylacrylamide) and release of incorporated hemoglobin. *Journal of Physical Chemistry C, 113*(36), 16104-16109. doi:10.1021/jp903589a

Yixian, W., Zunzhong, Y., & Yibin, Y. (2012). New Trends in Impedimetric Biosensors for the Detection of Foodborne Pathogenic Bacteria. *Sensors (14248220), 12*(3), 3449-3471. doi:10.3390/s120303449

Zelada-Guillén, G. A., Bhosale, S. V., Riu, J., & Rius, F. X. (2010). Real-time potentiometric detection of bacteria in complex samples. *Analytical Chemistry, 82*(22), 9254-9260. doi:10.1021/ac101739b

Zhang, R. (2005). Synthesis, characterization and reversible transport of thermo-sensitive carboxyl methyl dextran/poly (N-isopropylacrylamide) hydrogel. *Polymer, 46*, 2443-2451. doi:10.1016/j.polymer.2005.02.006

Zhao, X., Liu, Y., Lu, J., Zhou, J., & Li, J. (2012). Temperature-responsive polymer/carbon nanotube hybrids: Smart conductive nanocomposite films for modulating the bioelectrocatalysis of NADH. *Chemistry - A European Journal, 18*(12), 3687-3694. doi:10.1002/chem.201103259

Zhou, J., Liu, J., Wang, G., Lu, X., Wen, Z., & Li, J. (2007). Poly(N-isopropylacrylamide) interfaces with dissimilar thermo-responsive behavior for controlling ion permeation and immobilization. *Advanced Functional Materials, 17*(16), 3377-3382. doi:10.1002/adfm.200700286